

# THE RADIO AND ELECTRONIC ENGINEER

## The Journal of the Institution of Electronic and Radio Engineers

FOUNDED 1925 INCORPORATED BY ROYAL CHARTER 1961

*"To promote the advancement of radio, electronics and kindred subjects by the exchange of information in these branches of engineering."*

VOLUME 29

MAY 1965

NUMBER 5

### ON STATION

*The second issue of the N.E.R.C. Review contains the following article by Mr. L. H. Bedford, C.B.E., a Past President of the Institution and vice chairman of the Projects Committee of the National Electronics Research Council. Reproduced here by permission of the Council, it will be of undoubted interest to all radio engineers.*

**A**PRIL 9th, 1965 was a very important day in the history of electronics. On that day *Early Bird*, the first communication satellite with a commercial role, arrived on station.

The history of the geo-stationary satellite is worth recalling. Perhaps the first explicit statement of the idea is that of A. C. Clarke. In retrospect one may say, as in the case of other major 'inventions', that the idea was obvious. It must be remembered that Clarke's paper† pre-dated the achievement of the first *Sputnik*, so there would be some reason for arguing that if the idea was obvious to Clarke it was equally so to Newton. The difference was perhaps that Clarke was not daunted, as were some of those more closely concerned with the practical rocket problems, by the tremendous booster problems implied.

*Early Bird*, and its *Syncom* predecessors, have not been achieved without a struggle. The opponents of the stationary communications satellite have argued—

- (a) that the launching, injection, and station-keeping problems were in advance of the art, and
- (b) that the propagation time of approximately 270 milliseconds was unacceptably high.

The first argument would seem to have received the *coup-de-grace* in that *Early Bird* is not the last commercial satellite to be launched but the *first*.

It remains to see whether the propagation-time problem proves to be real or ephemeral. Incidentally, it should be remarked that the launching of a satellite is rather an expensive way of making this particular trial, which would seem wholly amenable to simulated ground tests. Such tests have indeed been carried out on quite a large scale but no clear conclusion has been stated.

Finally, one may inquire, what has this particularly brilliant space effort to do with electronics? The answer is three-fold:

The whole orbiting procedure is essentially an electronic control operation.

The electronics of the '*Bird*' is most advanced in both concept and execution; especially is this true with regard to component reliability. There are no mechanical moving parts other than the gas-jet control valves, which are 'bang-bang' devices with a movement of a few thousandths of an inch.

Finally, *Early Bird* heralds a new era—electronic communication by satellite. It is designed not as an experiment but as a means of providing permanent commercial communication channels. Its 240 two-way channels (to C.C.I.R. standards) about double the present transatlantic capacity.

The fact that this is achieved with a single 6-watt repeater at a range of some 22,000 miles is somewhat surprising. To accomplish this has required the application of the most advanced communication techniques, but one sacrifice has had to be made: *Early Bird* is essentially a trunk system, that is to say it provides a trunk circuit between two stations only. Multi-access would reduce the total channel capacity drastically. But it is precisely the possibility of multi-access that gives satellite communication its operational and economic appeal. While so much has been achieved, there still remains the multi-access problem, and it is an electronic one.

† "Extra-terrestrial relays", *Wireless World*, 51, pp. 305-8, October 1945.

## INSTITUTION NOTICES

### Symposium on Microelectronics

A symposium of over thirty papers concentrating primarily on the applications of microelectronics will be held at the University of Southampton from 21st to 23rd September 1965. The meeting is being organized jointly by the Southern Section of the Institution of Electronic and Radio Engineers, the Southern Electronics Section of the Institution of Electrical Engineers, and the Department of Electronics, University of Southampton.

Sessions will deal with thin-film and integrated-circuit linear applications, digital-stores, computer and switching applications, the use of metal-oxide-semiconductor transistors, system design and inter-connection methods, and human and economic aspects.

Registration forms are now available from The Symposium Secretary, Department of Electronics, The University, Southampton.

### Conference on Non-Metallic Thin Films

The Electronics Group of The Institute of Physics and The Physical Society is arranging a conference on "Non-metallic thin films" to be held at Chelsea College of Science and Technology, London, from 23rd to 24th September 1965.

The conference will discuss the physical properties of continuous non-metallic films deposited on substrates of a different material. It is proposed to include the following main subjects: formation of thin films, electronic structure, electrical conduction, electron emission, and electronic applications, especially in active devices.

Further details and application forms are available from The Meetings Officer, The Institute of Physics and The Physical Society, 47 Belgrave Square, London, S.W.1.

### International Aerospace Instrumentation Symposium

The Fourth International Aerospace Instrumentation Symposium (formerly Flight Test Instrumentation) will be held at the College of Aeronautics, Cranfield on 21st to 24th March 1966. The Symposium is sponsored by the College of Aeronautics and the Aerospace Division of the Instrument Society of America.

Papers are invited for presentation at this symposium and authors are requested to submit a 300-500 word summary for consideration by the organizers. Appropriate subjects in the applied science and technology of instrumentation of aerospace vehicles may be chosen, but papers which are concerned with new measurement techniques and the application of computers to large-scale data handling problems are particularly welcome.

Further information may be obtained from Michael A. Perry, Symposium Organizer, The College of Aeronautics, Cranfield, Bedford, England, or E. K. Merewether, I.S.A. Aerospace Division, 4515 Canoga Avenue, Woodland Hills, California, U.S.A.

### Montefiore Foundation Prize

The Association of Electrical Engineers of the Institut Electrotechnique Montefiore, Liège, awards every five years an international prize for the best original work submitted on scientific advance and progress in the technical applications of electricity in all spheres. The value of the award is 100,000 Fr. (Belgian) (about £725).

The closing date for submission of entries to the Secretary of the Fondation George Montefiore is 1st July 1965. Further information may be obtained from the Institution or from the Association direct at 31 Rue Saint-Gilles, Liège, Belgium.

### Conference on Medical Physics

The First International Conference on Medical Physics is to be held at Harrogate, Yorkshire, from 8th to 10th September 1965.

This Conference, which is being organized by the U.K. National Committee for Medical Physics under the sponsorship of the International Atomic Energy Agency and the World Health Organization, will consist of a series of sessions on all aspects of medical physics, including applications in obstetrics, neurology, orthopaedics, physiology and radiology. Work in artificial environments, in functional replacements of artificial organs and limbs, in haemodynamics, electrophysiology, the use of mathematical techniques and computers, ultrasonics in diagnosis and therapy, infra-red thermography, radiation dosimetry, and the use of radioactive isotopes in medicine will also be discussed.

All inquiries should be addressed to The Secretary, First International Conference on Medical Physics, 45-47 Little Britain, London, E.C.1.

### Back Copies of the Journal

Because of the increasing number of requests by new subscribers, notably libraries overseas, several issues of *The Radio and Electronic Engineer* for 1963 are now out of print, namely, January, February, March, April, May and June (Volume 25). Members who are willing to part with their copies of any or all of the above six issues (in good condition) are invited to send them to the Publications Department, I.E.R.E., 8-9 Bedford Square, London, W.C.1; payment of 5s. per copy will be made. Please note that these are the only issues required.

# Performance Calculations for High-definition Q-band River Radar

By

Ir. J. M. G. SEPPEN †

*Presented at a meeting of the Radar and Navigational Aids Group in London on 26th February, 1964.*

**Summary:** This paper discusses vital aspects of high-definition radar sets. It specially examines radial resolving power in connection with video bandwidth. A radio frequency sensitivity-time control circuit and a new technique for checking the correct tuning of the radar set are described.

P.p.i. photographs from a Q-band river radar and a waterway supervision radar system are included.

## 1. Introduction

Considerations of economy increasingly stress the need to keep shipping traffic on rivers moving in periods when visibility is poor owing to fog, snow, rain or darkness. Radar goes a long way towards meeting this need, but it can only do so if it does not endanger traffic. The importance of this is illustrated by the fact that the countries on the Rhine have agreed on a minimum-performance specification for all radar sets to be used on the river. In Holland similar specifications are in force for all inland shipping. An essential requirement for safe navigation is high definition of the radar picture even on long ranges. Other fields where such detailed information is demanded are those of shore-based waterway supervision radar and airfield surface movement detection equipment.

## 2. Tangential Resolving Power

In river and canal navigation and also where shipping is supervised by harbour radar, the usefulness of a plan-position display depends largely on the dimensions of echoes measured at right angles to the radial sweep.

Navigation in a narrow fairway under conditions of reduced visibility is not safe unless the navigator can observe an unobstructed path extending from his vessel to a point beyond stopping distance. The situation is complicated by such factors as the direction and speed of the current and the character of the vessel (push-boat, tug or tanker). Let us illustrate this with an example.

In a fairway which is  $w$  metres wide two ships, S1 and S2, each  $b$  metres wide and at a distance of  $d$  metres from the shore are closing with each other. The question which arises is: at what maximum distance does the radar set of one vessel permit the navigator to con-

clude that there is a clear passage between the other vessel and the shore?

The answer varies with the type of radar set used. Let us examine the situation with three radar sets I, IIA and IIB; I has a 'broad' antenna beam, IIA and B a 'narrow' beam, while IIB uses a larger picture tube. All sets are supposed to comply with the regulations for Rhine navigation. Their characteristics are shown in Table 1.

**Table 1**

Parameter	I	IIA	IIB
Horizontal beamwidth between $-3$ dB points $\theta_{H(-3\text{ dB})}$	1.2°	0.6°	0.6°
Effective picture tube diameter $\Delta_T$	19 cm	19 cm	26 cm
Spot diameter $\Delta_S$	0.05 cm	0.05 cm	0.05 cm

Let us install these radar sets on board S1 and set them to a range of 1200 m, off-centred to cover the situation up to 1800 m ahead. Now we have to examine the effect of ship-to-ship distance  $D$  (see Fig. 1) on the detail with which the radar screen represents clearance  $H$  between S2 and the shore. It will be assumed that the jitter in the synchro system transmitting the aerial rotation to the display is negligible.<sup>1</sup>

Let us also assume that  $\theta_{H(-20\text{ dB})} = 2\theta_{H(-3\text{ dB})}$ , and that the reflective areas offered by S2 and the shore near S2 are so large that the effective antenna beamwidth in the case of radar set I can be equated to  $\theta_{IH(-10\text{ dB})}$  for  $H = 0$ . A further assumption is that the radiation energy of the antenna drops off linearly between the  $-3$  dB and  $-20$  dB points on each side of the beam. This can be plotted on linear graph paper with energy shown on a decibel scale on the vertical and degrees on the horizontal axis.

† Philips Telecommunicatie Industrie, Huizen, Holland.

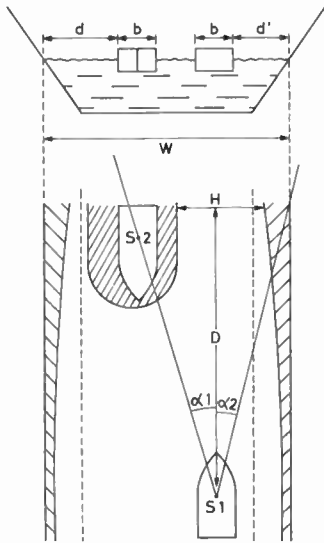


Fig. 1. Waterway situation illustrating the importance of tangential resolving power.

Because  $\theta_{IH(-3dB)} = 1.2$  deg, it follows that  $\theta_{IH(-10dB)} = 1.7$  deg. The application of the equation shown on Fig. 2 now gives curve I. This takes account of the fact that the effective  $\theta_H$  increases for lower values of  $D$  because stronger signals are received.

Curves IIA and IIB are obtained along similar lines. In spite of the higher antenna gain, the signals are weaker as they are returned by objects at a longer range. Therefore the effective  $\theta_{IH}$  for  $H = 0$  has been corrected accordingly.

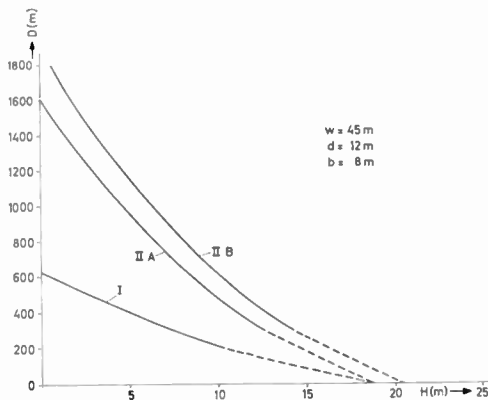


Fig. 2. Relationship between width of clear passage  $H$  and the distance  $D$  from which  $H$  is observed. Cf. Fig. 1.

$$H = w - d - b - \frac{\theta_H D}{114.6} - \frac{2R}{\Delta_T} \cdot \Delta_S$$

where  $\frac{\theta_H D}{114.6}$  is the lateral echo extension due to antennae beam-width and  $\frac{2R}{\Delta_T} \cdot \Delta_S$  represents the spot width in metres.

It is clear from Fig. 2 that S1 can observe a free passage between S2 and the shore at a distance as great as 1800 m if a type IIB radar is used, but not beyond a distance of 600 m if the radar used is of type I.

With the ever increasing volume of traffic, and particularly with the advance of round-the-clock operation using push-boats, there is a rising demand for radar sets which give a higher standard of performance than that demanded by existing specifications. It will be clear now that the tangential resolving power as worked out above is one of the principal items of a specification which is to ensure safety of navigation.

### 3. Radial Resolving Power

This is another important property which enables a navigator to see what is beyond a buoy, a bend in the river, a harbour pier, etc.

A radial resolving power of  $x$  metres means that two pin-point targets, say buoys, both located at the same bearing position but differing in range by  $x$  metres, can just be discerned as two separate objects on the radar screen. Let us now picture the situation with a large number of such pin-point targets in a line at intervals of  $x$  metres. The radar set is assumed to transmit perfectly rectangular pulses having a duration of  $T_p$  microseconds,  $T_p$  being  $\leq x/150$ . If the echoes returned by the pin-point targets are dealt with by an ideal detector, they appear as in Fig. 3.

The application of Fourier analysis to this pulse train,  $E$  representing the amplitude, gives the function:

$$s(t) = E \left\{ \frac{T_p 150}{x} + \frac{2}{\pi} \left( \sin \frac{T_p 150}{x} \pi \cdot \cos \frac{300\pi \cdot 10^6}{x} t + \frac{1}{2} \sin \frac{300 T_p \pi}{x} \cdot \cos \frac{600\pi \cdot 10^6}{x} t + \dots + \frac{1}{n} \sin \frac{n T_p 150}{x} \pi \cdot \cos \frac{n \cdot 300\pi \cdot 10^6}{x} t \right) \right\}$$

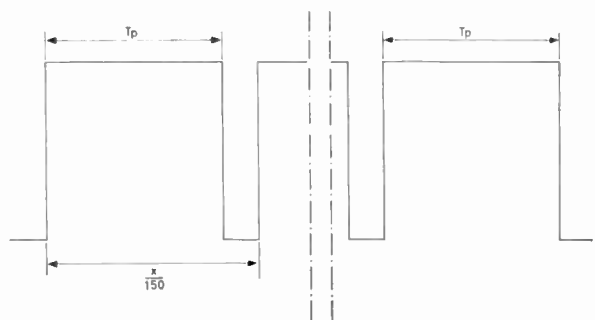


Fig. 3. Echoes of pin-point targets arranged on a single line of sight at intervals of  $x/150 \mu s$ , obtained with a pulse of  $T_p \mu s$  duration.

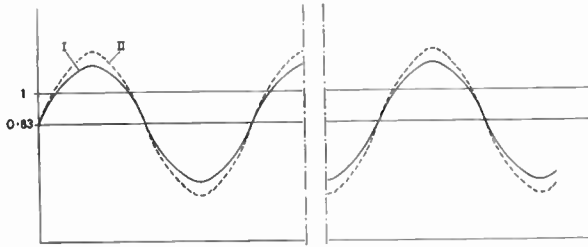


Fig. 4. D.c. and fundamental wave components obtained from a Fourier analysis of the echo pattern shown in Fig. 3.

In this series we recognize the d.c. component  $E(T_p 150/x)$ , the fundamental wave of frequency  $(150/x) \times 10^6$ , the 1st harmonic  $(300/x) \times 10^6$ , etc. In the practical calculation of the response of a video amplifier one does not proceed beyond the fundamental, whose amplitude is  $2/\pi E \sin T_p 150/x \pi$ .

If a value of, say, 5/6 is taken for  $T_p 150/x$ , curve I of Fig. 4 is obtained.

Comparing this with the original signal, we find distinct differences between the signal and no-signal states. When this signal is presented on a picture tube, however, the odds are that these differences are really no longer discernible, particularly if the signal threshold is low. At any rate it is useful to accentuate the differences between maximum and minimum. One way of achieving this is to give the  $(150/x) \times 10^6$  frequency component additional gain by means of a response curve as shown in Fig. 5. Dash curve II in Fig. 4 shows how the differences between maximum and minimum are brought out by the use of this response curve. The criterion of good resolution,

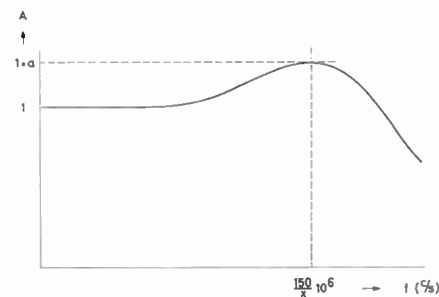


Fig. 5. Response curve of a peaked amplifier.

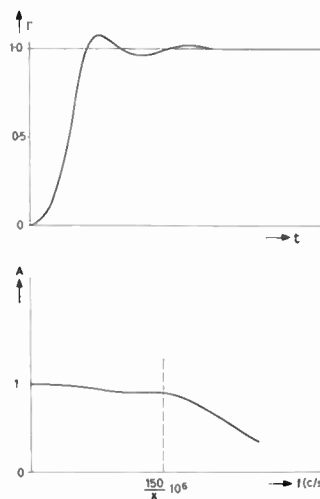


Fig. 7. Video and unit step response curves of VAI.

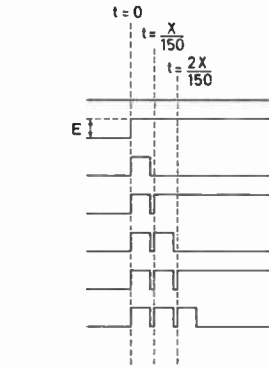


Fig. 6. Unit step responses.

for minima of II equal to or less than 0, or for the given values of  $x$  and  $T_p$ , could be put in the following terms:

$$(1+a) \frac{2}{\pi} \sin \frac{T_p 150}{x} \pi \geq \frac{T_p 150}{x}$$

The theory given here, as far as it concerns the amplitude of the fundamental wave, extends without loss of validity to the case of single targets. This has been verified by measuring the unit-step response of a few video amplifiers. By unit-step or transient response is understood the behaviour of the output signal of a video amplifier whose input circuit receives an instant voltage change  $E$  at time  $t = 0$ .

Once this type of response has been evaluated, we may proceed as indicated in Fig. 6 and apply this method to amplifiers VAI and VAII. Figure 7 illustrates the video response and unit-step response of VAI; Fig. 8 shows these responses for VAII.<sup>2</sup>

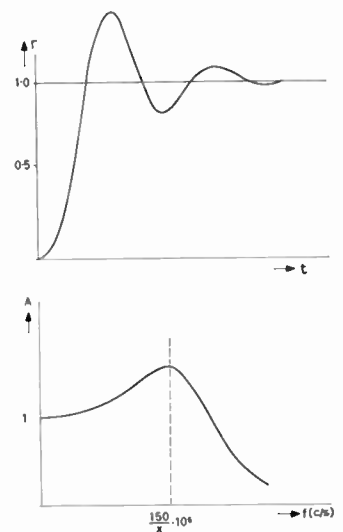


Fig. 8. Video and unit step response curves of VAII.

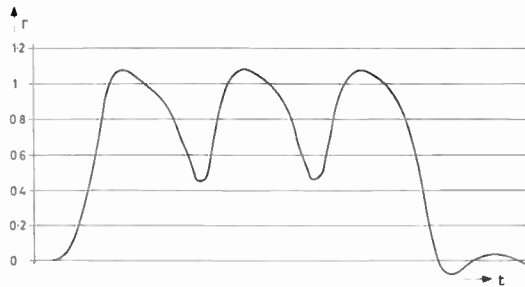


Fig. 9. Graphic evaluation of response of VAI to signal pattern shown in Fig. 6.

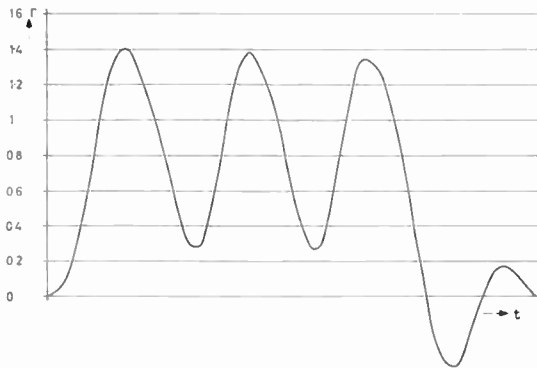


Fig. 10. Graphic evaluation of response of VAI1 to signal pattern shown in Fig. 6.

The result of applying the results given in Fig. 6 to VAI is shown in Fig. 9, whilst Fig. 10 gives the corresponding result for VAI1; in each case it was assumed that  $T_p 150/x = 5/6$ . It can be inferred that the amplitude of the fundamental wave of VAI and VAI1 is substantially equal to that obtained by multiplying the amplitude worked out according to the Fourier series by the amplification factor derived from the frequency response curve. This principle may, therefore, be applied to a radar set provided other elements which govern bandwidth are not overlooked.

Incidentally, the properties of the picture tube itself ( $2R/\Delta_T \cdot \Delta_S$ ) have to be taken into account in designing a radar set with a certain radial resolving power.

A means of improving the radial resolving power whilst maintaining flat video response is the use of a peaker or differentiator, which gives the higher frequencies more emphasis and thus produces the same effect as that accomplished in VAI1. This method, however, impairs the presentation of 'long' echoes.

#### 4. Some Circuits used in High-definition Radar

##### 4.1. Checking Frequency with a Curve on the Display Screen

A portion of the signal energy is taken from the video amplifier and applied to a low-frequency amplifier tuned to the pulse repetition frequency of the radar set. If this amplifier is made to operate as an integrator, its output provides a measure for the number of echoes picked up. The output signal, a rectified alternating voltage  $V_{\omega}$ , is fed to the time-base generator. The circuit is so arranged that the sweep stops when the sawtooth reaches the level of  $V_{\omega}$ . (See Fig. 11.) If this facility is introduced on a working radar set, the screen displays an endless trace formed by successive time-base stop pulses. In sectors where many echoes are picked up the sweep will be stopped later than in sectors of low echo density. Thus a bizarre outline is obtained on the screen as shown in Fig. 12 (trace I). If re-tuning the local oscillator causes the trace to spread to the position of trace II, it is evident that more echoes are received and the radar is tuned closer to its optimum frequency. When trace II is being written, trace I persists for a while so that it is easy to see whether the new trace is inside or outside the old one. When the trace encompasses the largest area, tuning is optimum.

During the frequency adjustment the radar image continues to be written normally inside the trace. A well-designed circuit ensures that the tuning trace

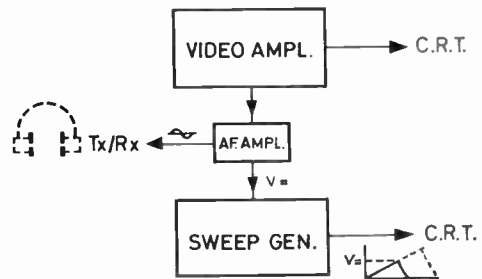


Fig. 11. Block diagram of circuit required to display a tuning trace on the display screen.

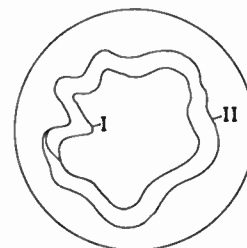


Fig. 12. Tuning trace patterns displayed in different frequency settings of the radar set.

keeps at least half a radius away from the deflection centre in order that echoes in this region are not obscured. No steps have to be taken to keep the trace stationary when the display unit is switched through its various range settings.

The circuit described offers an additional advantage. The alternating voltage output of the i.f. amplifier may be fed to the transmitter-receiver unit where it can be picked up with a pair of headphones. While the antenna is scanning, a tone of the radar pulse repetition frequency is heard, varying in intensity with the 'excursion' of the trace. (See I in Fig. 12.)

When a new magnetron has been fitted, the headphones will not, as a rule, give a tone immediately. The local oscillator can now be re-tuned until the tone of varying intensity is strongest; this indicates operation at the optimum frequency. This method is convenient in practice because it is aural and makes no demand on the serviceman's eyes or hands.

#### 4.2. R.F. Sensitivity-Time Control

Figure 13 depicts the mixer stage of a radar set. The echoes and the local oscillator signal are applied to left-hand extremity 1 of rectangular-section waveguide 2. Plunger 3 terminates the right-hand extremity. The waveguide incorporates mixer crystal 4. A phasing control is fitted between the crystal and the plunger. It contains ferrite rod 5 which is polarized axially by a variable current through a winding 6 which surrounds the waveguide. If the waveguide wall under the winding were conductive, it would behave as a shorted turn and produce eddy currents which would prohibit rapid changes in the magnetic field in the waveguide. For this reason a portion of the wall 7 is of insulating material having inside it a thin film of metal which acts as a screen. One end of winding 6 is connected via resistor 8 to negative voltage source  $V$ , the other is earthed via variable resistor 9. The latter resistor is shunted by the emitter-to-collector path of transistor 10. The effective electrical length of waveguide between mixer crystal 4 and plunger 3 depends on the polarization of ferrite rod 5 and hence on the current through winding 6. Now this current may be passed through the winding in such a manner that the length of the electrical path is an even multiple of a quarter wavelength during and briefly after each radar pulse. The mixer crystal is then located in a null or node of the electrical field, both for echo signals and for the local-oscillator signal, and cannot deliver any appreciable i.f. energy to output terminals 11 and 12. During the remainder of the interval between radar pulses the current through winding 6 has such a value that the electrical length between crystal 4 and plunger 3 is an odd multiple of a quarter wavelength. Being in an antinode, the crystal now delivers full output. The

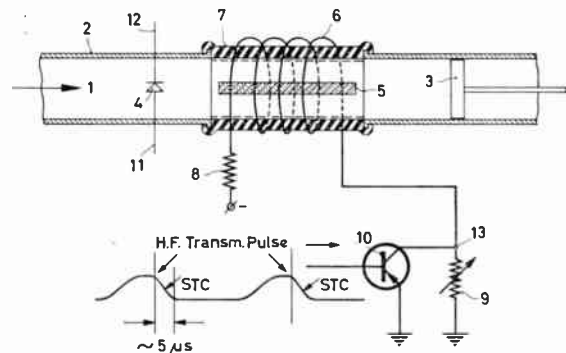


Fig. 13. R.f. sensitivity-time control circuit.

transfer loss of the crystal is 0.2 dB when in an antinode and of the order of 60 dB when in a node. As regards the adjustment of the system, plunger 3 should be set for optimum reception while transistor 10 is conductive; variable resistor 9 is then practically shorted out. When the transistor is cut off, the transfer loss can be adjusted with the variable resistor, which is located on the control panel of the display unit. The advantage of the r.f. sensitivity-time control is that it effectively prevents saturation of the mixer stage and the first stages of the i.f. amplifier.

### 5. Practical Results obtained with High-definition Equipment

#### 5.1. Tangential Resolving Power

The circuits described in Section 4 are employed in a transistorized river radar (Philips type 8GR 260) first produced in 1962.

To achieve the high tangential resolving power whose importance was stressed in Section 2, without having to resort to the use of a large antenna, a frequency as high as 33 Gc/s was adopted with a horizontal beamwidth of 0.6 deg between  $-3$  dB points. The reduction of antenna size is essential because river vessels rarely have space to spare. In this respect the use of transistors is another step forward. Other advantages offered by transistorization are greater reliability and low power consumption, which are marked assets on river vessels. Figure 14 shows how the display of the 9 mm radar is cluttered up by a rain-shower when the r.f.-s.t.c. is switched off; Fig. 15 illustrates the same display with the s.t.c. circuit in action. It may be of interest to know that the operative range of this circuit extends to 900 m.

Figure 15 shows residual rain clutter near the centre. This is due to the shape of the s.t.c. curve, which has to effect receiver regulation in the region corresponding to the fourth power of range  $R$  as given in the radar range formula. Rain clutter, however, has only a second-power relationship to  $R$ . A similar residue

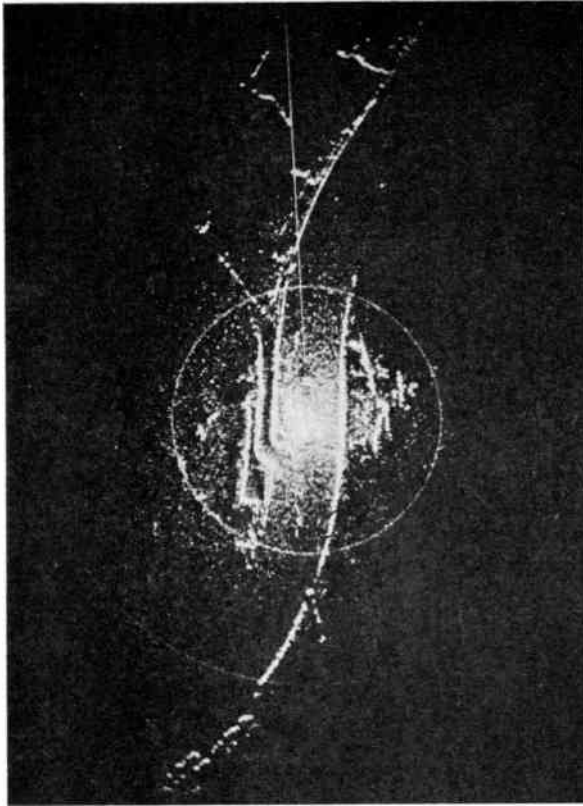


Fig. 14. Picture obtained with river radar set (type 8GR 260) in a rain shower with the r.f.-s.t.c. circuit switched off. Precipitation rate approx. 7 mm/h.

of rain clutter is encountered in practice with the use of circular polarization. The 8GR 260 uses a double-cheese antenna because a duplexer system for 8 mm waves is too costly and the t/r cells used in it are comparatively short-lived, thus defeating the design objective of highest possible mean-time-between-failures. The need for a high m.t.b.f. has also prompted the development of a solid-state modulator for the magnetron, producing an r.f. pulse of about 35 ns duration. As for the noise figure, components now available permit it to be reduced to some 12 dB; in the 8GR 260 it is a few decibels higher. Generally speaking the price of r.f. components for a millimetric radar is higher than for a centimetric radar, partly because closer tolerances have to be realized in production. On the other hand the antenna drive equipment is less expensive because the antenna is small and of light weight and presents a small area to the wind, so its power requirements are low. Admittedly, a millimetric radar is more sensitive to rain than a radar working in the centimetre-band, but on waterways, where a range of a few thousand metres is all that is needed, the loss of range coverage caused by rain plays only a minor role.

### 5.2. Radial Resolving Power

The 8GR 260 radar uses a video amplifier whose *a*-value (Fig. 5) is about 0.2 at 19 Mc/s. The radar pulse has a duration of 35 nanoseconds, which is accomplished by the use of a magnetic modulator.

It may be shown that these values permit good target discrimination at  $x = 150/19 = 8$  m. Applying eqn. (2) of Section 3 as a criterion:

$$(1+a) \frac{2}{\pi} \sin \frac{T_p 150}{x} \pi \geq \frac{T_p 150}{x}$$

Thus the radar comes within the limits laid down for good radial definition. The lowest range scale of the display unit is 600 m, the effective diameter of the cathode-ray tube is 26 cm (12 in. model) and each spot has an approximate diameter of 0.5 mm, so a spot represents a length of

$$\frac{2R}{\Delta_T} \cdot \Delta_s = \frac{1200}{260} \times 0.5 = 2.3 \text{ m}$$

Theory suggests that on the basis of this a radial resolving power of about 8 m is to be expected, and this is confirmed by practice. Figure 16 shows the 8 mm waterway radar on board a French push-boat.

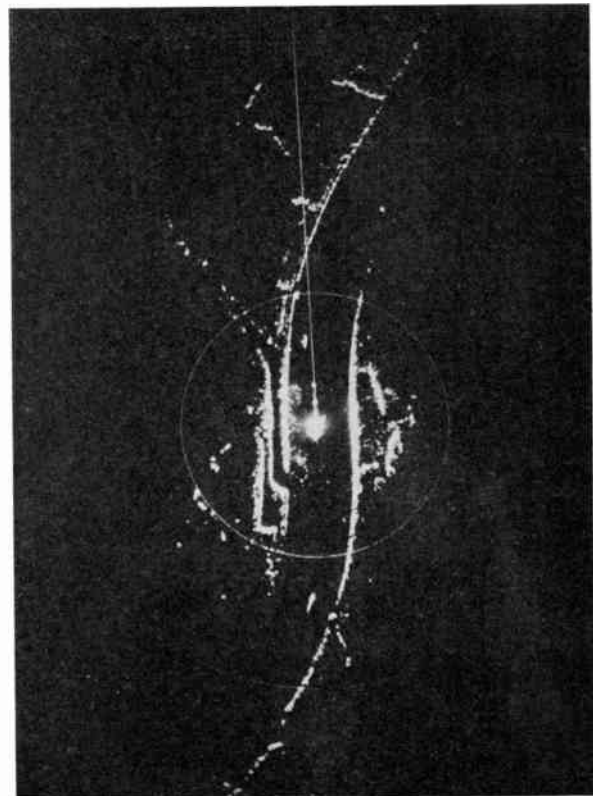


Fig. 15. The effect of the r.f.-s.t.c. circuit on the picture shown in Fig. 14.



Fig. 16. An 8 GR 260 set on board the push-boat *Sûre* (Communauté de la Navigation Française Rhénane).

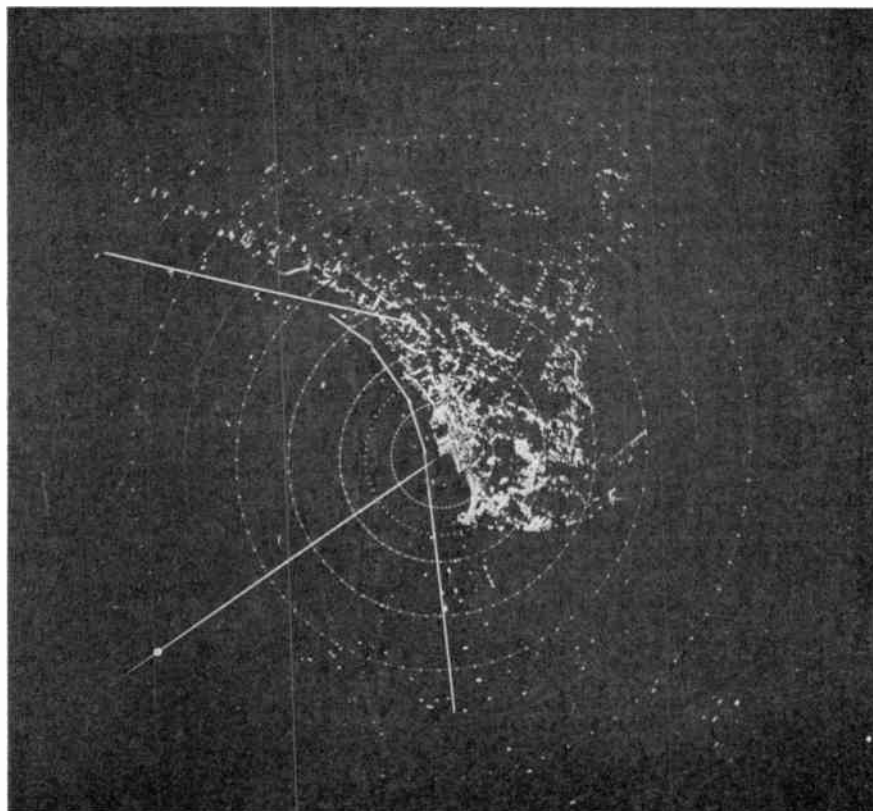


Fig. 17. Radar view of Cuxhaven area (Elbe estuary).

### 5.3. Narrow Beamwidth Antennae

Waterway supervision radar systems are not always strictly shore-based like those in use at IJmuiden (Amsterdam), along the Nieuwe Waterweg to Rotterdam, and along the Gironde (France). It may happen that supervision equipment is installed on lighthouses out at sea. Typical of this is the Elbe and Weser surveillance system<sup>3,4</sup> in which land-based operational centres handle information collected via radio links from various radar stations.

The topographical situation did not offer many sites where a radar unit could obtain a close-up view of the waterway, so stringent requirements had to be set for horizontal beamwidth in order that piloted vessels could be supplied with sufficiently accurate information. To meet these requirements the Nederlands Radar Proefstation (Netherlands Radar Research Establishment) developed slotted waveguide aerials with  $\theta_{H(-3\text{dB})}$  values which were occasionally as small as 0.4 deg (IJmuiden radar system). The use of slotted radiators was dictated by the fact that many of the antennae had to be installed on lighthouses. Such radiators have little weight and present only a small surface area to the wind. If a large reflector were used, the varying wind forces would set the optical system of the lighthouse vibrating, which would have an adverse effect on the light beam at long distances.

Figure 17 gives a radar picture of Cuxhaven on the Elbe. Full range is 16 km, and the interval between the calibrating circles is 2 km. In order to achieve a bearing accuracy of 0.4 deg, azimuth markers are written at intervals of 5 deg on ranges (in Fig. 17) of 2, 3, 4, 6, 8, 12 and 16 km. They are produced by a magnetic pulse generator fitted in the antenna control gear of the radar station. The cursor shown in Fig. 17 originates at this station from the point representing the radar site. A small circular range marker can be moved any desired distance along it. A north reference is provided by a row of dots. The fairway near the station is marked out with five 'lines of light'.

### 6. Conclusion

A significant reason for the increase of traffic density on inland waterways is the ever growing demand for efficient cargo handling. Means for satisfying this demand are push-boats and tankers of greater capacity in round-the-clock operation. In

order to ensure safe navigation with these vessels under poor visibility conditions the need for radar sets with better definition becomes apparent. To realize this better definition and to avoid large antennae a transistorized river radar has been developed which operates at 33 Gc/s. A criterion based on the Fourier analysis of a pulse train is formulated to assess radial resolving power. It is verified graphically on a small number of pulses with two video amplifiers whose unit-step responses are known. A radio-frequency sensitivity-time control circuit is used to overcome serious clutter.

A novel method enables a radar set to be tuned whilst retaining a picture of near-by echoes. A trace which outlines the inner part of the radar picture is adjusted for maximum enclosed area. The method is simple and easy to interpret.

A photograph giving a radar view of the Cuxhaven waterway area shows the visual aids which enable an operator in a waterway supervision radar system to supply ships' pilots rapidly with accurate navigational information.

### 7. Acknowledgment

I wish to thank Mr. C. le Comte of the Radar Laboratory of Philips Telecommunicatie Industrie for his valuable observations during the preparation of this paper.

### 8. References

1. R. B. R. Braun and P. Dick, "Verfahren zur Berechnung der Grösse eines Radarechos auf einer Radarbildröhre" *Schiffahrt, Schiffbau, Hafen*, 99, No. 11, pp. 1127-31, 1962.
2. Dr. Ir. A. van Weel, "Invloed van Amplitude en fase distortie op Sprongkarakteristieken van Electricische Neturerken. Deel III". Philips Research Report No. 2927.
3. O. Hilke, J. M. G. Seppen and W. J. Verhoeff, "The Elbe-Weser shore-based radar system", *Philips Telecommun. Rev.*, 22, pp. 124-38, May 1961.
4. C. le Comte, "Data transmission and display units for waterway supervision radar systems", *Philips Telecommun. Rev.*, 22, pp. 141-61, July 1961.

*Manuscript first received by the Institution on 3rd February 1964 and in revised form on 27th October 1964. (Paper No. 977/RNA41)*

© The Institution of Electronic and Radio Engineers, 1965

# Pulse Response of Delay Lines

## I. Constant-*k* Delay Lines

By

M. AVINOR, Ph.D.  
(Associate Member)†

AND

Y. PARTOM, M.Sc. †

**Summary:** Exact numerical solutions have been obtained for unit step response of constant-*k* delay lines. Results are given for finite lines terminated at one end and at both ends with a resistance equal to the characteristic impedance of the line, and for the voltage output tapped off an infinite line after a finite number of sections.

### 1. Introduction

The behaviour of delay lines has, until recently, been investigated mainly through the properties of frequency response and phase shift.<sup>1, 2</sup> With the advent of pulse and digital techniques the pulse response of delay lines became important. However, the solution of the mesh equations of multiple-section delay line with lumped constants is very tedious. Until now resort has been made to experimental techniques<sup>3</sup> or to calculations of a single section and simple extrapolation to composite lines.<sup>4</sup>

The tedium of numerical work can be considerably relieved by using a fast electronic computer and thus exact numerical solutions may be obtained. The only limit on the accuracy of the results is accumulation of rounding-off errors.

In this paper we give the results obtained for the response of a constant-*k* delay line to unit-step excitation. Unit-step response is usually the most interesting feature of delay lines used in pulse circuits. Calculations were carried out on a Philco 2000 (TRANSAC) computer operating in floating point arithmetic with 10 decimal significant figures. We have investigated the response of an infinite line and of finite lines terminated either on one side or on both sides with a resistance equal to the characteristic impedance of the line.

### 2. Line of Infinite Length

When a unit-step voltage, from a generator of zero internal impedance, is applied to an infinite line a solution in closed form, in terms of Bessel functions, may be obtained.<sup>5</sup> Let the first stage of the line have the form depicted in Fig. 1. Since the line is infinite in length the impedance 'looking' into the output of the section is equal to the input impedance and the Laplace

transform of the line impedance turns out to be

$$\mathcal{L}(z) = L \cdot \sqrt{s^2 + \alpha^2} \quad \dots\dots(1)$$

where

$$\alpha = \sqrt{\frac{2}{LC}}$$

After infinite time, when the transients die away, the input impedance becomes  $(2L/C)^{\frac{1}{2}}$  and has dimensions of pure resistance. Using eqn. (1), the solution of the mesh for the Laplace transform of the output voltage yields

$$\mathcal{L}\left(\frac{E_1}{E_0}\right) = \frac{1}{s} \cdot \frac{(\sqrt{s^2 + \alpha^2} - s)^2}{\alpha^2} \quad \dots\dots(2)$$

The transform of the output voltage tapped off after *n* sections is similarly

$$\mathcal{L}\left(\frac{E_n}{E_0}\right) = \frac{1}{s} \cdot \frac{(\sqrt{s^2 + \alpha^2} - s)^{2n}}{\alpha^{2n}} \quad \dots\dots(3)$$

The inverse of the numerator in eqn. (3) is known<sup>5</sup> and is given by

$$\mathcal{L}^{-1}(\sqrt{s^2 + \alpha^2} - s)^{2n} = \frac{2n \cdot \alpha^{2n}}{t} J_{2n}(\alpha t) \quad \dots\dots(4)$$

where  $J_{2n}(xt)$  is the ordinary Bessel function of order  $2n$ .

By the convolution theorem the inverse of eqn. (3) is obtained in the form:

$$\frac{E_n}{E_0} = 2n \int_0^{\alpha t} \frac{J_{2n}(\tau)}{\tau} d\tau \quad \dots\dots(5)$$

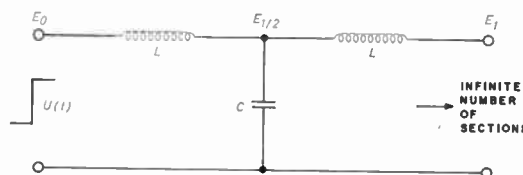


Fig. 1. First section of a constant *k* delay line with lumped constants.

† Scientific Department, Ministry of Defense, Israel.

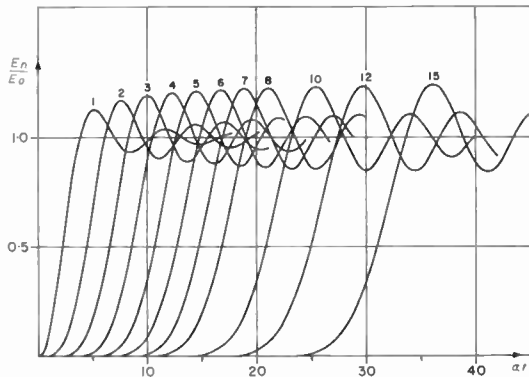


Fig. 2. Voltage output of an infinite delay line after various numbers of sections. The input is a unit step.

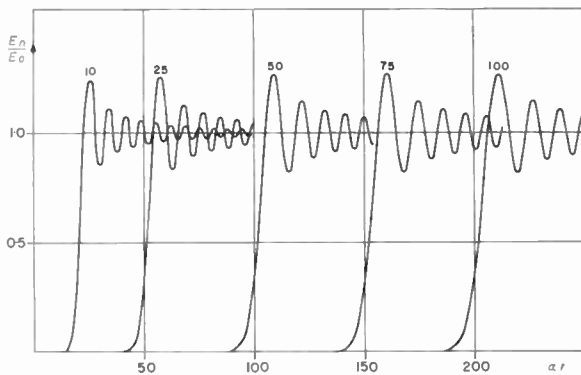


Fig. 3. Voltage output of an infinite delay line after various numbers of sections. The input is a unit step.

A subroutine for calculating the value of Bessel functions was available in the library of the computer and the right-hand side of eqn. (5) was evaluated by numerical integration for various values of  $n$  and  $t$ . To make the curves universal the time axis is measured in dimensionless units of  $\alpha t$ . The results are shown in Figs. 2 and 3. The delay time (rise to 50% of final value) after  $n$  sections is found to exceed the value of  $\alpha t = 2n$  (i.e.  $t = n\sqrt{2LC}$ ). However, the relative deviation decreases as the number of sections increases. The excess delay time (over  $\alpha t = 2n$ ) as a function of the number of sections in the line is shown in Fig. 4.

The increase in rise-time (10% to 90% of final value) is shown in Fig. 5. It may be shown that the rise time deteriorates in the beginning more slowly than  $n^{1/3}$ .

The results were checked in an independent way by obtaining the inverse of eqn. (3) in a different form. Thus if the square in eqn. (2) is expanded we obtain

$$\mathcal{L}\left(\frac{E_1}{E_0}\right) = \frac{1}{s} - \frac{2}{\alpha^2}(\sqrt{s^2 + \alpha^2} - s) \quad \dots\dots(6)$$

and inversion gives directly the output voltage after one section as

$$\frac{E_1}{E_0} = 1 - \frac{2}{\alpha t} J_1(\alpha t) \quad \dots\dots(7)$$

This scheme can be extended further to yield

$$\frac{E_n}{E_0} = 1 - \frac{2}{\alpha t} [J_1(\alpha t) + 3J_3(\alpha t) + \dots + (2n-1)J_{2n-1}(\alpha t)] \quad \dots\dots(8)$$

The simplicity of eqn. (8) makes it well adapted for hand calculation with the aid of tables.

Comparison of the results of using eqn. (8) with those from eqn. (5) showed good agreement to five significant figures or more. However, eqn. (8) was found more useful because it gave directly the desired value at any given point with no dependence on the results of all previous points, as required by the integral of eqn. (5). This feature was found convenient in calculating the response of lines with a large number of sections.

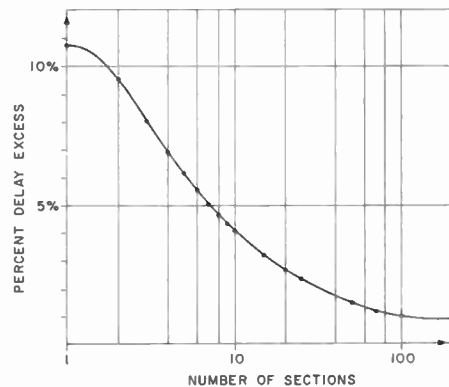


Fig. 4. Excess of delay time over  $\alpha t = 2n$  (i.e.  $t = n\sqrt{2LC}$ ) after  $n$  sections. Infinite delay line.

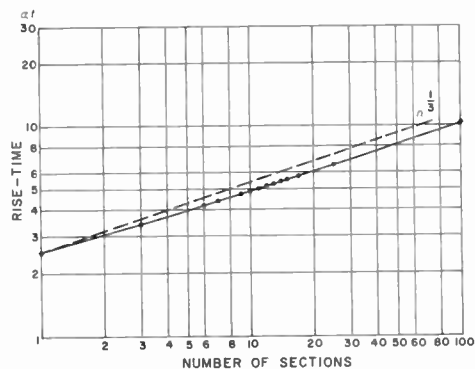


Fig. 5. Rise-time of an infinite delay line after variable number of sections.

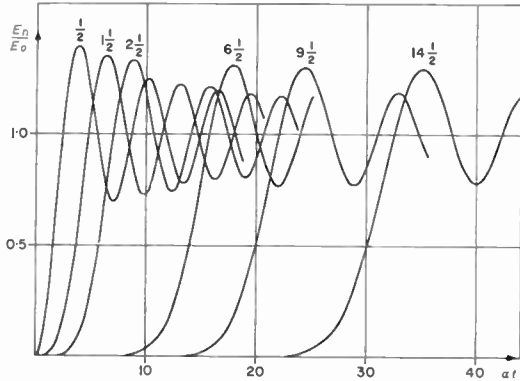


Fig. 6. Voltage output of an infinite delay line after various odd numbers of half sections. The input is a unit step.

Equation (5) shows that for each additional section the order of the Bessel function increases by two. This observation might suggest that the response after an odd number of half sections would be given by the same equation with functions of odd order. This, however, turns out not to be the case. The transform of the response after an odd number of half sections may be obtained by using eqn. (3) at the input and output of the *n*th section and calculating the voltage on the capacitor. The result is

$$\mathcal{L}\left(\frac{E_{n+\frac{1}{2}}}{E_0}\right) = \frac{1}{s \cdot \alpha^{2n}} \cdot \frac{(\sqrt{s^2 + \alpha^2} - s)^{2n+1}}{\sqrt{s^2 + \alpha^2}} \dots\dots(9)$$

and its inversion yields

$$\frac{E_{n+\frac{1}{2}}}{E_0} = \int_0^{\alpha t} J_{2n+1}(\tau) \cdot d\tau = 1 - [J_0(\alpha t) + 2J_2(\alpha t) + 2J_4(\alpha t) + \dots + 2J_{2n}(\alpha t)] \dots\dots(10)$$

The right-hand side of eqn. (10) is obtained, as before, by successive expansion of a second power factor in eqn. (9) before inversion.

The response of a delay line after several odd numbers of half sections is given in Fig. 6. These curves have an interesting mathematical property. Each curve intersects the curves of the adjacent even number curves (i.e. the curves of delay lines with one half section more and one half section less) at *all* their maxima and minima. The first overshoot decreases as one advances along the line and becomes 27.46% after 9999½ sections. For an even number of half sections the overshoot increases steadily as the number of sections increases (Fig. 7) and reaches 27.39% after 10 000 sections. The first overshoot after one half section is 40.21%, indicating that the first capacitor should be rated to withstand this excess voltage.

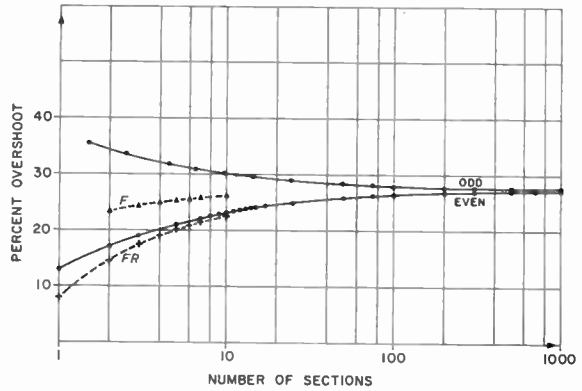


Fig. 7. The first overshoot of an infinite delay line for variable even and odd numbers of half sections. Curve F shows the overshoot of a finite line terminated only at one end and Curve FR shows the overshoot of a finite line terminated at both ends, as a function of the number of sections.

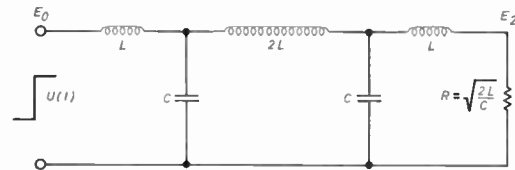


Fig. 8. Diagram of a two-section constant *k* delay line terminated with a resistance equal to the characteristic impedance of the line.

### 3. Line of Finite Length

Evaluation of the determinants obtained in solving the Laplace transform of the mesh equations quickly becomes quite involved. The polynomial in the denominator of the transformed voltage equation is of third power for a single section and increases by two for each additional section. For a two-section line, as in Fig. 8, the determinant is

$$PA_3 = \begin{vmatrix} A & -1/Cs & 0 \\ -1/Cs & F & -1/Cs \\ 0 & -1/Cs & B \end{vmatrix}$$

where  $A = sL + 1/Cs$ ;  $F = 2(sL + 1/Cs)$ ;  $B = sL + R + 1/Cs$  and  $R = (2L/C)^{\frac{1}{2}}$ , and the transform of the output voltage takes the final form:

$$\mathcal{L}\left(\frac{E_2}{E_0}\right) = \frac{1}{s(8s^5 + 8s^4 + 12s^3 + 8s^2 + 4s + 1)}$$

This third-order determinant and all the higher ones have some common features. The main diagonal is occupied only by the terms *F* except the first and last entries. The last is always *B*. The first entry is *A* when the pulse generator has zero internal impedance, or *B* if the internal impedance is *R*. The two adjacent diagonals contain only the terms  $-1/Cs$  and all the other entries are zero. These features enable us to

derive the polynomial of  $s$ , obtained by expanding the determinant, in a systematic way, convenient for computer programming.

Let us define the subsidiary determinant  $PF_m$  as follows: The determinant contains the entries  $F$  on the main diagonal  $m-1$  times, and the last entry is  $B$ . The two adjacent diagonals contain the terms  $-1/Cs$  and all the other entries are zero. Thus the fourth determinant is:

$$PF_4 = \begin{vmatrix} F & -1/Cs & 0 & 0 \\ -1/Cs & F & -1/Cs & 0 \\ 0 & -1/Cs & F & -1/Cs \\ 0 & 0 & -1/Cs & B \end{vmatrix}$$

It is easily verified that beyond  $m \geq 2$  the following recursion formula holds:

$$PF_m = F.PF_{m-1} - PF_{m-2} \cdot 1/(Cs)^2 \dots\dots(11)$$

By inserting convenient numbers for  $R$ ,  $L$  and  $C$  (e.g. 2, 2 and 1 respectively), starting with  $PF_1 = B$  and  $PF_0 = 1$ , and using eqn. (11) a series of polynomials in  $s$  is obtained as far as needed.

Now if  $PA_m$  and  $PB_m$  are the polynomials in  $s$  for a generator impedance zero and  $R$  respectively, then:

$$PA_m = A.PF_{m-1} - PF_{m-2}/(Cs)^2 \dots\dots(12)$$

$$PB_m = B.PF_{m-1} - PF_{m-2}/(Cs)^2 \dots\dots(13)$$

For a delay line of  $n$  sections these equations hold with  $m = n+1$ . On insertion in the mesh equation, the Laplace transforms of the output voltage take, respectively, the form:

$$\mathcal{L}(E_n/E_0) = 1/s \cdot A_n \dots\dots(14)$$

$$\mathcal{L}(E_n/E_0) = 1/s \cdot B_n \dots\dots(15)$$

where

$$A_n = PA_{n+1} \cdot s^{n+1}/2 \quad \text{and} \quad B_n = PB_{n+1} \cdot s^{n+1}/2$$

$A_n$  and  $B_n$  are the required polynomials for a delay line with  $n$  sections. These polynomials are conveniently obtained by using recursion formulas (11), (12) and (13). The coefficients of the first few polynomials are given in Table 1.

Solution and inversion of eqns. (14) and (15) were approached in two different ways. In the first way the polynomials were factorized and inversion was carried out by summation of residues.

It should be observed that the polynomials are of odd power and one real root is negative. The root is  $-1$  for a single section terminated on both sides with resistances and increases towards zero as the number of sections increases. The real root was isolated by the Newton-Raphson method. All the other roots are complex and distinct. The reduced polynomial was factorized into second degree equations using the Bairstow process. The trial factor  $x^2 + px + q$  was

**Table 1**

Coefficients of the network polynomials in  $s$  (eqns. (14) and (15)) for finite delay lines with  $n$  sections

$n$	Power of $s$	$A_n$	$B_n$
1	0	1	2
	1	2	4
	2	2	4
	3	2	2
2	0	1	2
	1	4	8
	2	8	16
	3	12	20
	4	8	16
3	0	1	2
	1	6	12
	2	18	36
	3	38	70
	4	48	96
	5	64	96
	6	32	64
4	0	1	2
	1	8	16
	2	32	64
	3	88	168
	4	160	320
	5	272	464
	6	256	512
	7	320	448
	8	128	256
5	0	1	2
	1	10	20
	2	50	100
	3	170	330
	4	400	800
	5	832	1504
	6	1120	2240
	7	1696	2720
	8	1280	2560
	9	1536	2048
	10	512	1024
11	512	512	

**Table 2**

Values of the constants in eqn. (16) for delay lines terminated on one end only

<i>n</i>	<i>K</i>	<i>L</i>	<i>M</i>	<i>X</i>	<i>Y</i>	<i>W</i>
1	- 0.801223	- 0.198776	0.643692	- 0.647799	- 0.176101	0.860717
2	- 0.982304	- 0.188217 0.170522	1.051539 - 0.108721	- 0.414567	- 0.259020 - 0.033696	0.525075 0.937260
3	- 1.143755	- 0.101317 0.328700 - 0.083627	1.347947 - 0.231471 0.031042	- 0.316395	- 0.236474 - 0.094546 - 0.010783	0.367889 0.735741 0.968696
4	- 1.290648	- 0.004677 0.426135 - 0.178929 0.048119	1.599001 - 0.343749 0.067720 - 0.012780	- 0.259953	- 0.209459 - 0.114182 - 0.041715 - 0.004668	0.282696 0.585637 0.840171 0.981674
5	- 1.426875	0.093602 0.501581 - 0.245492 0.108238 - 0.031055	1.822613 - 0.453440 0.101050 - 0.028237 0.006456	- 0.222577	- 0.186855 - 0.117614 - 0.060121 - 0.021703 - 0.002418	0.229696 0.482417 0.718165 0.894489 0.988055

**Table 3**

Values of the constants in eqn. (16) for delay lines terminated on both ends.  
Normalized to give unity final output

<i>n</i>	<i>K</i>	<i>L</i>	<i>M</i>	<i>X</i>	<i>Y</i>	<i>W</i>
1	- 1.000000	0.000000	1.154700	- 1.000000	- 0.500000	0.866025
2	- 1.473680	0.000000 0.473680	2.000000 - 0.149605	- 0.647799	- 0.500000 - 0.176101	0.500000 0.860717
3	- 2.000000	0.171041 1.000000 - 0.171041	2.897327 - 0.377964 - 0.069389	- 0.500000	- 0.428633 - 0.250000 - 0.071367	0.345733 0.661438 0.905146
4	- 2.565018	0.434574 1.505305 - 0.434574 0.059713	3.840884 - 0.721008 - 0.159116 0.053387	- 0.414567	- 0.371467 - 0.259020 - 0.128533 - 0.033696	0.264543 0.525075 0.764543 0.937260
5	- 3.163277	0.768488 2.000000 - 0.743751 0.163277 - 0.024737	4.824964 - 1.154700 - 0.219319 0.143569 - 0.032558	- 0.357613	- 0.328157 - 0.250000 - 0.153699 - 0.071194 - 0.018144	0.214696 0.433013 0.648265 0.833074 0.956712

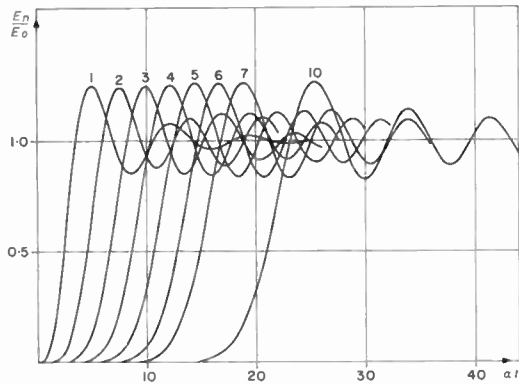


Fig. 9. Voltage output of a finite delay line terminated only at one end for various numbers of sections. Input is a unit step.

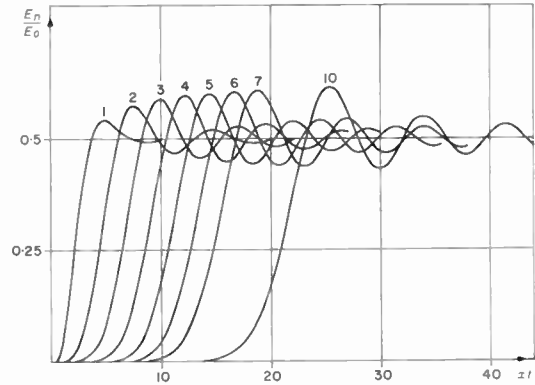


Fig. 10. Voltage output of a finite delay line terminated at both ends for various numbers of sections. Input is a unit step.

found always to converge to a solution by starting with  $p = q = 0$ . The method of Lin was also successful for factorizing these polynomials. The second degree equations yielded pairs of complex roots. The real part is always negative (damping exponent) and the imaginary part gives the frequency. Summation of the residues at the poles yields the solution as a sum of a finite trigonometric series

$$E_n/E_0 = 1 + K \cdot \exp X \cdot \alpha t + \sum_{j=1}^n \exp Y_j \cdot \alpha t (L_j \cdot \cos W_j \cdot \alpha t - M_j \cdot \sin W_j \cdot \alpha t) \quad j = 1, 2, \dots, n \dots (16)$$

The coefficients of the first few equations are given in Tables 2 and 3. The results are shown graphically in Figs. 9 and 10.

In the second way the denominator of eqns. (14) and (15) was divided into the numerator for obtaining an infinite series in powers of  $1/s$ . The result was inverted term by term to yield a series in ascending powers of time (in  $\alpha t$  units). In order to reduce the rate of rounding-off error accumulation, the operations of advancing from one term of the series to the next were carried out partly by double precision calculations. However, rounding-off error accumulation limited the useful number of terms in the series to less than fifty. Results were found to be accurate for small values of  $\alpha t$ . At values of  $\alpha t$  of about 20 the results were still good to five significant figures but beyond that accuracy deteriorated rapidly. Thus this

method served as a check on the results of the trigonometric computations up to about 10 sections.

The response of the finite lines approaches the response of the infinite line as the number of sections increases. Beyond ten sections the response of a delay line terminated on both sides is practically the same as the response of an infinite line. Finite delay lines terminated on one side only approach the response of the infinite line more slowly, as can be seen in Fig. 7.

#### 4. Acknowledgment

The authors wish to thank Mr. G. Frieder and Mrs. N. Nizan of the Computing Group for their help in the programming for the computer.

#### 5. References

1. M. H. Hebb, C. W. Horton and F. B. Jones, "On the design of networks for constant time delay", *J. Appl. Phys.*, **20**, p. 616, 1949.
2. L. Weinberg, "Network Analysis and Synthesis" (McGraw-Hill, New York, 1962).
3. W. C. Elmore and M. Sands, "Electronics" (McGraw-Hill, New York, 1949).
4. J. Millman and H. Taub, "Pulse and Digital Circuits" (McGraw-Hill, New York, 1956).
5. J. Mikusinski, "Operational Calculus" (Pergamon Press, London, 1959).

Manuscript first received by the Institution on 20th January 1964 and in final form on 17th September 1964. (Paper No. 978.)

© The Institution of Electronic and Radio Engineers, 1965

# A Radar Receiving Array with I.F. Multiple-beam Forming Matrix

By

J. SALOMON,†

S. PICHAFFROY †

AND

P. HURBIN †

Reprinted from the Proceedings of the Symposium on "Signal Processing in Radar and Sonar Directional Systems", held in Birmingham on 6th-9th July 1964.

**Summary:** The type of radar array outlined in this paper utilizes individual receiving aerials followed by amplifiers and an intermediate-frequency phasing matrix. This matrix simultaneously issues data corresponding to orthogonal aerial lobes covering a wide angular sector. The general principles involved are outlined as well as supporting experimental work and current developments.

## List of Symbols

$u$	distance between array elements	$p, q$	integers
$A$	voltage gain	$Q$	total radiated field
$b$	index for 'noise'	$r, R$	resistance
$B$	noise voltage	$S, S', S_0$	signal, image, local oscillator voltages
$D$	aperture width	$t$	increase in side-lobe level intensity
$E(x)$	aperture distribution	$T_0$	290° Kelvin
$f$	frequency	$u, U_0$	spurious and no-error radiated fields
$F$	'radiation' pattern	$V$	voltage
$G$	conductance	$\alpha$	phase-shift
$H$	'power illumination' radiation pattern	$\gamma$	correlation coefficient
$i$	numbering of matrix rows	$\lambda$	wavelength
$I$	current	$\Gamma$	antenna gain
$k, l$	numbering of matrix columns	$\theta$	angle
$K$	Boltzmann's constant	$\theta_0$	maximum radiation direction
$L$	signal/noise ratio loss	$\bar{\theta}$	beamwidth
$m$	number of matrix rows	$\theta_T$	angular sector (coverage)
$n$	number of matrix columns	$\rho_b$	noise resistance
$N$	noise factor	$\sigma$	standard deviation

## 1. Introduction and General Description

Arrays can be used either for providing the almost instantaneous scanning of one radar beam, or for delivering received signals (e.g. echoes) in several simultaneous channels. This latter type of array radar can provide an angular coverage  $\theta_T = n\bar{\theta}$  with  $n$  channels of individual coverage  $\bar{\theta}$ .

The present paper describes a small-scale experimental model set of this latter type of receiving array. This model makes use of an i.f. phasing matrix and

its object is to verify the feasibility of such a technique.<sup>1</sup> The general principles of the receiving system are shown on Fig. 1.

The antenna itself includes  $m$  sources lined up side-by-side. (These sources can be disposed along the focal line of a parabolic cylinder in order to narrow the beams in the transverse planes.) The r.f. signals received by each of these sources are mixed with a local oscillator and are in this way converted into i.f. signals, their respective amplitudes and phases being left unchanged.

The output voltages  $V_i$  of the  $m$  identical receivers are delivered on the inputs of the  $m$  rows (1, 2, . . . ,

† Compagnie Française Thomson-Houston, Systèmes Electroniques Radars, Bagnaux, Seine, France.

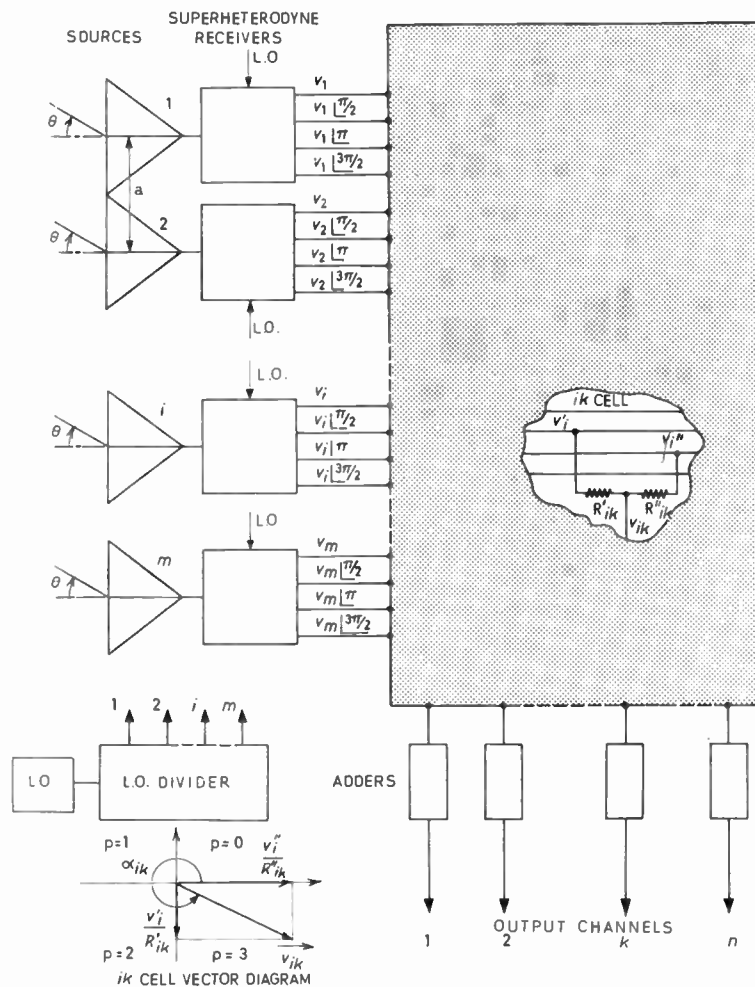


Fig. 1. Basic details of the receiver array.

$i, \dots, m$ ) of the phasing matrix. The outputs of the matrix are taken from the  $n$  columns (1, 2,  $\dots, k, \dots, n$ ). Each of these columns gives the equivalent of an individual antenna with its own equivalent 'radiation' pattern.

The phasing matrix operates as follows: The voltage  $V_i$  from the  $i$ th receiver is divided into four voltages  $V_i \exp(jp\pi/2)$  ( $p = 0, 1, 2, 3$ ), in quadrature, which feed the  $i$ th row of the matrix. Through two of these voltages [ $V'_i = V_i \exp(jp\pi/2)$  and  $V''_i = jV'_i$ ], each element (or cell)  $ik$  of the matrix delivers an output voltage:

$$V_{ik} \approx \frac{V'_i}{R'_{ik}} + \frac{V''_i}{R''_{ik}} \approx V_i \exp(j\alpha_{ik})$$

(Refer to the vector diagram of Fig. 1.)

If the resistors  $R'_{ik}$  and  $R''_{ik}$  across  $V'_i$  and  $V''_i$  are:

$$R'_{ik} = \frac{r_{ik}}{\cos(\alpha_{ik} - p\pi/2)} \quad R''_{ik} = \frac{r_{ik}}{\sin(\alpha_{ik} - p\pi/2)} \quad \dots(1)$$

and if  $V'_i$  and  $V''_i$  (that is to say  $p$ ) are properly chosen, the input voltage  $V_i$  can be outphased by any phase angle  $\alpha_{ik}$  ( $0 \leq \alpha_{ik} \leq 2\pi$ ). All the voltages  $V_{ik}$  from the  $m$  cells of the  $k$ th column are summed in an adder of very low input impedance.

A plane electromagnetic wave falling on the array under an incidence  $\theta$  induces in each source equal amplitude, progressively phased voltages. The object of the matrix is to restore these voltages in phase for  $n$  particular angular directions  $\theta = \theta_{0k}$ . The equivalent 'radiation pattern' thus measured at the output of the  $k$ th column adder has a maximum in the  $\theta_{0k}$  direction if the phases are:

$$\alpha_{ik} = \frac{2\pi}{\lambda} ia \sin \theta_{0k}$$

( $i$  can have any integral value between 0 and  $m-1$ ,  $a$  is the array element spacing, and  $\lambda$  the wavelength).

The proper value of  $r_{ik}$  (eqn. (1)) is determined by the matching conditions of the receiver outputs. In

the common case of uniform amplitude arrays all the  $r_{ik}$  are equal ( $r_{ik} = r_0$ ), but a proper choice of these  $r_{ik}$  can offer the possibility of tapering the amplitude (side-lobe reduction) of the  $k$ th column. As will be seen in Section 2, the maxima of the equivalent radiation patterns are usually chosen in order that these patterns are two-by-two orthogonal functions. For a uniform amplitude array the matrix cell phases are in this case:  $\alpha_{ik} = ik2\pi/m$  (with  $i$  comprising every integral value between 0 and  $m-1$  and  $k$  between 0 and  $n-1$ ; the integral values of  $k$  can also be chosen symmetrically around 0).

The experimental model set which is described is an array of  $m = 8$  sources. Thus the phase-shifts to be included in the matrix ( $\alpha_{ik} = ik\pi/4$ ) only require resistor values  $R'_{ik}$  (or  $R''_{ik}$ ) =  $r_0$  or  $r_0\sqrt{2}$ , plus, of course, infinite value ( $V'_i$  or  $V''_i$  disconnected).

The h.f. components of the model set are in the X-band. The i.f. of the matrix is 3 Mc/s. On the schematic diagram (Fig. 1), each superheterodyne receiver actually comprises two frequency converters. The first one mixes the h.f. received signals with in-phase local signals fed from an oscillator through a splitter network. The first i.f. is 36 Mc/s in order to obtain a reasonably good noise-factor (about 8 dB). The 36-Mc/s amplifiers are adjusted in order to minimize their differential phase shift and gain (that is, in order to render each amplifier as identical as possible to the others). These amplifiers, which have a much wider bandwidth (20 Mc/s) than the matched bandwidth are of a similar design to the monopulse radar i.f. amplifiers. The second converter which follows these amplifiers transposes the i.f. to 3 Mc/s. This converter is of the single-sideband-type in order to suppress the image noise due to the wide bandwidth of the 36 Mc/s amplifiers.

The basic principles of the technique have been tested using this model (Sect. 4) and their extension to more realistic problems, which would need wider arrays, is being considered.

## 2. Principles of Operation

This section outlines some points of the theory of multi-beam receiving arrays with special regard to i.f. matrix arrays.

### 2.1. Orthogonality Conditions. Equivalent Radiation Patterns

It has been shown<sup>2,3</sup> that the radiation patterns  $F_k(\theta) \dots F_l(\theta) \dots$  of a lossless multi-beam aerial must be represented by orthogonal functions in order to avoid coupling between the different channels:

$$\int_{-\infty}^{+\infty} F_k(\sin \theta) F_l(\sin \theta) d(\sin \theta) = 0 \quad \dots\dots(2)$$

This expression is rigorous only in the small angles approximation, i.e. for narrow, slightly deflected beams. The significance of the orthogonality relation in the post-amplification beam-forming-array case is explained in Appendix 1.

If the pattern functions  $F(\sin \theta)$  are the same, except for their deflection angle, this condition becomes:

$$\int_{-\infty}^{+\infty} F(\sin \theta - \sin \theta_{ok}) \cdot F^*(\sin \theta - \sin \theta_{ol}) d(\sin \theta) = 0$$

$\theta_{ok}, \theta_{ol}$  being the angles of the maxima of the radiation patterns for the channels  $k$  and  $l$ .

Finally, this condition can be written:

$$H(\theta) = 0$$

with

$$H(\theta) = \int_{-D/2}^{+D/2} E(x) \cdot E^*(x) \exp(-j2\pi/\lambda \cdot x \sin \theta) dx$$

$E(x)$  is the illumination function of the equivalent 'radiating aperture' and  $D$  the width of this aperture.

Thus the angular intervals  $\sin \theta_{ol} - \sin \theta_{ok}, \dots$  between the directions  $\theta_{ok}, \theta_{ol} \dots$  of the maxima of the radiation patterns must be equal to the zeros of the function  $H(\sin \theta)$ . This function can be called the 'radiation pattern of the aperture power distribution'.

For a uniform array with an element spacing  $a$ :

$$E(x) = \sum_{i=0}^{i=m} E_e(x - ia)$$

$$F_k(\theta) = F_e(\theta) \frac{\sin \left[ m \frac{\pi a}{\lambda} (\sin \theta - \sin \theta_{ok}) \right]}{\sin \left[ \frac{\pi a}{\lambda} (\sin \theta - \sin \theta_{ok}) \right]} \quad \dots(3)$$

$$H(\theta) = H_e(\theta) \frac{\sin \left[ m \frac{\pi a}{\lambda} \sin \theta \right]}{\sin \left[ \frac{\pi a}{\lambda} \sin \theta \right]}$$

$E_e(x)$  is the field intensity across an individual source,  $F_e(\theta)$  is the radiation pattern of a source (element factor),

$H_e(\theta)$  is the radiation pattern of one fictitious individual source with a field intensity  $[E_e(x)]^2$ .

Usually, the individual sources have a broad pattern  $F_e(\theta)$ . In this case the first zeros of  $H(\theta)$  are also the zeros of the array factor. This means that:

$$\sin \theta_{ol} - \sin \theta_{ok} = \frac{q\lambda}{ma} \quad \dots\dots(4)$$

$q$  being an integer.

The maximum of a 'radiation pattern' then coincides with the zeros of the other 'radiation patterns'.

2.2. Phase Differences within the Matrix

It can be shown from this equation that the phase differences within a matrix, which has uniform amplitude distribution and gives independent beams, are:

$$\alpha_{ik} = ik \frac{2\pi}{m}$$

as mentioned above. The orthogonality condition appears as a natural property inside the matrix: a plane electromagnetic wave with angle of incidence  $\theta_{ok}$  gives a voltage which is proportional to

$$\sum_{i=0}^{m=1} \exp ji(l-k) \frac{2\pi}{m}$$

at the output of the  $l$ th column. This voltage is maximum for  $l = k$  (output of the  $k$ th column) and is zero for  $l \neq k$ .

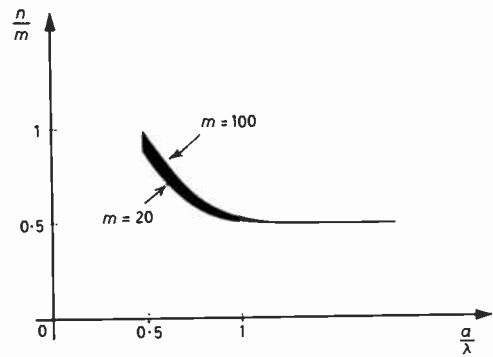
2.3. Maximum Number of Effective Beams. Grating Lobes

Shannon's Sampling Theorem can be applied to antenna theory<sup>4</sup>: in this sense, an angular sector  $\theta_T$  can be analysed with an antenna of aperture  $D$  by resolving this sector in a number  $\theta_T D/\lambda$  of independent samples. Thus  $\theta_T D/\lambda$  is the number ( $n$ ) of independent (orthogonal) beams which can be received in this sector  $\theta_T$  by an uniform array whose aperture is  $D (= ma)$ . Now, the number of degrees of freedom in the array is, of course, equal to the number  $m$  of sources. Hence  $n \leq m$ : the number of independent beams (number of columns) of the matrix cannot be greater than the number of sources (number of rows).

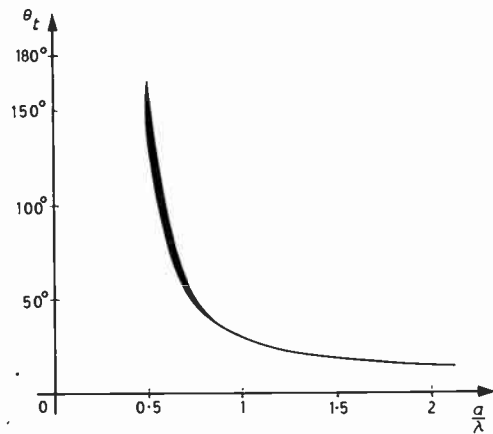
The condition  $n = m$  would be realizable only if the array distribution had been kept uniform in all the directions of the  $\theta_T$  sector. In other words, this imposes the condition that the element factor  $F_e(\theta)$  should be approximately constant (with 1 dB tolerance for instance) in the whole  $\theta_T$  coverage.

The number of utilizable beams can be calculated in another way from the tolerance to be kept on the maximum level of the grating lobes (10 dB for instance). The side (and grating) lobes can also be considered as the consequence of the regular 'stepped' phase errors on the aperture distribution for deflected beams.

The main results are outlined in Fig. 2. Figure 2 (a) shows that the number of independent (orthogonal) beams  $n$  can be almost equal to the number of  $m$  sources in the case of half-wavelength elements, but cannot be greater than  $m/2$  if the element (source) width, exceeds about  $0.9\lambda$ . Figure 2(b) shows the



(a) Number of beams/number of sources vs. element spacing.



(b) Total coverage vs. element spacing.

Fig. 2. Array coverage capability.

$\theta_T$  angular sector which can be covered by these  $n$  beams.

Note that: (1) These results are valid only for a totally filled aperture distribution. The sources (elements) must be lined up side-by-side and their own aperture distribution must be uniform. Nevertheless, this latter condition can be relaxed for elements shorter than one wavelength.

(2) Some special methods can be used, in particular applications, to reduce the number of elements (and consequently the number of rows in the matrix) without impairing the system performances.

(3) In the theoretical case  $n = m$ , the first and the last beams are symmetrical about the broadside direction and have identical amplitudes; each one forms the grating lobe of the other one.

2.4. Tolerances on Phases and Amplitudes

The theory of the influence of manufacturing errors on antenna performances<sup>5-8</sup> can be applied to the post-amplification arrays in order to calculate the tolerances on the alignment and stability of the

differential phase shift and amplitude (gain) between the  $m$  receivers. Such random variations of phase and amplitude:

(a) Involve a loss  $L$  in the signal/noise ratio (equivalent to a loss in antenna gain).

(b) Raise the side-lobe level. The spurious radiation pattern produced by the errors has an envelope which is the element factor  $F_e(\theta)$  and a maximum 'gain'  $(1-L)\Gamma_e$ ,  $\Gamma_e$  being the element gain. This diffused radiation compounds with the no-error radiation pattern (according to random outphasing conditions).

The main practical results can be summarized by the following formulae:

(i) Loss of signal/noise level (equivalent loss of antenna gain) (decibels)

$$= -10 \log(1 + \sigma^2) \\ \approx -4.3\sigma^2 \quad (\text{for } \sigma \leq 0.3)$$

$\sigma$  is the total standard deviation of the errors  
 $\sigma^2 = \sigma_p^2 + \sigma_a^2$ .

$\sigma_p$  and  $\sigma_a$  are the standard deviations of the phase errors and amplitude errors.

When the aperture amplitude distribution is not uniform,  $\sigma$  must be tapered according to this distribution.

$\sigma_p$ , the standard deviation on differential phase shifts is, of course, measured in radians.

$\sigma_a$  can be measured by the differential receiver gain:

$$20 \log(1 + \sigma_a) \approx 8.7\sigma_a$$

(ii) Side-lobe level: In proximity to the broadside direction, the side-lobe level is raised (within a probability limit  $P$ ) by an amplitude ratio  $t$  (see Appendix 2):

$$t = 1 + \frac{z}{h\sqrt{2}} \frac{\sigma}{\sqrt{m}} \quad \dots\dots(5)$$

$z$  is a constant quantity which depends on  $P$ .†

† This expression is valid for a uniform aperture distribution and for  $\frac{\sigma}{h\sqrt{2}\sqrt{m}} \leq \frac{1}{3}$ ,  $z$  is given by the following table:

P: Probability limit of the increase for:		
One side-lobe	The two symmetrical side-lobes	$z$
0.71	0.5	0.55
0.89	0.8	1.25
0.95	0.9	1.63
0.975	0.95	2
0.995	0.99	2.58

$h$  is the relative amplitude of the theoretical side-lobe.

For instance, if the theoretical level ( $-13$  dB or  $h = 0.224$ ) of the first two side-lobes is to be raised not more than 1 dB ( $t = 1.12$ ) within 90% probability ( $z = 1.63$ ), it is necessary that:

$$\sigma \leq 0.023\sqrt{m}$$

For  $m = 100$  elements  $\sigma \leq 0.23$  which can be divided (for instance) into:

$$|\sigma_p| \leq 9^\circ, \quad \sigma_a \leq 0.05 (\pm 0.4 \text{ dB})$$

For  $m = 8$  elements  $\sigma \leq 0.065$  and, for example:

$$|\sigma_p| \leq 2.5^\circ, \quad \sigma_a \leq 0.05 (\pm 0.4 \text{ dB})$$

(iii) Errors can be divided into:

(a) Errors on r.f. components, which principally divide into:

(1) Errors on T-R cells (not used on the present experimental set). These cells must be of the 'controlled phase' type. The standard deviations of differential phase shift and amplitude errors for this type of cell can amount to  $\pm 3^\circ$  ( $\pm 5^\circ$  specification value) and  $\pm 0.1$  dB.

(2) Errors on r.f. mixers. These errors are very small ( $\pm 1^\circ$ ). The conversion loss (amplitude errors) have a standard deviation about  $\pm 0.25$  dB.

(b) Errors on the 36 Mc/s i.f. amplifiers. These errors can be adjusted to  $\pm 2^\circ$  and  $\pm 1$  dB (or less). These limit values are valid on the whole dynamic range.

(c) Errors on the matrix elements: These errors are usually negligible.

To sum up, the required tolerances are easily kept when the number of sources ( $m$ ) is greater than thirty or so. For small arrays, very accurate adjustments are necessary. For big arrays, these initial adjustments are easy but the permanent test devices, which could be necessary in operational conditions, become complex and cumbersome.

2.5. Noise Factor

Firstly, it is necessary to recall the fact that the sensitivity of an array-type radar comprising  $m$  sources (elements) of individual gain  $\Gamma_e$  is the same in the two following hypotheses:

The electromagnetic fields received in the elements are added by a r.f. process in one receiver.

Or: The voltages induced by these fields are frequency transposed and amplified in identical receivers of a type similar to the single receiver of the first case. Then they are added by an i.f. process.

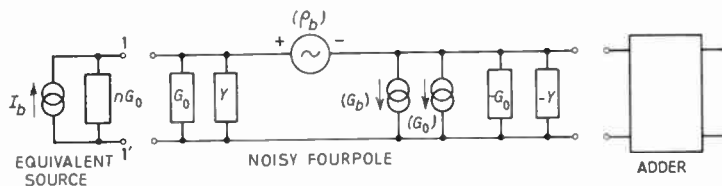


Fig. 3. Noise equivalent diagram of summation process.

In the first hypothesis, the ratio of the maximum received signal voltage to the receiver noise voltage  $B$  is  $\sqrt{m\Gamma_e}/B$ . In the second hypothesis, this ratio appears unchanged, being equal to  $m\sqrt{\Gamma_e}/\sqrt{mB}$ , due to the fact that the total noise power is the sum of the uncorrelated noise powers from each of the  $m$  individual receivers.

Now, it is nevertheless necessary to investigate, in the present case, the influence on the noise factor of the matrix resistors and of the adding process. The calculation has been carried out, for the sake of simplification, in the case of a broadside beam, i.e. for a column of identical resistors  $R'_{ik} = r_{ik} = 1/G_0$ . The noise current  $I_b$  (per unit bandwidth) arising from the  $m$  receivers and the  $m$  resistors is given at the adder input by:

$$\overline{I_b^2} = 4m \left( W_0 + \frac{N-1}{W_0} \right) K T_0 N_0 W_1 G_0$$

where  $N_0, W_0$  are noise factor and power gain of the r.f. part of one receiver,†

$N_1, W_1$  are noise factor and available power gain of the section comprising the 36-Mc/s amplifier, the 3 Mc/s transposition mixer and the matrix resistors.

The addition of voltages is performed in a feedback amplifier whose input effective resistance ( $r$ ) is very small, in order to obtain a good decoupling between the  $m$  cells of one particular column. This decoupling ratio is equal to  $rmG_0$ . The feedback resistor is also  $1/G_0$ , thus providing a closed-loop gain equal to  $-1$ . The calculation of the adder's noise factor ( $N_2$ ) can be carried out by considering the equivalent diagram of Fig. 3. In this diagram, a noise equivalent fourpole stands for the internal noise sources of the amplifier.<sup>9,10</sup>

The equivalent noise sources of the above-mentioned fourpole are:

A noise voltage generator (inducing the same noise as a resistor  $\rho_b$ ).

A first noise current generator. (This induces the same noise as a conductance  $G_b$ , and the current

noise is correlated to the voltage noise. This correlation is represented by an equivalent admittance  $Y$ .)

A second noise current generator (inducing the same noise as the feedback conductance  $G_0$ ).

The parameters  $\rho_b, G_b, Y$  can be derived from the noise characteristics of the components (transistors) of the adding amplifier.

The result of the calculation is:

$$N_2 = 1 + \frac{G_0 + G_b}{mG_0} + \frac{\rho_b}{mG_0} [(m+1)G_0 + Y]^2$$

which, for  $m > 2$ , can be approximated by

$$N_2 \approx 1 + mG_0\rho_b$$

The total noise factor of one array channel (column) is:

$$N = N_0 + \frac{N_1 - 1}{W_0} + \frac{N_2 - 1}{W_0 W_1}$$

In the present case, for instance

$$\rho_b = 100 \text{ ohms}, \quad G_b = 5 \times 10^{-3} \text{ mhos}, \\ Y = 3 \times 10^3 \text{ mhos}^\ddagger$$

and

$$m = 8, \quad 1/G_0 = 675 \text{ ohms}, \quad N_0 = 4.6, \\ W_0 = 0.32, \quad W_1 = 270$$

From these data

$$N_2 = 3.8$$

and

$$N = 4.6 + 1.9 + 0.01 \quad (\text{that is } 8.2 \text{ dB})$$

The noise contribution of the adder is thus negligible. But the result would have been quite different if the summation had been carried out on a simple resistor  $r$  followed by an amplifier. This amplifier would have been to give the same voltage gain  $A_2 = 1/rG_0$  as the open-loop feedback amplifier which is actually used. The total voltage gain would have been the same ( $-1$ ) but the noise factor would have been:

$$N'_2 = 1 + \frac{A_2 G_0 + G_b}{mG_0} + \frac{\rho_b}{mG_0} [(m + A_2)G_0 + Y]^2 \\ \approx 1 + \frac{\rho_b A_2^2 G_0}{m}$$

† In our experimental model set, there is no provision for r.f. amplifiers. Then,  $W_0$  is smaller than 1 (conversion loss of the crystal mixer).  $N_0$  is the ratio (noise temperature coefficient of the crystal)/ $W_0$ .

‡ The calculation of the adder's noise factor includes only the contribution of the first and second stages (which make use of high cut-off 400-Mc/s transistors).

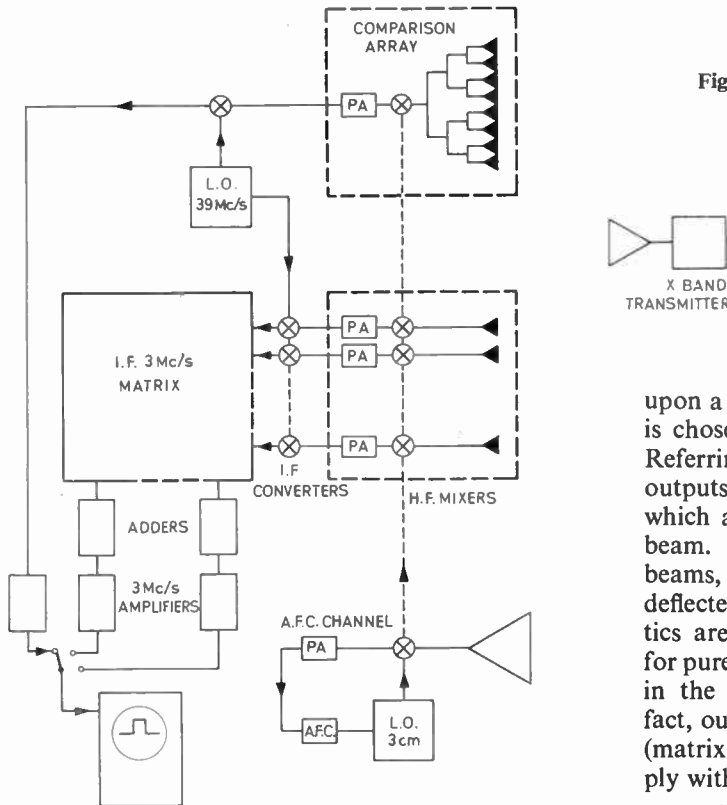
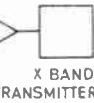


Fig. 4. Experimental model set and test equipment.



upon a rigid framework (Fig. 5). The horn directivity is chosen in order to obtain sufficient antenna gain. Referring to Fig. 2(a), it can be seen that only four outputs correspond to effective beams, i.e. beams which are only slightly different from the theoretical beam. (There would actually be only three effective beams, i.e. one central beam and two symmetrically deflected beams. Moreover, the pattern characteristics are still more disturbed owing to the fact that, for purely mechanical reasons, the horns are positioned in the H-plane (cosine illumination).) In point of fact, our one concern is to verify, on the eight outputs (matrix columns), that the experimental results comply with actual computed patterns.

To the rear of each horn is located a balanced mixer followed by an i.f. pre-amplifier. The local oscillator signals are distributed by a staggered divider, electrically-balanced and made up of magic-tees.

The comparison antenna is an array identical to the above-described one, the addition of r.f. signals being effected on one receiver, via a divider of the same type.

Thus the ratio  $\frac{N'_2 - 1}{N_2 - 1}$  is about  $\left(\frac{A_2}{m}\right)^2$  which is equal to the decoupling ratio, between the matrix cells, as is to be expected. In our present instance, the noise contribution ratio of the summation device would have been equal to 55.

### 3. Description of Main Components

Figure 4 represents the experimental model set. It also shows the various equipments used for c.w. (or pulsed) experimentation, i.e. transmitter, various circuits (a.f.c., synchronizer, etc.), and, furthermore, two devices whose purposes are adjusting and testing, one comparison antenna and one i.f. simulator (monitor see, see Fig. 9).

It should be borne in mind, however, that this set is constructed in the simplest possible manner so as to verify the principle involved. Thus, it is obvious that some components are of a standard-type and have not been specially selected. The array uses uniform amplitude elements, thereby achieving equivalent beams which constitute sampling patterns. (The actual form  $F_e(\theta)$  of these beams is as given in equation (3).)

#### 3.1. Microwave Sub-assembly

The array proper comprises eight horns, the aperture of which is  $1.65 \lambda$  positioned side-by-side

#### 3.2. The 36-Mc/s I.F. Pre-amplifiers

The technique applied in the 36-Mc/s i.f. pre-amplifiers is very similar to that used on phase-monopulse radar receivers. Studies carried out on the latter show good reproducibility in production and identical transfer curves can be obtained. The components are defined with a tolerance value of 1%, and special attention is given to the wiring. The phase frequency curve slope (group-propagation time) is rendered very small in the signal-frequency band owing to the selection of an overall pre-amplifier pass-band which is much wider than the spectral bandwidth (20 Mc/s for a  $1 \mu s$  pulse). Under these conditions, the phase variation could be rendered to approximately 1 deg. On the other hand, the amplitude variations are not in excess of 1 dB (for amplifier gain of 35 dB) over a 60 dB/noise dynamic range. A trimming attenuator positioned at the amplifier output enables this amplitude variation to be lowered still further.

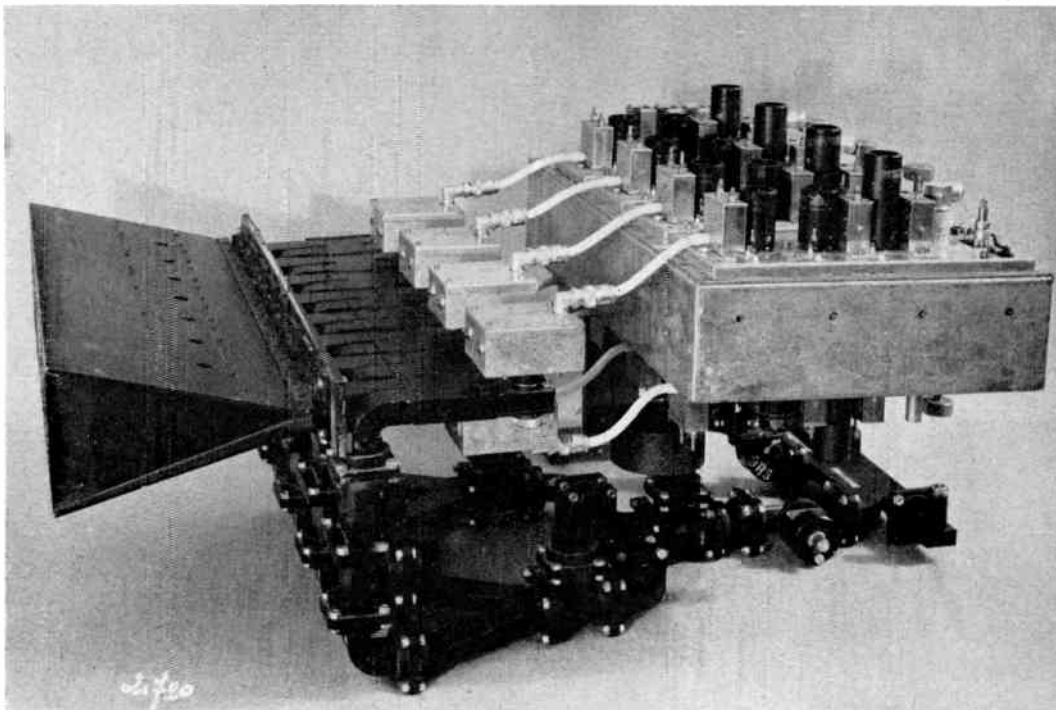


Fig. 5. R.f. and i.f. (36 Mc/s) sub-assembly.

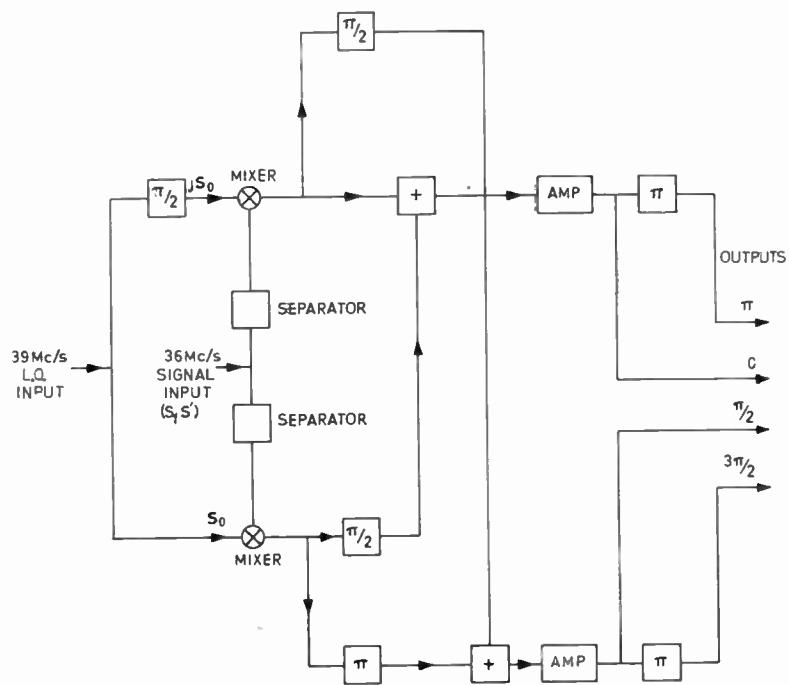


Fig. 6. Phase-shifting converter.

### 3.3. Second I.F. Mixing and Quadrature Outputs (Phase Shifting Converter)

Here again use is made of the simplest technology; thus the matrix is achieved for a 3-Mc/s i.f. On the other hand, each row input must be fed by four voltages. The  $\pi/2$  outphasing between these voltages must be frequency independent, otherwise the aperiodic characteristic of the matrix would be hardly worthwhile. Finally, the i.f. mixing from 36 Mc/s to 3 Mc/s should be so devised as to avoid the wide bandwidth of the r.f. and first i.f. (36 Mc/s) causing a deterioration in noise-factor. To this end, the noise components located around the image frequency must be suppressed, and this is aperiodically achieved using a single-sideband circuit.

Figure 6 shows a block diagram of this outphasing i.f. second mixer. At the output of both mixers, through beats between signal voltage  $S$  (36 Mc/s) and l.o. voltage  $S_o$  (39 Mc/s), i.f. (3 Mc/s) voltages  $jS_o \cdot S^*$  and  $S_o \cdot S^*$  are obtained.

Each of these voltages is split up into two parts and each part is added to the other after a  $\pi/2$  outphasing. The signal voltages thus restored in phase give voltages  $jS_o \cdot S^*$  and  $-S_o \cdot S^*$  at the adding circuits' outputs. The image-frequency voltages are subtracted from each

other and therefore cancel out. Finally, two  $\pi$  outphasing circuits, moreover, enable effective voltages of  $-jS_o \cdot S^*$  and  $S_o \cdot S^*$  to be obtained.

These circuits are entirely transistorized, and are linear over a 60-dB dynamic range with image-frequency suppression better than 20 dB. The output voltages are held in perfect quadrature in the 1-Mc/s bandwidth.

### 3.4. Matrix and Adders

Figure 7 depicts the sub-assembly comprising the phase-shifting converter, the matrix and the adders (shown at the top of the photograph). The achievement of this matrix has not entailed any special technology. The resistors are defined with a tolerance value of 1%. The columns of the matrix correspond to  $k = -3, -2, -1, 0, +1, +2, +3, +4$  ( $k$  value of the phases formula:  $\alpha_{ik} = ik2\pi/8$ ).

The operation of the adder has been described in Section 2.5. This adder comprises one high-gain amplifier with heavy feedback. Special precautions must be taken to secure its stability: near the frequency of unity gain, the slope of the gain-frequency curve must be about 8 dB/octave (and, in any case, lower than 12 dB/octave). The need for high frequency circuits and transistors can be avoided if this

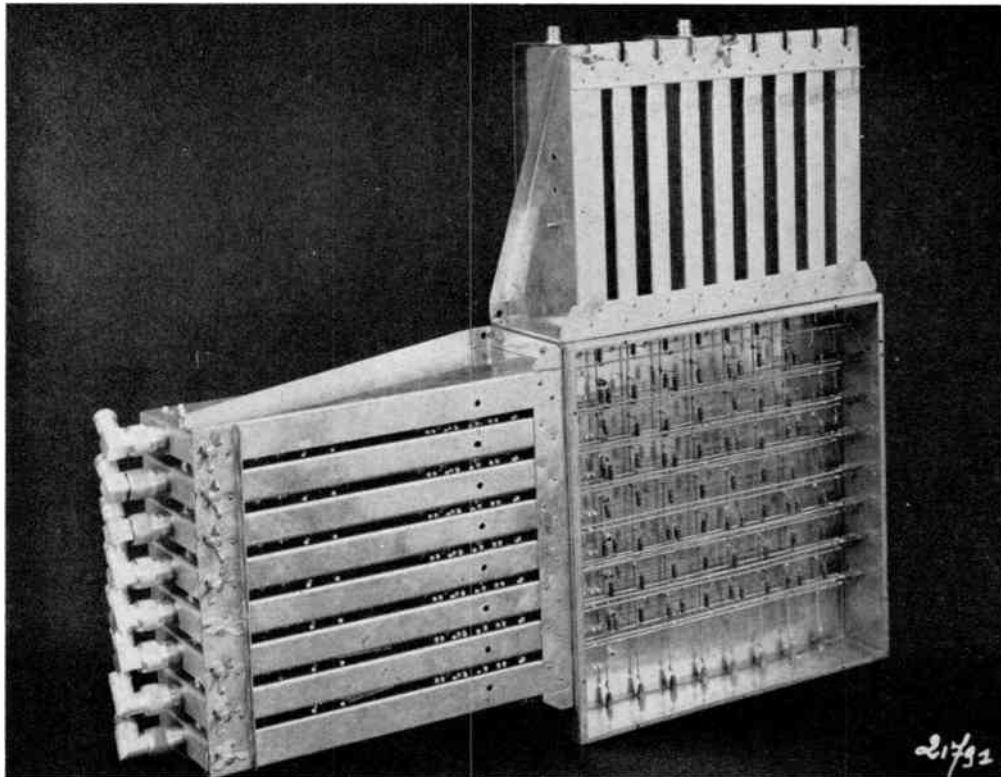


Fig. 7. 2nd i.f. phase-shifting converters, matrix and adders sub-assembly.

slope is increased, close to the operating frequency (3 Mc/s), which is effected by the insertion of one high-gain frequency-sensitive stage in the amplifier. Furthermore, the high-frequency stability is still improved by a frequency-sensitive (near 100 Mc/s) phase-leading cell within the feedback impedance.

**4. Experimental Set-up and Results**

A phase-shifted i.f. signals simulator (monitor set) has been developed to allow accurate and easy adjustments. This monitor is also used to test new circuits and components and is a veritable antenna simulator. The block diagram (Fig. 9) shows that it is founded upon the same principle as a type of scanning array.<sup>11</sup> A frequency modulated voltage is mixed with a fixed frequency (36 Mc/s) voltage and the modulated voltage thus generated is divided into *m* voltages which, via *m* delay lines, are mixed again and restored to their original frequency (36 Mc/s). Each voltage (*i*) is thus phase-swept over  $2\pi i$  radians during one modulation period and simulates the signal received at the source *i* during an angular scanning over the whole coverage of the array.

The trials consisted of 'equivalent' radiation pattern measurements for the eight matrix columns as we'll as signal/noise ratio tests. The measured patterns and their computed counterparts are shown on Figs. 10 and 11 for the central beam (*k* = 0) and the second right deflected beam (*k* = +2). The correlation is rather good, especially as regards the

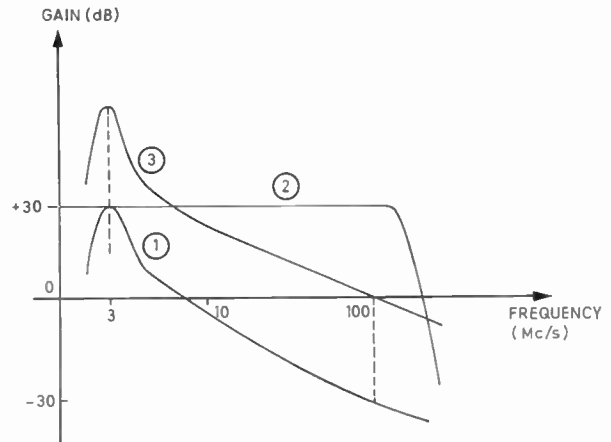


Fig. 8. Gain/frequency curve of the adding amplifier.

- (1) 3 Mc/s tuned circuit.
- (2) Video amplifier.
- (3) Open-loop curve (1) + (2).

beam deflections, the side-lobe level and position, and the depth between side-lobes.

The sensitivity (signal/noise ratio) measurement has been made with reference to a comparison antenna: the two sensitivities are the same with a 1 dB uncertainty, which approximately amounts to the accuracy of measurement.

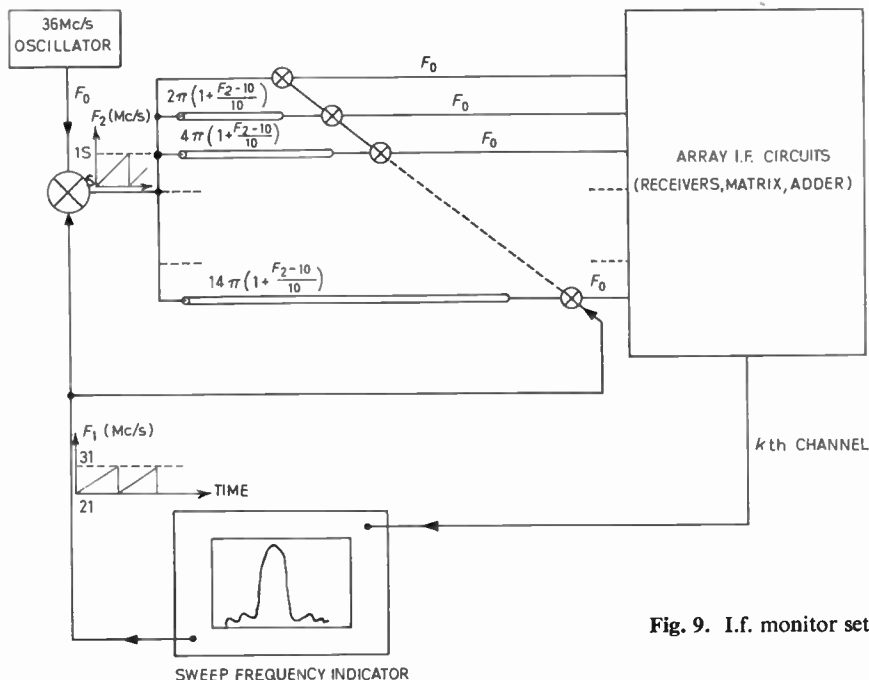


Fig. 9. I.f. monitor set.

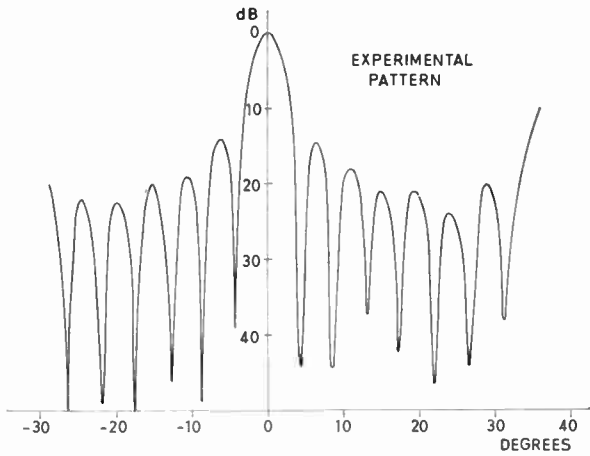


Fig. 10. Central beam.

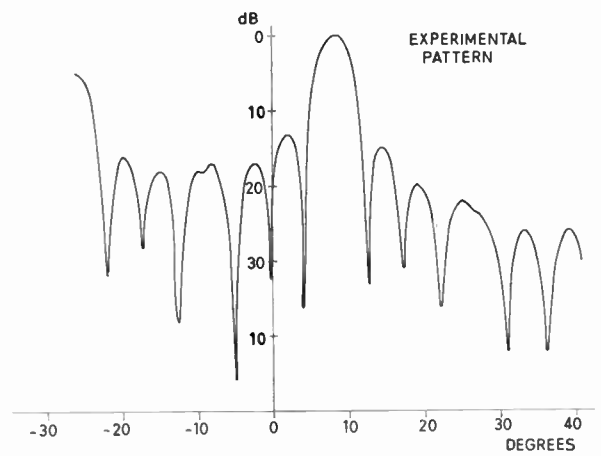


Fig. 11. Third right beam.

**5. Developments and Operational Modes**

Two main developments are now being considered in order to improve the above-mentioned studies:

(1) Array comprising a large number of elements: The i.f. matrix technique seems particularly useful for large arrays. The adder circuits which have been described require some amendments in order to be adapted to large arrays. However, it is possible to envisage arrays comprising from 50 to 100 rows (and the number of corresponding columns).

(2) Wide-bandwidth arrays: The term 'wide bandwidth' actually expresses two different meanings:

(a) R.f. wide-bandwidth: Although the device itself is intrinsically aperiodic, some 'radiation' characteristics are frequency-sensitive. For instance, beam-width and deflection angles are in inverse ratio to the frequency (in the case of small angles approximation, i.e. for near broadside directions). On the other hand, the shape and orthogonality property are frequency-insensitive.†

If the received signal frequency is known, it is possible to determine the actual direction of the receiving beam.

(b) I.f. wide-bandwidth: A wide i.f. bandwidth appears necessary either if the received signals' frequency is unknown, or if these signals themselves have a wide spectrum. The i.f. bandwidth of the model set is approximately 1 Mc/s.

The elaboration of a wide i.f. bandwidth array implies the utilization of a high i.f. The miniaturization of the matrix elements therefore becomes indispensable. Moreover, line effects within the matrix are of considerable importance. Not only must

† Some types of multi-beam arrays use delay lines as phase-shifting circuits. In this case, the deflection angles are frequency-insensitive if the i.f. (and thus also the l.o. frequency) are kept proportional to the r.f. This latter condition implies wide-bandwidth i.f. circuits. On the other hand, the orthogonality property is, in this case, frequency-sensitive.

great care be taken in the arrangement of elements within a column, but, still further, special means must be taken in the addition of the voltages from the column elements. These problems are the subject of current studies.

The operational utilization modes of multi-beam arrays must also be considered: from an information theory standpoint it appears logical to utilize uniform-amplitude arrays (as has been done on the model set) since the corresponding patterns behave similarly to sampling functions. However, these patterns comprise high side-lobe levels. It would then be appropriate to contrive an operational utilization mode in which this characteristic would not be adverse.

It is also possible to envisage tapered distributions, for instance, the simple cosine distribution resulting from the addition of two neighbouring columns, but too low a cross-over of the independent sampling patterns may then be a drawback. It might then appear necessary to sacrifice the orthogonality condition at the expense of a sensitivity loss in the signal comparison (see Appendix 1). At all events, such a comparison (monopulse interpolation) is usually necessary to determine angular directions.

In all of the foregoing, we have only considered receiving factors. It is obvious, in effect, that the best operational field as regards multi-beam antennas is that of simultaneous reception in all of the various channels. It is therefore, normal to associate this type of receiving antenna with a transmitting antenna, which radiates according to a wide sector pattern ensuring the same coverage. It is a well-known fact that under these circumstances such a radar possesses the same performance factors as a radar scanning the same sector, via a narrow transmitter/receiver beam, when a given measurement time is allotted, when the receiver is of the coherent-integration-type, and when the gain of the scanning antenna is identical to the equivalent gain corresponding to the various channels of the multi-beam receiving antenna.

The choice between a scanning radar and a multi-beam radar depends on the operational specifications and on the various available technologies. It should be borne in mind that electronic scanning high-power array radars give rise to difficult design problems where the transmitter energy division as well as the scanning devices (phase-shifters, etc.) are concerned.

In the multi-beam antenna category, the following solutions can be compared:

- (a) i.f. matrix array (dealt with in this paper);
- (b) r.f. matrix array<sup>12-15</sup>;
- (c) antennas comprising focusing optics and multiple feeds (especially of the parabolic-torus-type).

All of these solutions usually comprise, for a given number of beams, the same quantity of receivers. However, solution (c), the optical system of which acts as a matrix, may necessitate a certain number of additional r.f. or i.f. channels in order to comply with orthogonality conditions or to compensate optical aberrations. Solution (b) necessitates extremely cumbersome r.f. circuits in cases of large arrays. There is no ready-made solution and the choice depends upon specifications applicable to each case.

The i.f. matrix is a member of the 'family' of the means available to the system designer, and is in a position to promote relatively simple and advantageous equipments.

## 6. Conclusion

Although the model set, described therein, is a small-scale, non-sophisticated entity, it has, nevertheless, enabled a contribution to be made to multi-beam array radar technique. More research into the matter is of course required, but it would appear that the i.f. matrix technique affords a simple and efficient solution to the multi-beam receiving radar.

## 7. Acknowledgments

Similar ideas have been developed in various countries for some years past, particularly since 1956.

We especially appreciated the discussions which have taken place between Major Dole and Mr. Turriere, representatives of the French Air Forces (S.T.T.A.) and engineers of the Radar Division of the Compagnie Française Thomson-Houston.

We extend our thanks also to Mr. S. Drabowitch for his contribution to Appendix 1 during valuable discussions on the matter.

## 8. References

1. This matrix technique is somewhat similar to that described by F. C. Ogg in "Steerable array radars", *I.R.E. Trans. on Military Electronics*, MII-5, pp. 80-94, April 1961 (Section 8).
2. W. D. White, "Pattern limitations in multiple beam antennas", *I.R.E. Trans. on Antennas and Propagation*, AP-10, p. 430, July 1962.
3. J. C. Allen, "A theoretical limitation of the formation of lossless multiple beams in linear arrays", *I.R.E. Trans. on Antennas and Propagation*, AP-10, p. 350, July 1961.
4. J. S. Drabowitch, "Applications de la Théorie du Signal à technique des Antennes", *Revue Technique C. F. T. H.*, No. 33, pp. 7-27, October 1960.
5. J. Ruze, "The Effect of Aperture Distribution Errors on the Radiating Pattern", Side-Lobe Conference, 28th April 1952, pp. 13-29 (NRL Washington).
6. J. Robieux, "Influence de la précision de fabrication d'une antenne sur ses performances", *Annales de Radioélectricité*, 11, pp. 29-56, January 1956.

7. J. Guittet, "Le rayonnement diffus lié aux erreurs de distribution", *Revue Technique C. F. T. H.*, No. 33, pp. 29-57, October 1960.
8. S. Drabowitch, J. F. Decaux, *Rapports C. F. T. H.* (unpublished).
9. W. Dahlke, "Transformationsregel für rauschende Vierpole", *Archiv der Electr. Übertrag.*, 9, p. 397, September 1955.
10. H. Rothe and W. Dahlke, "Theory of noisy fourpoles", *Proc. I.R.E.*, 44, pp. 811-18, June 1956.
11. D. E. N. Davies, "A fast electronically scanned radar receiving system", *J. Brit.I.R.E.*, 21, pp. 305-18, April 1961.
12. J. Blass, "Multidirectional antenna—a new approach to stacked beams", *I.R.E. Conv. Rec.*, 1960, Part I, pp. 48-50.
13. J. Butler and R. Lowe, "Beam-forming matrix simplifies design of electronically scanned antennas", *Electronic Design*, 9, pp. 170-73, 12th April 1961.
14. J. P. Shelton and K. S. Kelleher, "Multiple beams from linear arrays", *I.R.E. Trans. on Antennas and Propagation*, AP-9, pp. 154-61, March 1961.
15. W. P. Delaney, "An r.f. multiple beam-forming technique", *I.R.E. Trans. on Antennas and Propagation*, AP-10, pp. 179-86, April 1962.

9. Appendix 1

Orthogonality Relation in the Case of Multiple-Beam Forming Arrays

The orthogonality relation (equation (2)) has a very straightforward significance in the case of multi-beam arrays which do not include individual receivers: this relation means that, in each channel, the radiation pattern and the antenna gain are the same as if the other channels were non-existent. It is possible to devise radiation patterns whose shape and/or directions do not meet orthogonality conditions, but this can only be achieved at the expense of losses introduced within junction circuits and, therefore, at the expense of gain.

But, in the present case, the addition of signal voltages takes place after the introduction of the noise sources emanating from first amplification stages. Under these circumstances, the reception conditions might appear independent of the relative angular position of the various beams. But this is not actually the case, and the relation (2) expresses, even in this instance, the independence of the various channels (matrix columns).

This independence arises from the uncorrelated character of the noise voltages from these various channels. If the noise from two channels are correlated, all and any comparison between the signals delivered from these channels, is effected in non-optimum conditions regarding sensitivity (signal/noise ratio) and, hence, precision.

Now, such a comparison can be used to measure accurately a target's direction (monopulse inter-

polation). It is, in any case, always necessary to weigh the strongest signal, i.e. to determine which lobe is the nearest to the direction of the target.

We shall establish the condition of uncorrelation of noise voltages in the simple case of a uniform amplitude array. The proof is closely related to the reasoning of Section 2.2.

Let  $B_{1o}, B_{2o}, \dots, B_{io}, \dots, B_{mo}$  be the (uncorrelated) instantaneous noise output voltages from the 1, 2, . . . ,  $i, \dots, m$  rows' individual receivers. These receivers being identical:

$$\overline{B_{1o}^2} = \dots = \overline{B_{io}^2} = \dots = \overline{B_{mo}^2} = \overline{B^2}$$

Let  $B_k$  and  $B_l$  be the instantaneous total output noise voltages from the  $k$  and  $l$  column adders.

$$B_k = \sum_i B_{ik} \quad B_l = \sum_i B_{il}$$

The main directions of the beams corresponding to channels  $k$  and  $l$  are  $\theta_{ok}$  and  $\theta_{ol}$ .  $B_{ik}$  is the output noise voltage from  $ik$  cell, i.e. phase shifted by  $2\pi/\lambda \cdot ia \sin \theta_{ok}$

$$B_{ik} = B_{io} \exp(j \cdot 2\pi/\lambda \cdot ia \sin \theta_{ok})$$

and similarly

$$B_{il} = B_{io} \exp(j \cdot 2\pi/\lambda \cdot ia \sin \theta_{ol})$$

The correlation coefficient† of  $B_k$  and  $B_l$  noise voltages is:

$$|\gamma| = \frac{\overline{B_k \cdot B_l^*}}{\sqrt{\overline{B_k^2}} \cdot \sqrt{\overline{B_l^2}}} = \frac{\overline{B_k \cdot B_l^*}}{mB^2}$$

The time averages of products like  $B_{ik} \cdot B_{il}$  are zero if  $i \neq i'$  (uncorrelated noise output voltages from two different receivers  $i$  and  $i'$ ).

Thus

$$\overline{B_k \cdot B_l^*} = \left| \sum_i B_{io}^2 \exp \left\{ j \frac{2\pi}{\lambda} ia (\sin \theta_{ok} - \sin \theta_{ol}) \right\} \right| = \overline{B^2} \left| \sum_i \exp \left\{ j \frac{2\pi}{\lambda} ia (\sin \theta_{ok} - \sin \theta_{ol}) \right\} \right|$$

$$|\gamma| = \frac{\left| \sin \left[ m \frac{\pi a}{\lambda} (\sin \theta_{ok} - \sin \theta_{ol}) \right] \right|}{m \cdot \left| \sin \left[ \frac{\pi a}{\lambda} (\sin \theta_{ok} - \sin \theta_{ol}) \right] \right|}$$

† A coherent demodulator, which can be used in the signal voltages comparison between  $k$  and  $l$  channels, delivers a voltage somewhat similar to that coefficient.

whence

$|\gamma| = 1$  for  $\sin \theta_{ok} = \sin \theta_{ol}$  (two identical channels) and

$|\gamma| = 0$  for  $\sin \theta_{ok} - \sin \theta_{ol} = q\lambda/ma$  which is the same condition as (4).

10. Appendix 2

Influence of Aperture Distribution Errors on Side-Lobe Level

We want to give a proof of formula (5)

$$t = 1 + \frac{2}{h\sqrt{2}} \frac{\sigma}{\sqrt{m}}$$

The various symbols are defined in Section 2.4. Let  $U_0$  be the electric field 'radiated' in a given direction by a perfect (no-error) antenna and  $u$  the disturbing field introduced in the same direction, because of the presence of phase and amplitude errors.

The probability-density function of the absolute value of the total field  $Q = U_0 + u$  is given by:

$$P_0(Q) dQ = \frac{1}{u^2} \exp\left(-\frac{Q^2 + U_0^2}{u^2}\right) \times Q \cdot 2\mathcal{J}_0\left(-\frac{2QU_0}{u^2}\right) dQ$$

$\mathcal{J}_0$  is the Bessel Function of order zero and imaginary argument. This formula is founded upon the fact that each of  $u$  components (projected on  $U_0$  and transverse to  $U_0$  components) obeys a Gaussian probability distribution.

In the vicinity of the broadside direction and for  $u \ll U_0$  the formula can be approximated by a

Gaussian distribution:

$$P_0(Q) dQ = \frac{1}{\sqrt{\pi}\sqrt{u^2}} \exp\left(-\frac{(Q - U_0)^2}{u^2}\right) dQ$$

Now  $\bar{u}^2 = (\sigma^2/m)\Gamma$  for an antenna whose maximum gain is  $\Gamma$  and which comprises an array of  $m$  equal-amplitude sources. The probability that  $Q$  does not exceed a limiting value  $Q_{lim}$  is

$$P(Q_{lim}) = \frac{1}{2} + Y\left(\frac{Q_{lim} - U_0}{\sqrt{\frac{u^2}{2}}}\right)$$

$Y$  is the Galton function

$$Y(z) = \frac{1}{\sqrt{2\pi}} \int_0^z \exp\left(-\frac{y^2}{2}\right) dy$$

If  $z$  is the value corresponding to the chosen probability (see Table in Section 2.4)

$$\frac{Q_{lim} - U_0}{\sqrt{\frac{u^2}{2}}} = z$$

whence:

$$\frac{Q_{lim}}{U_0} = z \frac{\sigma}{\sqrt{2}\sqrt{m}} \cdot \frac{\sqrt{\Gamma}}{U_0} + 1$$

This formula is identical to (5) with

$$h = \frac{U_0}{\sqrt{\Gamma}} \quad (\text{relative field intensity})$$

$$t = \frac{Q_{lim}}{U_0} \quad (\text{relative increase of this field intensity})$$

Manuscript first received by the Institution on 27th April 1964 and in final form on 12th November 1964. (Paper No. 979/RNA42)

© The Institution of Electronic and Radio Engineers, 1965

DISCUSSION

Under the chairmanship of Dr. M. I. Skolnik

**Dr. R. Benjamin:** In passive reception, would the phase relation between four i.f. outputs associated with each source be conveniently maintained by means of phase changes applied to a common l.o. signal feeding four separate mixers?

**Mr. J. Salomon (in reply):** By the term common l.o., I presume that Dr. Benjamin means the second l.o., that is, the second i.f. conversion (36 to 3 Mc/s). The process described, which does not make use—in each cell—of the four quadrature voltages, would entail a loss in the signal/noise ratio, if four separate first mixers were used in each source. Therefore, referring to the second i.f. conversion, Dr. Benjamin's suggestion appears quite feasible. In the present case, however, it has not been used owing to the fact that the single-side-band circuit chosen for the mixer almost systematically delivers the four quadrature voltage.

**Mr. P. Bradsell:** I understand that the Maxson array uses some 500 elements to produce 100 beams. Would this by your standard be an inefficient array?

**Mr. Salomon (in reply):** Maxson's array was only mentioned for the sake of comparison. I gathered that an F.A.A. air-height surveillance radar uses three Maxson's arrays, each one of which covering 120 deg in azimuth. The elevation beamwidth of the lobes is approximately 1/8th deg and the number of sources in the region of one thousand (per array). I do not know the number of elevation lobes, but I imagine that about 100 beams are sufficient to cover the required measurement range of the elevation angles (say up to 13°). But, of course, the array, whose elements seem to be spaced at approximately one half-wavelength, would be intrinsically able to give many more beams and is by no means an inefficient array.

Naturally, the question of the efficiency regarding the waveguide losses is quite another problem.

**Dr. J. B. Payne:** What is the loss in the matrix beam-forming network?

I would like to draw attention to similar technique which has been investigated by the Lincoln Laboratory and is described in their report "Phased Array Radar Studies".†

**Mr. Salomon (in reply):** The loss in the matrix resistors must not be considered as an individual entity. In fact,

† Lincoln Laboratory Technical Reports 228 (August 1960), 236 (November 1961) and 239 (February 1963).

one column of the matrix cannot be dissociated from its output adder. The open-loop gain of the amplifier of this adder is approximately 50 dB. It has been explained in Section 2.5 of the paper that under the chosen conditions there is no noticeable loss in the signal/noise ratio for each column. This means that each adder delivers the same signal/noise ratio which would have been delivered by the conventional process comprising one antenna of the same dimensions feeding one source and one receiver.

Regarding the point raised in connection with studies similar to the subject discussed in our text, we are aware that such techniques have been broached in the U.S.A. (cf. reference 1 in our paper).

## STANDARD FREQUENCY TRANSMISSIONS

(Communication from the National Physical Laboratory)

Deviations, in parts in  $10^{10}$ , from nominal frequency for April 1965

April 1965	GBR 16 kc/s 24-hour mean centred on 0300 U.T.	MSF 60 kc/s 1430-1530 U.T.	Droitwich 200 kc/s 1000-1100 U.T.	April 1965	GBR 16 kc/s 24-hour mean centred on 0300 U.T.	MSF 60 kc/s 1430-1530 U.T.	Droitwich 200 kc/s 1000-1100 U.T.
1	-149.4	-149.8	-6	16	-148.7	-150.4	-4
2	-150.7	-150.3	-6	17	-149.7	—	-5
3	-150.0	-148.9	-6	18	-148.6	-148.0	-5
4	-149.0	-149.3	-5	19	-150.0	-149.1	-4
5	-148.9	-151.6	-6	20	-151.0	-151.7	-6
6	-151.1	-150.2	-6	21	-151.2	-151.4	-5
7	-149.6	-149.8	-5	22	-149.3	-148.4	-5
8	-149.3	-150.8	-7	23	-151.1	-150.7	-5
9	-150.0	-149.4	-7	24	-150.3	-150.2	-5
10	-150.6	-150.5	-5	25	—	-150.4	-5
11	-150.0	-149.9	-5	26	-150.0	-150.6	-4
12	-150.1	-151.7	-5	27	-150.2	-150.2	-4
13	—	-150.3	-7	28	-149.9	-150.4	-4
14	—	-152.0	-5	29	-149.5	-149.1	-4
15	—	—	-5	30	-150.4	-151.3	-4

Nominal frequency corresponds to a value of 9 192 631 770 c/s for the caesium  $F_m(4,0)-F_m(3,0)$  transition at zero field.

## CHANGES IN N.B.S. RADIO BROADCASTS

The time signals broadcast by the U.S. National Bureau of Standards stations WWV (Greenbelt, Md.) and WWVH (Maui, Hawaii) were retarded 0.1 second at 0000 U.T. on 1st March, 1965. This follows the announcement by the Bureau International de l'Heure (B.I.H.) of such a retardation to be made by all coordinated stations, due to changes in the speed of the earth's rotation.

The time pulses will continue to occur at intervals greater than 1 second by 150 parts in  $10^{10}$ , a frequency offset also coordinated by the B.I.H.

Station WWV has been transmitting audio tones of 400 and 600 c/s by upper single-sideband modulation on 2.5, 5, 10, 15, and 20 Mc/s and on double-sideband only for the 25 Mc/s transmission. Beginning 1st March, 1965, at 0000 U.T. these tones were modulated by double-

sideband modulation at all carrier frequencies and all single-sideband transmissions were discontinued. These audio tones are now included with the voice announcements, time ticks, code announcements and time code which are transmitted at all frequencies used with double-sideband modulation. This change was made to simplify station operation and because of the results of a recent questionnaire which indicated that few users need the single-sideband feature of the past transmissions.

The time signals broadcast by NBS Station WWVB (Fort Collins, Colo.) will be retarded 0.2 second at 0000 U.T. 1st April, 1965. This phase adjustment ensures that these second pulses will remain within about 0.1 second of the U.T.2. scale. It is made necessary because of changes in the speed of rotation of the earth, with which speed the U.T.2. scale is associated.

**Joint I.E.R.E.–I.E.E. Symposium on  
“MICROWAVE APPLICATIONS OF SEMICONDUCTORS”**

UNIVERSITY COLLEGE, LONDON, 30th JUNE–2nd JULY 1965

OUTLINE PROGRAMME

The papers listed under each Session are not complete: in most cases two or three more papers and short contributions will be included in the final programme which will be sent to those registering to attend.

**Wednesday, 30th June (10.30 a.m.—11.15 a.m.)**

‘Microwave Applications of Semiconductors’—Survey by PROFESSOR G. D. SIMS (*University of Southampton*).

(11.15 a.m.—12.30 p.m.; 2—5.30 p.m.)

**MICROWAVE PROPERTIES OF SEMICONDUCTOR DEVICES**

Papers will include the following:

‘Advances in Microwave Transistors and Mixer Diodes’—H. F. COOKE.

‘Silicon Variable Capacitance Diodes for Use at Low Temperatures’—A. H. BENNY.

‘The Development and Properties of Microwave p-i-n Diodes’—J. G. GISSING.

‘Intrinsic Frequency Limitations for Semiconductor Microwave Devices’—H. V. SHURMER.

‘The Applications of Instabilities in Semiconductors to Microwave Oscillators and Amplifiers’—J. S. HEEKS and C. P. SANDBANK.

‘Acoustic Amplification in Semiconductors’—H. W. HARCOURT, J. FROOM and C. P. SANDBANK.

‘Evaluation of High Quality Varactor Diodes’—D. A. E. ROBERTS and K. WILSON.

‘Varactor Diode Measurements’—F. J. HYDE, S. DEVAL and C. TOKER.

**6–8 p.m.—Symposium Reception**

**Thursday, 1st July (9.30—11 a.m.)**

**p-i-n DIODE CIRCUITS**

Papers will include the following:

‘p-i-n Diode Modulators for the K and Q Frequency Bands’—L. F. BURRY and L. J. T. HINTON.

‘Broad-band p-i-n Diode Switches in the Range 7–16 Gc/s’—N. A. D. PAVEY.

‘Wideband Coaxial Variable Alternators using p-i-n Diodes’—J. R. JAMES and M. H. N. POTOK.

(11.30 a.m.—12.30 p.m.; 2—3.30 p.m.)

**GENERATORS**

Papers will include the following:

‘An Investigation into the effects of Charge Storage on the Efficiency of a Varactor Diode Doubler’—B. C. HEAP.

‘Broad-band Varactor Frequency Multiplier Chains—Fundamental Problems and Realization’—W. HEINLEIN and A. KURZL.

‘Transient Analysis of Varactor Bridge Doublers’—A. UHLIR.

(4—5.30 p.m.)

**TUNNEL DIODE CIRCUITS AND MIXERS**

Papers will include the following:

‘A Tunnel Diode Oscillator with Wide Tuning Range (0.7–4.9 Gc/s)—D. R. PERSSON.

‘An S-band Tunnel-diode Mixer’—S. BASU MALLICK and W. A. GAMBLING.

‘Up-Converter Type Transmitter for Radio Link’—W. KWIATKOWSKI.

**7 for 7.30 p.m. Symposium Dinner**

Friday, 2nd July (9.30 a.m.—12.30 p.m.)

LOW NOISE DEVICES

Papers will include the following:

- 'Noise Limitation of a Helium Cooled Parametric Amplifier for Satellite Communication'—K. GARBRECHT.
- 'Parametric Multi-port Networks for Microwave Signal Processing'—H. B. HENNING.

(2—5 p.m.)

SYSTEMS

Papers will include the following:

- 'Applications of Parametric Amplifiers in Satellite Communications'—H. N. DAGLISH and D. CHAKRABORTY.
- 'Parametric Amplifiers in Radioastronomy'—R. D. DAVIES.
- 'A Survey on Possible Applications of Tunnel Diodes in Antenna Systems'—H. H. MEINKE.
- 'Recent Advances in Microwave Diode Switches and Limiters'—R. TENENHOLTZ.

*Synopses of some of the Papers to be presented at the Symposium*

**Advances in Microwave Transistors and Diodes**

H. F. COOKE. (*Texas Instruments Inc., Dallas, Texas.*)

This paper will discuss solid state microwave devices in three specific areas:

- Microwave power generation with transistors;
- Low noise amplifiers and power amplifiers using transistors;
- Low noise mixers using the Schottky barrier diode.

The advances in performance which will be described are a result of much improved high-frequency characteristics. A number of new technologies now being applied to semiconductor fabrication have made possible the many improvements which give better device performance.

**Silicon Variable Capacitance Diodes for Use at Low Temperatures**

A. H. BENNY. (*Ferranti Limited, Wythenshawe, Manchester.*)

The main source of noise in variable capacitance diode parametric amplifiers is that contributed by the diode itself. This noise may be reduced by lowering the temperature of the diode, a convenient operating temperature being the liquefaction point of nitrogen ( $-196^{\circ}\text{C}$ ). At this temperature the cut-off frequency of silicon diodes has been found to be considerably poorer than the room-temperature value.

This paper describes the design and construction of silicon variable capacitance diodes with cut-off frequency at  $-196^{\circ}\text{C}$  as good as, or better than the  $25^{\circ}\text{C}$  value. Such diodes have been operated in an S-band parametric amplifier at  $-196^{\circ}\text{C}$  to give a noise figure of 1 dB.

**The Development and Properties of Microwave P-I-N Diodes**

J. G. GISSING. (*Associated Electrical Industries Limited, Rugby.*)

The course of development of a p-i-n device from the first attempts to use an alloyed wire type power frequency rectifier to the final form of the alloyed sphere diode, type CV7599, is traced. The merits and demerits of the use of an evaporated and alloyed metal film or of solid state diffusion to produce p-i-n devices are discussed and a reference is made to recent methods employing epitaxy.

The equivalent circuit for a p-i-n diode is examined with reference to its form at microwave frequencies, and in terms of the changes due to application of bias. The problems of measurement of the basic diode parameters in its conducting and non-conducting states at microwave frequencies are difficult and the most direct way of allowing the element to terminate coaxial line of suitable dimensions is described.

The necessity to correct the measurements for line attenuation is demonstrated. Such measurements can now differentiate between the basic properties of p-i-n's made by different processes such as alloying, diffusion and epitaxy. The order of resistance change attainable with current p-i-n's produced by different processes is indicated.

**Intrinsic Frequency Limitations for Semiconductor Microwave Devices**

H. V. SHURMER. (*Associated Electrical Industries Ltd., Rugby.*)

The upper frequency of operation for a semiconductor microwave device is usually considered in terms of the equivalent circuit parameters associated with the immediate neighbourhood of the active element, together with any stray reactances of the package. Whilst it is generally recognized that in the semiconductor contribution both the resistive and reactive terms may have a frequency dependence, the exact nature of this is difficult to determine experimentally and its importance is generally obscure. This paper seeks to give a brief survey of the various mechanisms which can conceivably introduce frequency dependent effects and attempts to gauge which of them is likely to be important in devices of present interest—crystal valves, varactors, tunnel/backward diodes and p-i-n switches. The mechanisms discussed include such items as skin effect, carrier/phonon collisions, dielectric relaxation, carrier lifetime, transit time, etc.

**The Application of Instabilities in Semiconductors to Microwave Oscillations and Amplification**

J. S. HEEKS AND C. P. SANDBANK. (*Standard Telecommunication Laboratories, Harlow, Essex.*)

The type of oscillation obtained in GaAs and InSb (the Gunn effect) represents one of the most important advances leading to the use of bulk semiconductor devices at microwave frequencies. The oscillations occur when the d.c. field across a thin wafer of the semiconductor exceeds a well defined threshold. This causes a current instability associated with a sharp voltage step to move through the crystal.

This paper describes work aimed at a better understanding of the effect so that the full potentialities of devices might be realized. Coherent signals at repetition rates of 50 Mc/s to 4 Gc/s and peak powers up to 10 watts have been studied. The technique for studying the instabilities is to apply a short trigger pulse superimposed on the d.c. drive. By independently varying the amplitude of the triggering pulse and the d.c. drive, the conditions around the threshold are investigated. Using this technique to trigger only one cycle of operation, it is shown that instabilities of increasing amplitude are launched across the specimen as the d.c. field is raised towards the threshold for self-oscillation. There is a certain minimum d.c. field required if instabilities are to be launched across the specimen by the trigger pulse. This minimum field corresponds typically to 50% of the threshold field required for self-oscillation. The apparent gain observed when operating the device in the triggered mode suggests ways in which devices may be used for amplification as well as oscillation at microwave frequencies.

**Acoustic Amplification in Semiconductors**

R. W. HARCOURT, J. FROMM AND C. P. SANDBANK. (*Standard Telecommunication Laboratories, Harlow, Essex.*)

If the application of semiconductors is to be extended to microwave frequencies, the limitations due to electrode capacitance and transit time must be overcome. To a certain extent this can be done by reducing junction size and using majority carriers where possible. However a much more sophisticated way of overcoming these difficulties is to try to realize, in semiconductors, the type of continuous interaction obtained in travelling wave tubes.

In the paper the present state of the art on acoustic amplification in semiconductors is reviewed. Although net gain at microwave frequencies has not yet been obtained, the experiments at lower frequencies have given some general indications about the feasibility of achieving this. The main problems lie in coupling into the crystal in such a way that the insertion losses are minimized and the shape of the acoustic wavefront within the crystal is not disturbed. The amplifiers described use quartz transducers to couple into and out of a CdS crystal. Recently, deposited CdS transducers have been operated at X band for this type of application. This suggests that there are reasonable chances of making low loss delay lines and ultimately amplifiers for microwave applications.

The importance of the acoustic amplifier as a diagnostic tool, leading to a better understanding of other microwave phenomena in semiconductors, is discussed briefly. The experiments relevant to the mechanism of the Gunn effect are reported in the paper on microwave instabilities in semiconductors.

**Varactor Diode Measurements**

F. J. HYDE, S. DEVAL AND C. TOKER (*University College of North Wales.*)

The effects of losses in the measuring systems on the values of the small-signal parameters have been investigated experimentally for the well-established relative-impedance method originally described by Harrison and Houlding. Both silicon and gallium arsenide diodes have been considered. Measurements have been made using coaxial components in the u.h.f. band and microwave components at X-band and the results correlated. A comparison is made with results obtained using De Loache's transmission method at X-band.

**Evaluation of High Quality Varactor Diodes**

D. A. E. ROBERTS (*Mullard Research Laboratories*) AND K. WILSON (*A.S.M. Wembley Laboratories.*)

Recent measurements procedures used between 1 Mc/s and 40 Gc/s in evaluating very high cut-off frequency varactor diodes are discussed. The types of measurement are: bridge measurements at low frequencies, microwave coaxial line measurements, a transmission method near the diode series resonant frequency, and a transmission method at diode parallel resonance.

Typical results from each type of measurement are given. The effect of bias on the parameters of the simple equivalent circuit is described.

Correlation of data from the four types of measurement has led to the adoption of a new equivalent circuit for the varactor, which recognizes the effect at the junction of stray capacitance.

Some attempt is made to relate parametric amplifier performance to the results of diode measurements.

**p-i-n Diode Modulators for the K and Q Frequency Bands**

L. F. BURRY AND L. J. T. HINTON. (*E.M.I. Electronics Ltd., Hayes, Middlesex.*)

An experimental investigation into extending the operation of p-i-n diode modulators from 18 Gc/s to 40 Gc/s is described. Wafers of stacked p-i-n diodes are considered but most success is achieved with arrays on unencapsulated post-mounted diodes. By reducing the dimensions of diodes of this type used at lower frequencies, broad-band modulators can be designed to operate at frequencies up to 30 Gc/s. A minimum on/off ratio of about 10 dB and an insertion loss of 2 dB can be obtained over a 1.5 to 1 band of frequencies.

Operation at frequencies higher than about 30 Gc/s is at present restricted by a resonant condition in the p-i-n diode microwave circuit.

**Broad-Band p-i-n Diode Switches in the Range 7 to 16 Gc/s**

N. A. D. PAVEY. (*Royal Aircraft Establishment, Farnborough, Hampshire.*)

It is shown that the bandwidth of a microwave p-i-n diode switch is limited by reactances which are partly inherent in the diode and partly result from the mechanism of coupling into the transmission line. Three techniques to optimize switch performance over a given bandwidth are described. These are:

- (i) The choice of a suitable transmission line geometry to minimize reactive effects;
- (ii) Local tuning of the diode using reactive transmission line elements;
- (iii) The employment of multiple diodes in a filter configuration.

Design features of a number of microwave switches using CV7599 diodes are described, and the performance of an experimental broad-band switch is given. This switch has an insertion loss of approximately 1 dB and an attenuation of at least 20 dB over the frequency band 7 to 16 Gc/s.

**An Investigation into the Effects of Charge Storage on the Efficiency of a Varactor Diode Doubler**

B. C. HEAP. (*Department of Electrical Engineering, University College, London.*)

A paper on power dissipation in fourpole networks by A. Weissfloch is adapted to calculate the power dissipation in the input and output matching networks of an experimental varactor doubler and therefore to calculate the true input and output powers from semiconductor bulk material.

Experimentally measured values of input and output power for specified biases are then compared with predicted values for the same biases calculated using an approximate analysis suggested by D. B. Leeson which assumes a non-linear depletion layer capacitance mechanism for harmonic generation.

Reasonable agreement is achieved at power levels and biases which do not involve forward conduction. At high power levels the results show that if charge storage does occur when forward conduction takes place then it does not enhance the efficiency to any greater extent than could be accounted for by depletion layer non-linearities.

An analysis of the impedance changes of the varactor diode under high power conditions shows that this could account for the decrease in power loss in the surrounding circuits and could well explain the large increases in overall efficiency of the harmonic generator under these conditions.

**Wideband Coaxial Variable Attenuators Using p-i-n Diodes**

J. R. JAMES AND PROFESSOR M. H. N. POTOK. (*Electronics Branch, Royal Military College of Science, Shrivenham.*)

Using a conventional equivalent circuit for a p-i-n diode, a computer program has been written which permits the compilation of data for use in designing a coaxial wide band variable attenuator. Measurement on attenuators designed from the data agree well with calculated results. The data can also be used to design strip line attenuators and levellers.

Effects of inductance and capacitance are considered and steps taken to reduce the inductance are described.

**Broad-band Varactor Frequency Multiplier Chains—Fundamental Problems and Realization**

W. HEINLEIN AND A. KURZL. (*Siemens & Halske AG, Central Laboratory, Munich.*)

Broadbanding multipliers require the use of multiple tuned circuits, at least for input and output frequencies. In general frequency selectivity must be met over several octaves of bandwidth. This condition can scarcely be fulfilled in broadband multipliers with distributed circuitry. Therefore a new circuit technique was developed which is demonstrated with a three stage 3 times multiplier chain of 6 Gc/s output frequency.

The useful bandwidth is determined by the spectral purity of the output signal too. The output signal is more or less deteriorated by noise generated within the varactor multiplier. A model of noise generation showing the physical causes of noise is presented and experimentally and theoretically explained.

Stability problems are discussed and related to varactor properties. Criteria for stability are derived which result in design rules for multiplier circuits. The typical differences between commonly available GaAs- and Si-varactors and the requirements for optimum circuitry are discussed.

**Transient Analysis of Varactor Bridge Doublers**

A. UHLIR. (*Microwave Associates, Inc., Burlington, Massachusetts.*)

A direct digital integration of circuit equations is used to study the transient behaviour of a varactor bridge doubler circuit. A suddenly-applied sine wave is assumed for the fundamental drive and a piecewise-linear varactor characteristic used. The calculation shows that good efficiency and rapid transient response can be obtained for certain ranges of tuning and bias.

Experimentally observed input-output power relations are reproduced remarkably well by theoretically calculated results. These include an abrupt increase from negligible output to high efficiency as output is increased, for fixed bias voltage. Also, instabilities are observed when the power is too high for a given bias. The calculations thus prove that side-effects such as rectification and avalanche multiplication in the varactor diode are not necessary for the presence of spurious oscillations.

**An S-Band Tunnel-diode Mixer**

S. BASU MALICK AND PROFESSOR W. A. GAMBLING. (*Department of Electronics, University of Southampton.*)

The paper describes a theoretical and experimental study of a waveguide-mounted, S-band, tunnel-diode mixer. In designing a mixer the d.c. characteristic of the tunnel diode is first measured, from which the conductance/voltage and the equivalent shot noise current/voltage curves are obtained. In the presence of local-oscillator drive the dynamic conductance and the equivalent shot noise current can each be expressed as a Fourier series, and using a 24-ordinate scheme the appropriate Fourier coefficients are derived. A computer is used to determine values for the gain, bandwidth and noise figure over a wide range of parameters such as source and load impedances, d.c. bias and local-oscillator amplitude. From these results the optimum operating conditions and circuit parameters are obtained. Measurements have been made of gain, noise figures, bandwidth, dynamic range, etc. and are compared with the computed results.

**Up-Converter Type Transmitter for Radio Link**

W. KWIATKOWSKI. (*Standard Telecommunication Laboratories Ltd., Harlow, Essex.*)

An up-converter suitable for use as the transmitter of a 4 Gc/s f.m. radio link is described. The output of the transmitter is 1 watt. Some theoretical consideration regarding overall efficiency and bandwidth are discussed together with the characteristics of the i.f. and r.f. circuits. The up-converter transmitter described combines the features of high efficiency, ease of adjustment and freedom from spurious responses. The results of some overall performance tests are given.

*Continued on p. 312*

# Seismic Recording Techniques in Oil Prospecting

By

D. W. N. DOLBEAR, Ph.D.†

*Presented at a Symposium on "Modern Techniques for Recording and Processing Seismic Signals", held in London on 13th May 1964.*

**Summary:** Seismic methods for the detection of underground geological structures have been widely used since their introduction some forty years ago and a large manufacturing and research effort has gone into their development by oil companies and seismic contractors as well as the electronics industry.

Both reflection and refraction methods are practicable and details are given of the various sources of seismic energy, geophones, amplifiers, recorders and methods of presentation that are available. The design and operation of these are discussed in relation to the type of signal and the background seismic noise. Analogue systems are most widely used but in recent years digital recording and analysis has been introduced in attacking prospecting problems that are more easily solved numerically.

## 1. Introduction

Gas, oil and water exist in the ground in the pores of the rock. When the strata are of a suitable shape and are capped by a layer impermeable to these fluids, separation under gravity occurs. These rock structures may be some hundreds of feet high and some miles long and wide but at a depth below the surface of thousands of feet. Should the porous rock be permeable enough to allow the flow of the oil or gas such a structure is a potential oil or gas field.

A simple anticline was the first structure to be recognized as an objective for exploration but many other types of trap exist. All of these can be detected with varying degrees of certainty by seismic prospecting methods. It is emphasized that the structure, not the oil, is detected and when drilled it may contain only water.

Although the geology may be relatively simple, acoustically the layers are often complex and frequent increases and decreases in the velocity of sound occur with depth.<sup>1,2</sup> Figure 1 shows this variation over an interval of 900 ft in a borehole in England. Not only these changes in velocity but also any changes in density produce changes in acoustic impedance which are the discontinuities that are used in seismic prospecting. Elastic waves are generated near the surface of the ground by some means, generally by the detonation of an explosive charge, and the analysis of the travel times of particular wave groups which are detected at the surface after reflection or refraction in the rock yields the slope and depth of the principal layers.

† The British Petroleum Company Ltd., BP Research Centre, Sunbury-on-Thames, Middlesex.

## 2. Reflection Work

### 2.1. Shot, Cable and Geophones

Reflection prospecting uses the reflection at nearly vertical incidence of compressional waves within a bandwidth of, say, 10 c/s–100 c/s. A number, generally twelve, of seismometers, or geophones as they are called, is arranged in a line on each side of the shot point. The spread covers a distance of about

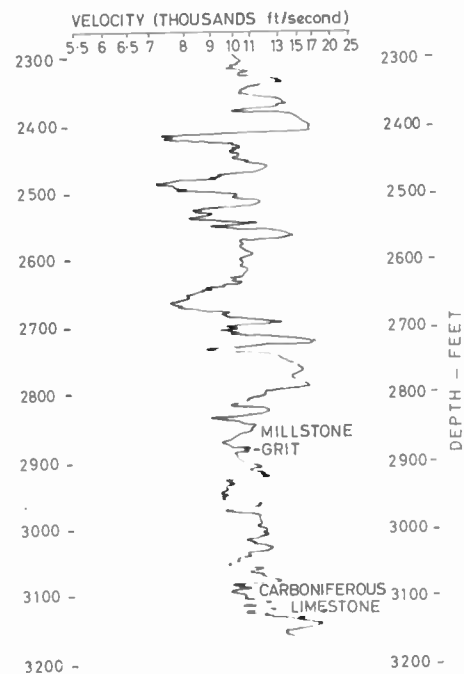


Fig. 1. Velocity log over a 900 ft interval of a borehole.

half a mile and reflections may be received from a depth of as much as 10 000 ft or 20 000 ft (3000 m or 6000 m). Half the spread is then moved and the next shot detonated at the centre point of the new spread; and so on.

A commonly used charge is about 20 lb (10 kg) of dynamite loaded into a shallow, drilled hole perhaps 50 ft (16 m) deep to get below the weathered layer. The hole should not be allowed to blow out as the debris interferes with the recording of the signal. The shots are often multiple,<sup>3</sup> that is, a pattern of small charges is detonated rather than a single larger charge, with the object of improving the signal/noise ratio under particular circumstances.

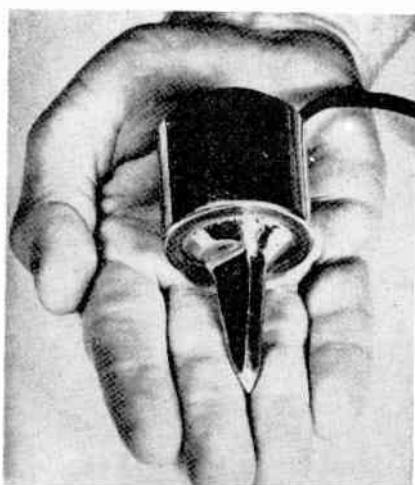


Fig. 2. Reflection geophone.

As there is a large component of low frequency noise at about 10 c/s in the ground motion after the explosion (the so-called ground roll) the natural frequency of the geophones is chosen to be higher, say 20 c/s, in order to filter out much of this motion. Just as the shot may be arranged in a pattern so the geophones, too, may be spread over a considerable area, as many as 36 small geophones being connected in a series/parallel arrangement to a single amplifier.<sup>4,5</sup> The geophones are moving-coil transducers each damped with a parallel resistor if necessary. Their design is such that they are rugged, keep a constant natural frequency and sensitivity and have no unwanted resonances to affect the output—sensitivity to horizontal vibrations is particularly undesirable. As Fig. 2 shows they are physically small and a seismic party may have as many as 1000.

The multi-core cables used for this work have connectors at each end so arranged that, with a choice of input sockets at the vehicle, the geophones

are connected to the appropriate amplifiers in spite of the change in observing position with successive shots. There are 13 twisted pairs and an insulated straining wire within a strong plastic sheath. Each pair is taken in turn at about 120 ft intervals to external tapping-points or 'take-outs' to which the geophone leads are temporarily clipped.

For so-called 'multiple cover',<sup>6</sup> when several shots at different positions are used for the same reflection point, switching boxes are used by the observer to enable each of the 24 amplifiers to be connected to the appropriate geophone position.

Multiple shots, geophone patterns and multiple cover are some of the field methods used to improve the signal/noise ratio. The term 'noise' includes unwanted multiple reflections from below the surface of the ground,<sup>7</sup> shot-induced reflections from elsewhere than vertically below the geophone spread, and any seismic disturbances produced, for example, by traffic or the wind.<sup>8</sup> Some thoughtful experimental work is often required to obtain optimum results and a considerable literature has accumulated on this side of the field operations.

## 2.2. The Signal and Analogue Amplifiers

In the more developed areas pick-up of mains-frequency signals is likely to occur and this is balanced out in a bridge arrangement on each channel before the input transformer. At this point the lines can be checked for open and short circuits. The input transformer matches the line and source impedance into the amplifier and converts the floating input to single-ended. These transformers are high-grade components with an excellent low-frequency response and well shielded with several screens of mu-metal.

Before discussing some details of the reflection amplifiers it is desirable to comment on the nature of the signal received from the geophones. In Fig. 3 is plotted the peak-to-peak amplitude recorded by two amplifiers using 4.5 c/s geophones under different filtering conditions with time variable gain. From the background level of 20  $\mu$ V the signal rose to a maximum of about half a volt soon after the shot instant. The wide band record still showed a predominantly 10 c/s signal 3 seconds later and even after 8 seconds the original background level was not regained; whereas the signal on the filtered record (30–60 c/s) returned to background after 3 seconds.

Such data vary with the nature of the ground—this record was taken in a fen district where the unsteady ground doubtless accounts both for the persistence of the low-frequency ground roll and the high level of background noise.

The sudden increase in signal by a factor of 10 000 or so and the rapid change in level afterwards pose the

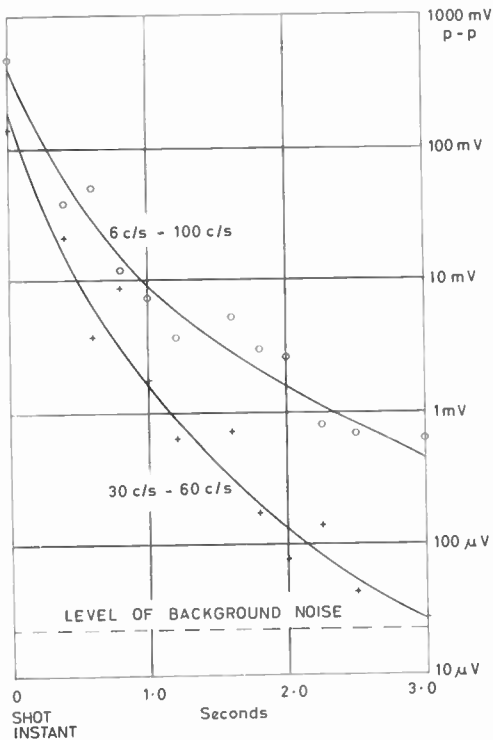


Fig. 3. Change of reflection signal level with time after the shot instant.

main technical problems. The dynamic range is too great for conventional analogue systems.

In order to avoid overloading of the amplifier at any stage in the record yet to keep the record easily readable, recourse is had to two practices, automatic gain control and initial gain suppression.

One method of providing a.g.c. over the required range uses the rectified signal from the output of the amplifier to provide a varying d.c. bias which controls the current in two double diodes which are normally cut-off.<sup>9</sup> These diodes shunt the incoming signal at the grids of two of the amplifying stages. Matching of diodes, bias batteries and other components is required for an acceptable performance.

An alternative method is to use the output, when further amplified, to increase or decrease the intensity of a small lamp which illuminates pieces of semiconductor material.<sup>10</sup> The semiconductor can be used as series or shunt resistors at suitable points in the amplifier circuit. A control range of 120 dB is achieved.

On either system a choice of compression or expansion times is often available, the time constants lying between, say, 50 and 500 ms. That is, the circuit may be set to give, for example, a fast compression but a slow expansion of gain.

Such an a.g.c. system is not suitable by itself for the conditions of working. Clearly before the detonation of the charge, when the geophones are picking up only background noise, the gain would be high and the sudden onset of energy immediately after the explosion would saturate the amplifiers. To avoid this, *initial gain suppression* is employed. This involves feeding into the first stage of the amplifier a signal from an oscillator at a frequency high enough (5–10 kc/s) so that none will appear on the final record owing to the high-cut filtering in the output stage. Any intermediate high-cut filter is by-passed for this frequency. The high frequency output is taken to the a.g.c. amplifier and control circuit which has already been described. Thus the same a.g.c. action occurs but using this artificial signal whose level can be separately controlled in each amplifier. The suppression signal can be removed simultaneously from all amplifiers by using the first break of seismic signal from a chosen channel (e.g. one farthest from the shot) or any other signal to open relay contacts—the so-called ‘trip’. The individual controls allow for giving more suppression to those channels nearest the shot where the signals will be of greatest amplitude. Time delays are generally available for use both at ‘trip’ and for the removal of suppression. The rate of removal is also variable.

The level of the suppression signal can be controlled by the integrated seismic energy on one channel which thus controls the gain of all the other channels. The suppression technique can also be used as the control in programmed gain applications. In the latter, skilful adjustment eliminates the need for a.g.c. in the ordinary sense.

The quiet record before the first breaks resulting from the use of suppression increases the accuracy to which the time of arrival of the first breaks can be read. This time is used as one of the corrections in the interpretation of the record.

A wide choice of low-cut and high-cut filtering is available in all types of analogue reflection amplifiers although in these days of magnetic recording it is perhaps less important than formerly when the use of filters could make or mar the once-for-all oscillograph record. Filtering is, of course, extensively used on playback as are suppression and a.g.c.

Both valve and transistor amplifiers are used. Little need be said here about the relative advantages and disadvantages but portability, ruggedness, versatility, reliability, power consumption, complexity, and sensitivity to climatic conditions are some factors of importance. A typical valve amplifier may have two or three double-triodes and two double diodes, excluding a central control amplifier common to all the seismic channels.

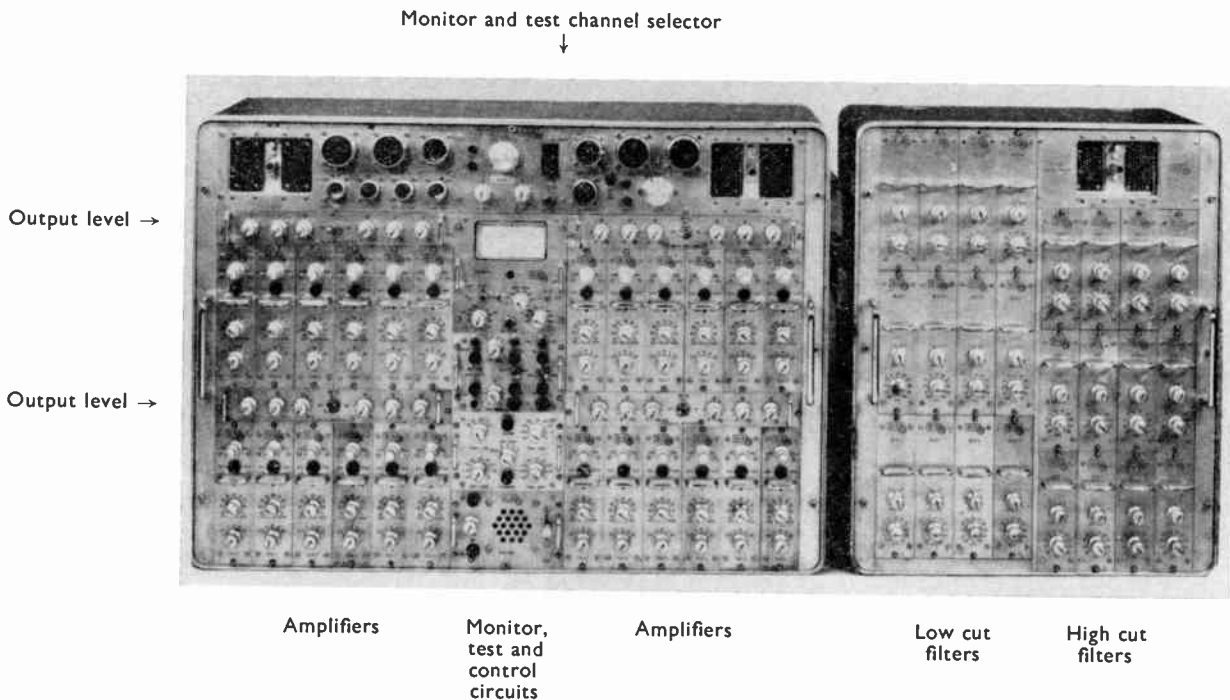


Fig. 4. Transistorized reflection equipment—SIE PT-100 (24 channels).

As an example of a recent transistorized design Fig. 4 shows the S.I.E. PT-100. The unit on the left includes the 24 amplifiers and, in the centre, the control circuits common to them all. The low-cut and high-cut filters are mounted in the right-hand unit. Each amplifier has 27 transistors plus a number of other semi-conductor elements. Photo-resistors are used for a.g.c. and suppression. Although germanium transistors are used, temperature compensation circuits allow operation up to an ambient temperature of about 120°F.

The input impedance is 500 ohms and the frequency response with a.g.c. off is 5 c/s to 500 c/s. There is a choice of four a.g.c. speeds with control for inputs from 1  $\mu$ V to 1 V; additional circuits control unusually large or small temporary changes in signal. A choice of eleven low-cut and ten high-cut filter frequencies is available.

2.3. Analogue Recorders

Formerly the records were taken only on photographic paper oscillographs as in Fig. 5 and these are

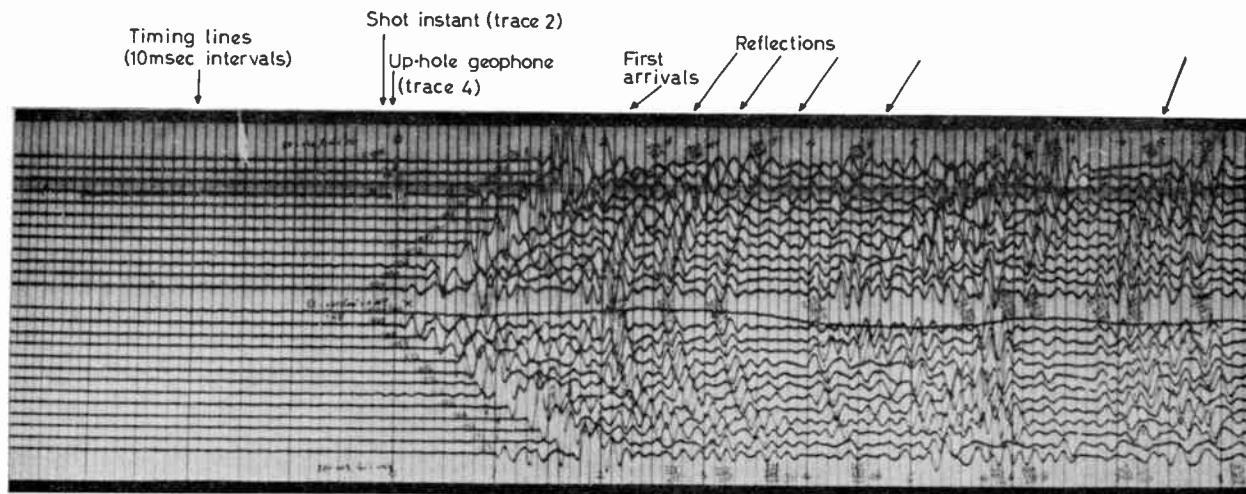


Fig. 5. Oscillograph reflection record.

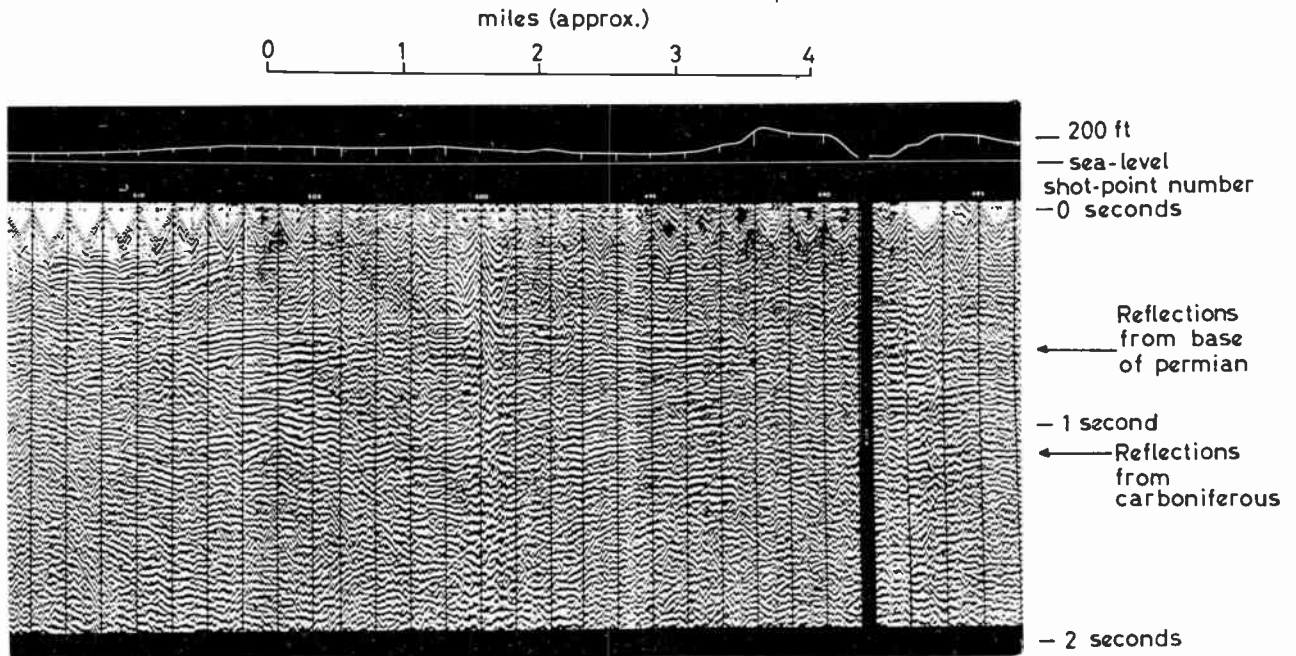


Fig. 6. Corrected variable density reflection cross-section.

still widely used. They contain 25 or 50 small moving-coil galvanometers each  $\frac{1}{8}$  in in diameter with a natural frequency of 100 to 200 c/s. Each is damped with a shunt resistor. The paper width is 6, 8 or 10 in and the paper speed for reflection work is 12 or 15 in/s. Accurate timing lines are flashed on the paper at 10 ms intervals by a rotating cylinder whose speed is controlled by a tuning fork. The timing accuracy is 1 part in 5000 or so within the temperature or voltage range normally encountered.

As already mentioned, records are now taken almost invariably on magnetic tape. This may be mounted on a drum or moved across a flat bed and a choice of direct recording with a.c. bias, pulse width or frequency modulation is available in different equipments. The tape speed is mostly  $7\frac{1}{2}$  in/s and tape width varies from  $2\frac{1}{4}$  in for two 14-track heads interleaved to 7 in or  $7\frac{1}{2}$  in for 27 heads individually movable along the tape. The operator will normally try to record so as to use most of the dynamic range on the recording medium, any further control being imposed at the playback stage. The same heads write and read.

For monitoring or for field playback the tape output may be fed into the seismic amplifiers again, using the movable heads for putting in corrections for the geometry of the geophone spread, velocity in the weathered layer, etc. The control of these heads may be with cams or servomotors. The immediate interpretation can then be carried out on this corrected

record which can be made on an oscillograph of the type described above or on a special camera which produces a variable-area or variable density record. Many records can be placed side by side as in Fig. 6. The individual shot-points, and therefore records, are numbered along the top and the surface relief and shot-hole depth are shown graphically. The correlation from record to record of the wave-groups is very striking and gives a useful impression of the changes in the sub-surface geology. A wide river is the cause of the gap in the section. Major changes in the strata, faults, salt-domes, etc., show clearly in this type of representation.

#### 2.4. General Performance

It is clear that since the basic measurement is time correlation the individual parts of the whole chain from geophone to recorder must be well matched between channels. It is generally accepted that the scatter in time-shifts due to the response of geophones, transformers, coupling circuits, filters, a.g.c., galvanometers and write and read amplifiers shall be not more than about 1 ms for the type of signal received. Tolerances of from  $\pm 2\%$  to  $\pm 5\%$ , depending on the particular component, are required to achieve this.

Because of the large signals that can occur at the input and the wide frequency band of interest, harmonic distortion can be troublesome. Cross-feed

between amplifiers must be low. Power supply impedances (including the common leads) are the usual built-in causes of cross-feed but wet and leaking cables and geophones give intermittent faults of this kind. Undamped resonances, particularly in geophones and galvanometers, are occasionally found and are particularly undesirable.

### 2.5. *Digital Conversion and Recording*

In recent years several oil companies and seismic contractors have been independently developing digital recording of seismic data with subsequent digital processing.

Programmed gain preamplifiers are required for two reasons: firstly, to raise the level of the geophone output to that specified for the digitizing equipment (typically  $\pm 10$  V), and second, to ensure that when the later, low-level signals are digitized they yield a reasonable number of bits. In addition these pre-amplifiers can filter the input signal to get rid of unwanted low and high frequencies which convey no useful seismic information. Otherwise the low frequencies, such as the ground roll, would use up dynamic range to no purpose; and the high frequencies would provide an unresolved noisy background to the highest frequency that can be analysed at the pre-determined sampling rate.

The outputs from the 24 pre-amplifiers are then switched in sequence by a high-speed multiplexer to a sample-and-hold unit at a rate which gives the bandwidth required (e.g. d.c. to 100 c/s). The analogue-to-digital converter must be presented with a constant input potential when operating and the sample-and-hold unit provides this. The switching time from sample to hold is finite so that the potential stored is within the range of values through which the input passes during the 'aperture time'. This results in the output of the converter being in error by an amount which increases with input frequency, amplitude and aperture time. Sample and hold units with an aperture time of less than  $1 \mu\text{s}$  are available and are suitable for reflection seismic work.

A fast 13-bit analogue-to-digital converter may operate at a rate of  $2 \mu\text{s}/\text{bit}$  plus  $2 \mu\text{s}$  and has an accuracy approaching 0.01% with a correspondingly low input noise level (13 bits is equivalent to  $\pm 4095$  on the decimal scale). To achieve this accuracy the multiplexer and sample-and-hold must be allowed adequate settling time and after allowing for this, with 24 input channels and a scanning rate of 1000/s in each channel, the converter is working at almost full capacity.

The dynamic range using such equipment is thus about 80 dB, a considerable improvement over any analogue recorder even under laboratory conditions.

The digitized information can be written on the magnetic tape in a number of formats. The simplest is to write each 13-bit word together with clocking, parity, etc., as a single character across the tape. This allows monitoring of records to be done, one channel at a time, easily and cheaply by simple logic and a digital-to-analogue converter feeding an amplifier and single track pen recorder. A more complex monitoring assembly will, of course, allow all 24 channels to be monitored simultaneously. Monitoring would normally be regarded as essential when the data processing is done elsewhere. Such a record would require either to be edited on replay into a format suitable for computation in a standard, general-purpose computer; or, if the economics justify such a step, a special-purpose computer might be designed.

Alternatively the field record might be produced directly in computer format. Monitoring is then more difficult and the field equipment becomes more complex and more expensive.

The same equipment can obviously be used to convert analogue records to digital form. This is being done by some companies in preference to direct digital recording of the geophone output.

Apart from the increase in dynamic range the interest in digital recording arises from the sophisticated approach to data analysis that is then possible.<sup>11</sup> Small amplitude events can be picked for correlation from larger amplitude noise more exactly than by analogue methods and numerical correlation, numerical corrections, numerical and inverse filtering are often more easily performed. Much effort is now being devoted to the programming side.

### 2.6. *Alternative Energy Sources*

A very large proportion of the work in seismic exploration is done by the method outlined above using an explosion as the source of seismic energy, but alternative sources are available. The dropping of a heavy mass (3 tons from 10 ft) on the ground,<sup>12</sup> a gas explosion in a heavy, inverted vessel resting on the ground, and the forced vibration of the ground by a programmed mechanical or electro-magnetic vibrator<sup>13</sup> are all in use. These are useful sources for work in towns or areas of hard outcrop where the drilling of shot-holes would be expensive or unpopular.

Such low-intensity sources are essentially repetitive and require a different recording technique from the conventional method. The signal is not much above background noise and may indeed be considerably below so that many recordings properly aligned in phase must be added to enhance the signal relative to the noise. An elegant way of doing this is a direct-recording magnetic drum with ten narrow, write heads which record ten successive records in phase

side by side. These records are then simultaneously read by a head of normal width which therefore sums all ten tracks. The output from this head can be recorded on a further narrow track and so on. Thus multiplicities of a hundred or so are not difficult to achieve for each geophone position.

The seismic amplifiers in these low-energy techniques are much simpler than those already described. Since the dynamic range of the signals along the record is small and there is no large onset of energy at the beginning, suppression and a.g.c. are not required.

The third system imposes a frequency-modulated wave on the ground rather than a sharp pulse. The frequency may change from, say, 15 c/s to 90 c/s in seven seconds and such frequencies are transmitted by the ground without any major change in their character. The final presentation is obtained by analogue cross-correlation of the original signal with the complex record composed of many small-amplitude signals of this kind in varying phase relationship and the background noise.

Large geophone patterns are used as well as source multiplicity in these techniques.

### 3. Refraction Work

The refraction method as used in the exploration for oil is essentially a long-range technique.

#### 3.1. *The Shot, the Signal and the Geophones*

A large charge of 1000 lb or so (500 kg), which may be loaded into many holes for ease in drilling and efficiency in propagation, is exploded perhaps 12 miles (19 km) from the line of 24 geophones which are themselves 1000 ft (330 m) apart. The sound wave spreads out and produces local reflections and refractions but if there is a deeper, high-velocity layer and the geophones are far enough away the first arrival at these points is the energy from this layer. The shot instant is transmitted to the observing van by radio which also provides a communication link between observer and shot-point.

If there are several successive layers of increasing velocity there may be later arrivals on the record which will occur as first arrivals if the distance between shot-point and geophones is further increased. Correlation between records often enables them to be picked out even when they are not the first arrivals.

The signals are of lower frequency than in reflection work and a band-pass of 1 c/s–60 c/s is required to cover all exploration areas.

The impedance of the geophones is, typically, a few hundred ohms and the cable resistance for the farthest geophones may bring up the source impedance to, say, a thousand ohms. This variation in

total source impedance may be corrected by additional resistors in the input of the amplifiers if it would result in unacceptable phase or sensitivity differences between channels.

The natural frequency of the refraction geophones may be as low as 1 c/s but these must be clamped during transport and positioning to avoid damage. A higher natural frequency (2 or 3 c/s) has an advantage in this respect since continued serviceability is required and non-technical local staff normally handle the geophones.

The amplitude of the signal, as well as depending on the transmission characteristics of the sub-surface will be determined by the amplitude of the seismic background noise. In quiet desert areas the noise signal may be as low as a fraction of a microvolt in terms of the impedance already mentioned. Relatively small charges can then be used and a satisfactory signal/noise ratio still obtained. In more noisy areas the charge, and therefore the signal, is proportionately increased.

#### 3.2. *Amplifiers*

All electrical noise associated with the equipment must be kept low compared with the signal corresponding to the seismic background noise of desert areas. As well as being technically satisfying this is economically important as explosive, especially if it has to be transported for thousands of miles, is expensive. This is a stringent specification and particular attention has to be paid to the design of the input stages, battery connections, the type of plug and socket, the lay-out of common leads, cross-feed between amplifiers and the absence of parasitic oscillations.

As the dynamic range of the signal along the record is small, straightforward high-gain amplifiers suffice. A choice of high-cut filters is useful to discriminate against wind-noise and the like.

The variation in input signal along the line and from area to area is accommodated by variable attenuation, some of which is applied at the input and some at a later stage in the amplifier. The first of these does not affect the amplifier noise whereas the second decreases the amplifier noise with the signal.

Both valve and transistor amplifiers are used. In terms of equivalent input noise a transistor input stage has to compete with valve noise decreased by a factor depending on the turns ratio of the input transformer. The design of a competitive transistor amplifier has awaited the manufacture of transistors in which the  $1/f$  noise is much lower than in those originally available. Recent improvements in this respect have been very welcome. Silicon rather than germanium transistors are preferred because of the severe temperature environment to which the ampli-

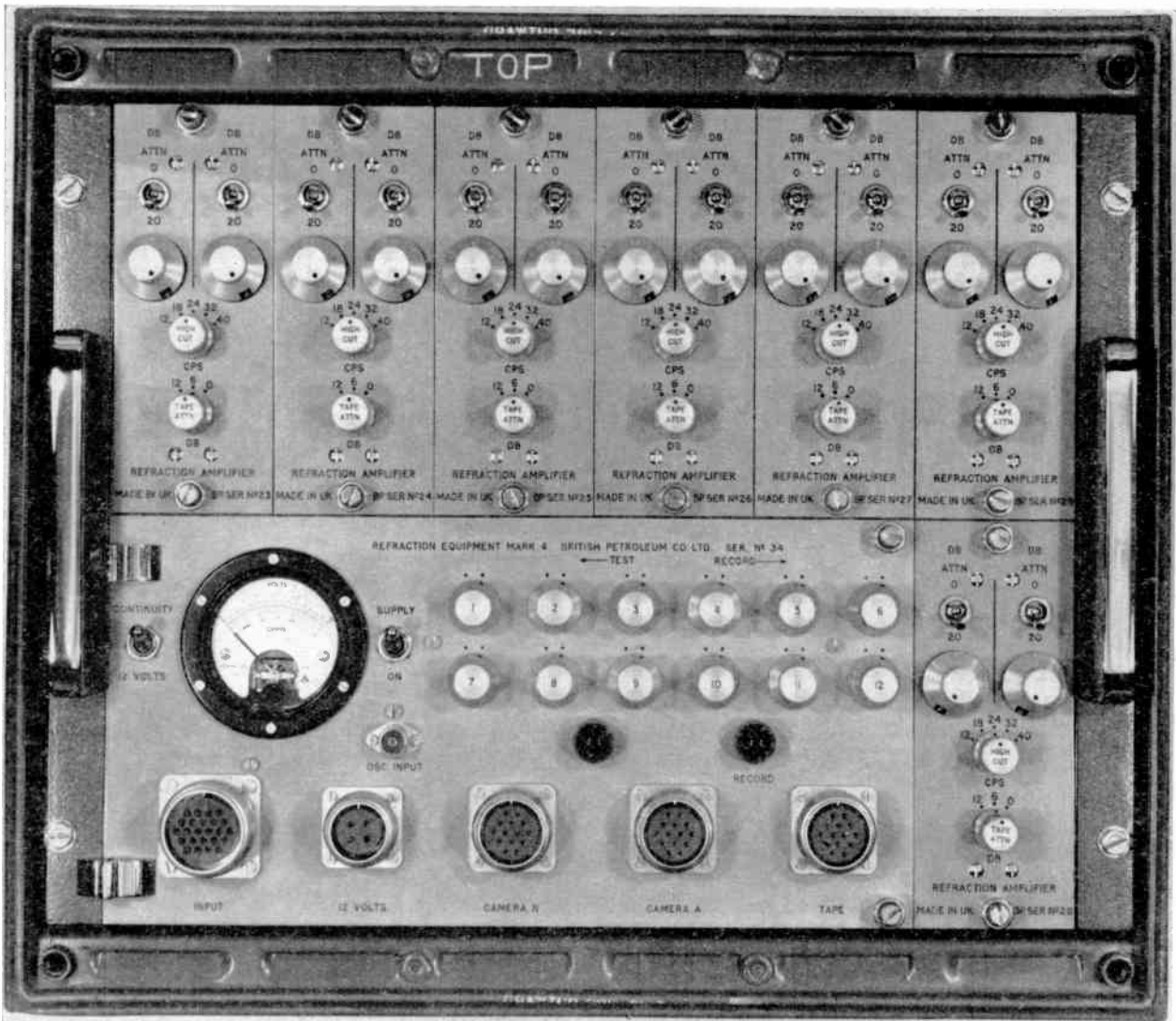


Fig. 7. Transistorized refraction equipment—BP Mark 4 (12 channels).

fiers are exposed—germanium transistors become too noisy at temperatures around 120°F. Much the same tolerances in performance are required as for reflection work but as some applications require the measurement of absolute amplitudes of the first arrivals careful calibration of the sensitivity of each channel is required. This requirement demands reasonable stability in the geophones, cables, amplifiers and galvanometers so that the calibration need be repeated only when one of these is changed.

Figure 7 shows a 12-channel refraction outfit (BP Mark 4) which is fully transistorized. Two of these may be used on a 24-geophone spread separated in order to minimize the amount of cable which is

required. Each sub-unit contains two amplifiers with some of the controls in common and there is a spare sub-unit.

The input impedance is 10 000 ohms so that the effect of variations in cable resistance on sensitivity can be ignored and the equivalent input noise (1000 ohm source) is 0.5  $\mu$ V peak-to-peak measured with a bandwidth of 1–24 c/s. At maximum gain the input without distortion is 100  $\mu$ V and attenuation, in 2 dB steps, up to 60 dB is available. There is a choice of five high-cut filters. Outputs for both galvanometers and magnetic tape recorders are available, the latter being unfiltered. This specification is maintained from 5°F to 150°F.

3.3. *Recorders*

The record is taken on a paper oscillograph of the same type as that used in reflection work but with a paper speed of 6 in/s as the record is rather long in time. Records may also be taken on magnetic tape, generally using frequency or pulse width modulation because of the required low frequency response. Direct recording can be used provided the tapes can be played back at an increased speed so that the lower sensitivity of the heads to long wavelengths on the tape is overcome. An increase of 8 or 16 times is required.

The numerical corrections are made on playback and a variable area record such as Fig. 8 produced of the survey line. With a single refracting layer of constant depth and velocity the effect of the corrections is to align the first arrivals in a straight line from left to right. The geological situation represented by this record is obviously much more complex and a detailed study is required to unravel the changes that are taking place along the line.

Digital recording has also been used.

4. *Work at Sea*

So far we have been concerned only with exploration on the land surface. With increasing demand for oil the effort has extended to cover the shallow seas of the continental shelves. The actual drilling

for oil is then much more difficult and much more expensive, but the search for suitable structures is, in terms of square miles covered, cheaper and quicker at sea.

Most of the seismic work done at sea in oil exploration is by reflection. The ships available for these surveys are owned or hired by contractors rather than by the oil companies. The economics demand full use of the equipment and the ships are suitable for working in any part of the world.

If a single ship is used, in one method of operation the receiving cable, which may be a mile long and contains hydrophones as sensitive elements, is towed from right aft while successive charges are exploded alternately from lines fixed to the port and starboard sides aft. Just before a charge is fired the receiving cable is allowed to run free so that the hydrophones are momentarily at rest in the water while the record is taken. While the next charge is reaching the firing position the cable is winched in to its towing position before again being released for the next shot. A record is taken every few minutes and the ship is stopped only when faults occur.

There is again a choice of analogue and digital systems. Both may be used if this is thought to be desirable. Since the ship machinery continues to operate during the record, analogue magnetic tapes tend to be noisy as these systems are usually sensitive

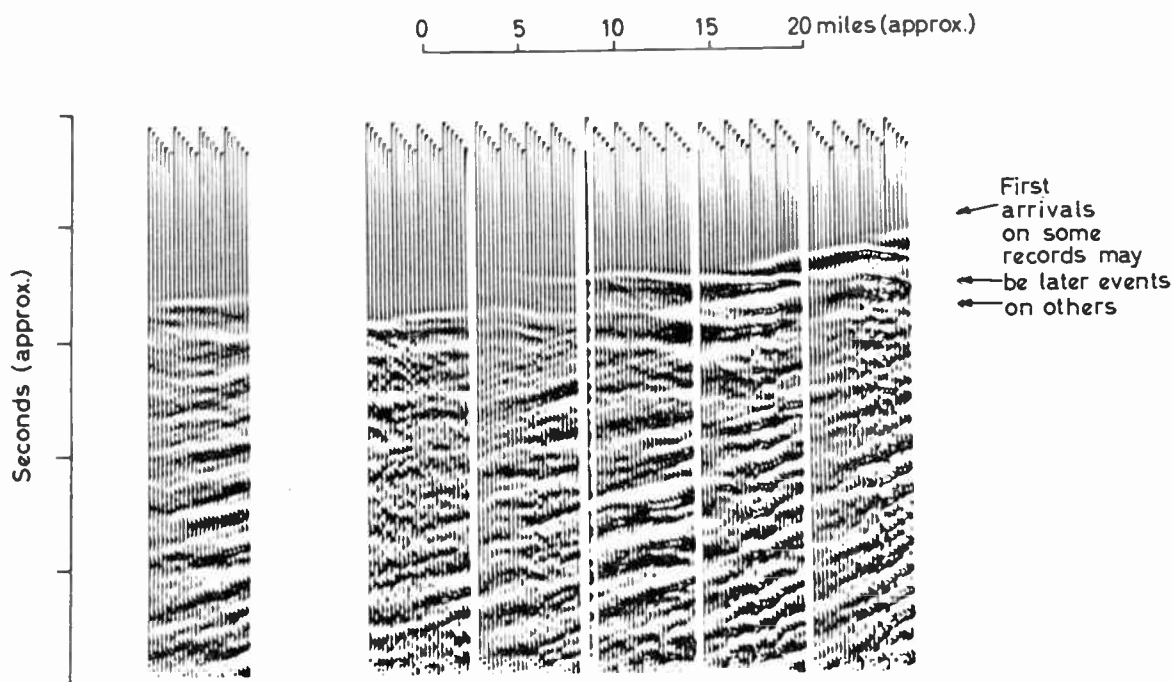


Fig. 8. Corrected variable area refraction cross-section.

to vibrations even when well insulated from the ship's structure. Digital recorders have therefore a substantial advantage in this respect. Smaller explosive charges can be used and the substantially bigger dynamic range eases the observing problems.

One peculiarity of marine reflection work is the occurrence of 'ringing'<sup>14, 15</sup> or large amplitude, interfering signals caused by multiple reflections generally between the sea surface and some deeper layer. At their worst this interference may completely obscure the ordinary reflections on an analogue visual record. While special analogue playback methods have been devised to assist interpretation under these conditions, the greater dynamic range available with digital recording and the flexibility of digital processing enable the difficulties to be overcome more effectively.

The transmission of sound through the sea-bottom is usually very efficient since with a soft bottom there is no sudden discontinuity from water to ground and the coupling between the water and the hydrophones is good. For deep reflections explosive charges are essential but for shallow work high energy spark sources or gas explosions may be used.

Radio navigational systems and ultrasonic depth indicators are in continual use during the survey to obtain the necessary positional and correction data.

Long-range marine refraction has hitherto been almost a monopoly of various academic research groups,<sup>16</sup> but recently the necessary equipment has become commercially available.<sup>17</sup> The signal either from a geophone on the sea-bottom or a neutrally buoyant hydrophone is transmitted by cable to a floating buoy where it frequency-modulates a 5-kc/s sub-carrier. The main radio-frequency carrier is then amplitude-modulated and the signal transmitted with a power of 1 watt. The r.f. carriers from the buoys are crystal controlled and 25 kc/s apart so that the signals can be readily separated by crystal-controlled filters on the receiver.

The receiver and recorder are mounted on the ship which steams away from the line of anchored buoys firing small depth charges at suitable intervals. Successive refraction records are thus obtained of horizons at increasing depth below the sea-bottom. The ranges from the ship to the buoys are based on the time of arrival of the direct water wave.

All the equipment is fully transistorized.

## 5. Acknowledgments

Thanks are expressed to the Chairman and Directors of The British Petroleum Company for permission to publish this review.

## 6. References

1. C. B. Vogel, "A seismic velocity logging method", *Geophysics*, 17, pp. 586-97, July 1952.
2. G. C. Summers and R. A. Broding, "Continuous velocity logging", *Geophysics*, 17, pp. 598-614, July 1952.
3. A. E. McKay, "Review of pattern shooting", *Geophysics*, 19, pp. 420-37, July 1954.
4. L. V. Lombardi, "Notes on the use of multiple geophones", *Geophysics*, 20, pp. 215-26, April 1955.
5. C. H. Savit, J. T. Brustad and J. Sider, "The moveout filter", *Geophysics*, 23, pp. 1-25, January 1958.
6. W. H. Mayne, "Common reflection point horizontal data stacking techniques", *Geophysics*, 27 (Part II), pp. 927-38, December 1962.
7. J. W. Hammond, "Ghost elimination from reflection records", *Geophysics*, 27, pp. 48-60, February 1962.
8. V. A. Olhovich, "The causes of noise in seismic reflection and refraction work", *Geophysics*, 29, pp. 1015-30, December 1964.
9. S. A. Scherbatskoy, "Automatic volume control", U.S. Patent 2,329,558, 1943.
10. F. W. Hefer, "The use of photo-resistive cells as lossier elements in a transistorised seismic amplifier", *Geophysics*, 26, pp. 550-9, October 1961.
11. E. A. Robinson and S. Treitel, "Principles of digital filtering", *Geophysics*, 29, pp. 395-404, June 1964.
12. E. B. Neitzel, "Seismic reflection records obtained by dropping a weight", *Geophysics*, 23, pp. 58-60, January 1958.
13. J. M. Crawford, W. E. N. Doty and M. R. Lee, "Continuous signal seismograph", *Geophysics*, 25, pp. 95-105, February 1960.
14. G. C. Werth, D. T. Liu and A. W. Trorey, "Off-shore singing—field experiments and theoretical interpretation", *Geophysics*, 24, pp. 220-32, April 1959.
15. M. M. Backus, "Water reverberations—their nature and elimination", *Geophysics*, 24, pp. 233-61, April 1959.
16. M. N. Hill, "The Sea", Volume 3, pp. 39-46. (Inter Science Publishers, London, 1963.)
17. J. B. Gurney, "A geophysical telemetry system", *Lucas Engineering Review*, 1, pp. 16-23, October 1964.

*Manuscript first received by the Institution on 9th September 1964 and in final form on 1st February 1965. (Paper No. 980/EA20.)*

© The Institution of Electronic and Radio Engineers, 1965

# An Apparatus for Automatic Quantitative Analysis of Electrolytes by Controlled Potential Coulometry

By

G. HALL, B.Sc.  
(Associate Member) †

**Summary:** An electronic instrument is described which is interesting as an application of the direct application of an electronic servo type system to chemical analysis. An outline of the basic physical chemical principles and of the circuits of the all-transistor control system is given, with a description of a special output circuit to control the smallest overshoot on switch-on of the electrolysis current. Consideration is given to the problems of preventing oscillations in such a system.

## 1. Physical and Chemical Principles

The apparatus described in this paper is used for controlled potential coulometric analysis, a highly precise technique for the determination of elements in solution by electrolytic reduction or oxidation under controlled conditions.

In this technique electrolytic reduction or oxidation is carried out at one electrode of a specially-designed electrolytic cell, the potential of which is accurately controlled with respect to a suitable reference electrode (calomel or silver half cells). The arrangement of electrodes in such a cell is shown in Fig. 1 and a practical arrangement is shown in Fig. 3.

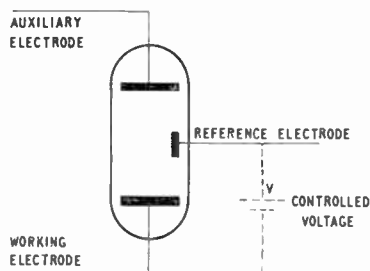


Fig. 1. Electrode arrangement.

The working electrode may be either mercury or a solid metal (e.g. platinum) and can be controlled within the range  $\pm 2$  V. The value of the working electrode potential is chosen by considering the electrochemical potentials of the systems involved and this potential has to be accurately maintained throughout the electrolysis in order to avoid interference from unwanted reactions. The optimum potential can be determined experimentally using solid electrodes with the equipment by means of a 'coulogram'. This is a graph showing the variation in electrode potential with integrated current, and a

† Formerly at the Atomic Weapons Research Establishment; now with the Central Electricity Research Laboratories, Leatherhead, Surrey.

typical example is shown for a mixture of two substances A and B in Fig. 2.

$E^0$  voltages are the standard electrode potentials for the materials concerned and represent the voltage at which equal amounts of reduced and oxidized species are present at equilibrium. It can be seen that any desired fraction of element may be reduced or oxidized by appropriate selection of working electrode potential and in practice for reactions involving a one electron change 100% reduction or oxidation takes place at voltages of  $(E^0 - 0.2)$  and  $(E^0 + 0.2)$  respectively.

Clearly quantitative determinations of A without interference from B is only possible if the difference in their standard potentials is greater than 0.4 V. If this difference is less than 0.4 V then interference results but its extent can be readily calculated provided the working electrode potential is known and remains constant.

During electrolysis the current falls exponentially with time and its integrated value, i.e. the total quantity of electricity involved, in coulombs, is related directly to the amount of material in solution by Faraday's law. By careful correction for background currents and reagent blanks a precision of 0.1% can be obtained.

A comprehensive treatment of the subject is given in references 1 and 2.

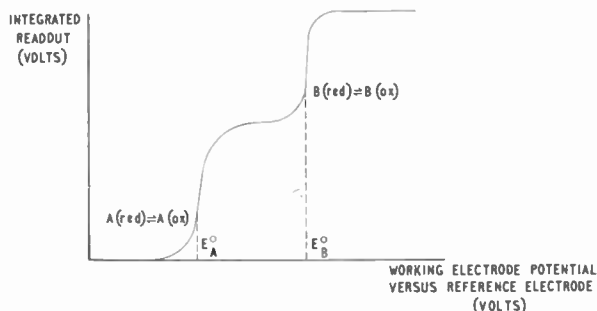


Fig. 2. Coulogram for a mixture of two substances A and B in solution.

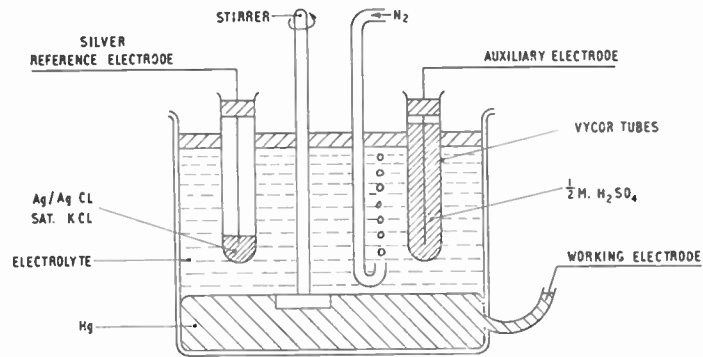


Fig. 3. Typical electrolytic cell.

2. Desired Performance

The earliest experiments in electrochemical analysis used an elementary manual system as shown in Fig. 4. The first automatic systems were those of Kelly, Jones and Fisher<sup>3</sup> and Hickling.<sup>4</sup> These were, in the main, systems where the manually-operated potentiometer was replaced by an amplifier and motor-driven potentiometer and the response was therefore slow. Some later systems<sup>5</sup> have used transistor output stages but no completely satisfactory system existed up to the time of development of this apparatus by the Atomic Weapons Research Establishment, where it has been in use for about three years.

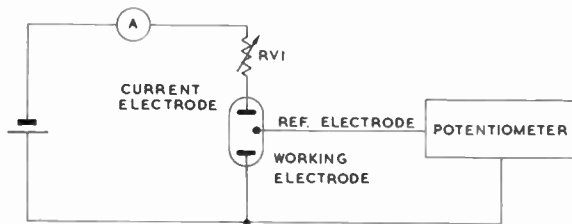


Fig. 4. A rudimentary manual system.

The design requirements were based on experience with earlier models and the requirements were:

1. A d.c. stability and accuracy of voltage at the controlled electrode of  $\pm 1$  mV with  $\pm 5$  mV ripple.
2. Automatic change-over in the machine from oxidation to reduction and therefore a need for centre-zero indicating instruments.
3. No surges of current through the cell or over-voltage at the control electrode at any time during the electrolysis.
4. The controlled current to be 100 mA down to a background current of several microamperes.

5. The whole apparatus was to be capable of being used by laboratory assistants and should be simple and rugged for routine analysis with an automatic read-out from the integrator.
6. The speed of response should be such as to correct for changes of resistance of the electrolyte with stirring which is particularly vigorous in the case of the mercury cathode cell. This stirring can be rapid and introduces alterations of cell resistance at up to several hundred cycles per second.

3. The Apparatus

The overall scheme of the apparatus (Fig. 5) is that of a straightforward control loop with the potentiometer backing off the voltage to be maintained. The difference voltage is amplified to operate the controller which varies the cell current and the integrator measures the total amount of charge which has passed during the experiment.

3.1. Amplifier

The resistance of the reference electrode varies from a few hundred ohms to 50 k $\Omega$  and it was thought that the input to the amplifier should have an impedance of greater than 100 k $\Omega$ . Also the input should

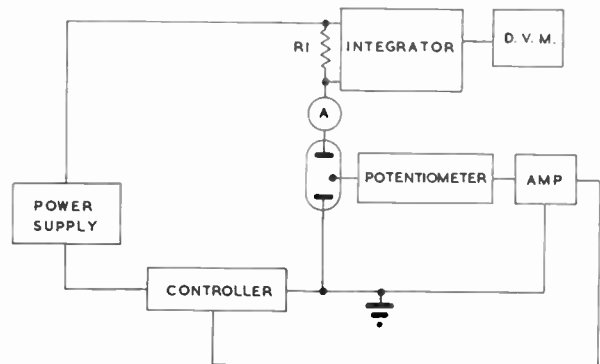


Fig. 5. Block diagram of apparatus.

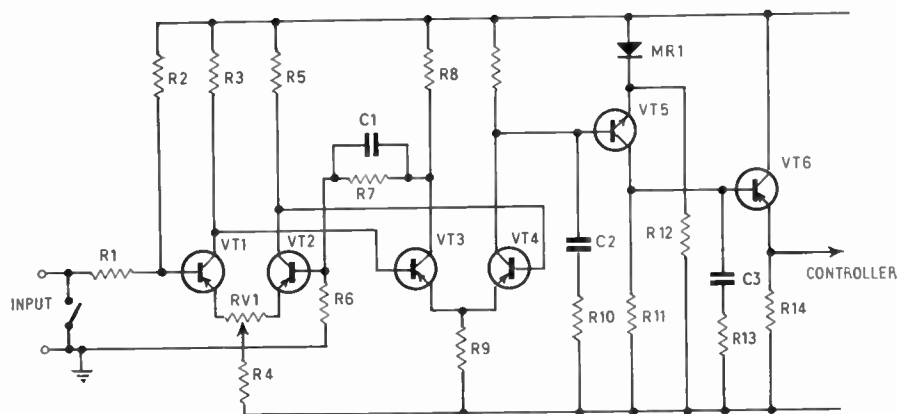


Fig. 6. Schematic of amplifier.

be arranged so that there should be negligible current drain through this electrode. In order to stabilize the gain to some extent and to obtain these input characteristics the input stage of the amplifier is arranged with feedback as shown in Fig. 6, where R6 and R7 are the feedback components.

An a.c. input impedance of greater than 100 k $\Omega$  was obtained and by varying R2 to supply base current with the input earthed, the d.c. drain at balance can be reduced to whatever level is required.

In order for this to be true and to obtain the required stability in a varying environment all the amplifier transistors were contained in a temperature controlled copper block. This system is very dependable and maintains the temperature of the block to within  $\pm \frac{1}{2}$  deg C. With silicon OC202 transistors in the input stage, stability of output voltage referred to the input and the d.c. drain from the reference electrode is always satisfactory. It is believed that by using planar transistors with lower leakage currents even better stabilities could have been obtained but this has never been found to be necessary. The remaining stages of the amplifier are conventional with one further amplifying stage and an emitter follower to drive the controller. The overall gain of the amplifier is about 2000 and the response is 3 dB down at about 5 kc/s. This response is modified by CR networks as described in Section 5.

### 3.2. The Controller

Because of the large range of current required and the very small minimum current to be controlled, some backing-off method for the  $I_{co}$  of the transistors used is necessary. Push-pull emitter followers could have been used but no voltage gain would then have been obtained from this stage and the amplifier would have had to provide  $\pm 25$  V, the maximum voltage available to the cell.

In this case, therefore, a composite grounded emitter stage with feedback to stabilize the gain is

used. Feedback is necessary as the resistance of the cell changes during electrolysis and therefore the gain of the stage without feedback would vary considerably. It is seen from the block diagram (Fig. 7) that the stage is essentially the usual grounded emitter stage with load and power supply exchanged and pnp and npn transistors working back to back. At low currents the feedback action of the system turns on one transistor to back off the  $I_{co}$  of the transistor which is passing the current in the desired direction through the cell. Feedback by R1 and R2 maintains the gain of the stage at about 15.

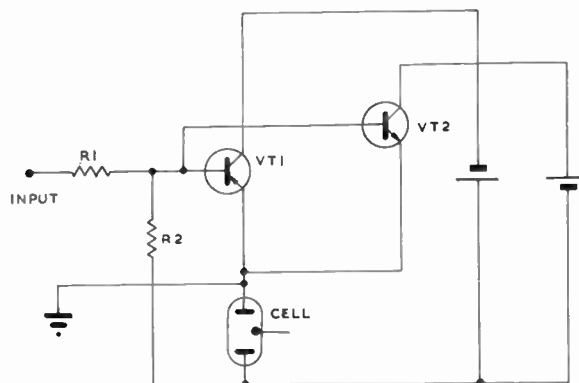


Fig. 7. Schematic of output stage.

The controller also includes extra transistor stages as shown in Fig. 8 to control the switching on of the equipment. Because of the nature of the chemical arrangement (the desired parameter being preset and the current being switched), it is impossible to avoid overshoots at switch-on merely by overdamping the system; and because of the exponential nature of the current decay, the slightest overshoot at switch-on will destroy completely the accuracy of the result.

When the circuit is completed by switching to RUN, VT1 and VT2 are biased hard off and their turn-on,

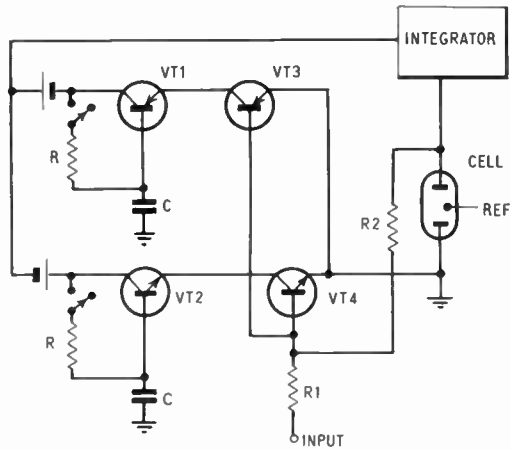


Fig. 8. Schematic of controller.

and therefore application of the supply voltage to the cell current control circuit, is controlled by the relatively long time-constant of several seconds of CR. The control system takes over smoothly when the current reaches the value necessary to obtain the desired voltage at the reference electrode. The 'switch-on' transistors VT1 and VT2 become bottomed and remain with no control on the circuit while the experiment takes place. This arrangement ensures that at no time does the controlled voltage exceed the desired value and in fact when viewed on an oscillo-

scope this voltage takes the form of a ramp with a flat top. The base of the ramp is the 'back e.m.f.' of the cell formed by control electrode and cathode, and the flat top after the ramp is the controlled voltage.

3.3. Potentiometer and Reference Voltage

The potentiometer, made of precision resistors, is fed from a Zener diode which is fed from a small stabilized power supply. It is possible to calibrate the potentiometer against a standard cell using the amplifier as detector, by switching the apparatus to CALIBRATE. A switch is provided to reverse the polarity of the voltage from the potentiometer in order that the working electrode can be held at positive or negative potentials with respect to the reference electrode. The potentiometer has a maximum output voltage of 3 V in steps of 10 mV.

3.4. The Integrator

The current from the cell is passed into a precision Miller integrator which is composed of a high stability commercial amplifier, and precision resistors and capacitors. This apparatus has ranges which closely approximate to the ranges marked on the range switch but is not absolute and is calibrated with a known current source before use. In order to obviate drift due to zero setting at the input a switch position is provided which gives a gain of 1000. The output can then be set with the digital voltmeter

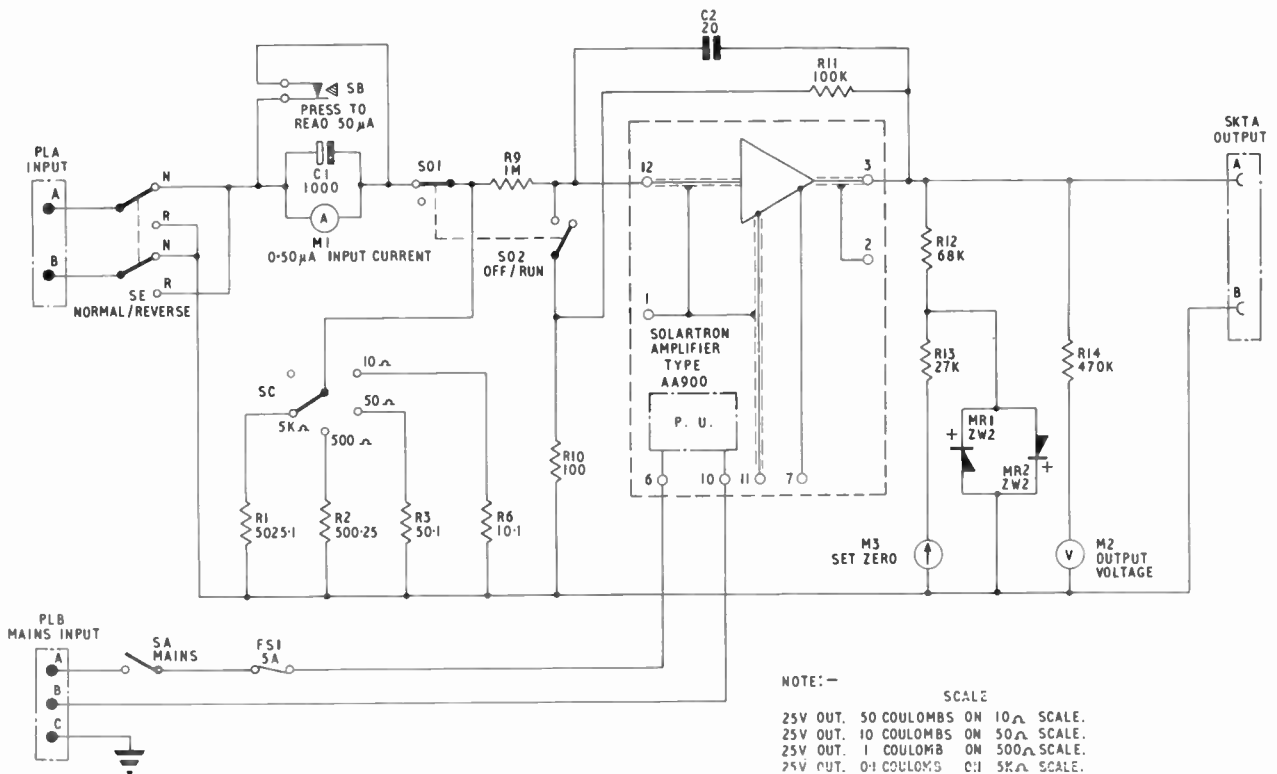


Fig. 9. Circuit diagram of integrator.

to within a millivolt ensuring that the zero error at the input is less than  $1 \mu\text{V}$ . A circuit diagram of the integrator is shown in Fig. 9.

#### 4. Stability

Various cells are used with the equipment depending on the material to be analysed. Response curves of the cells are difficult to measure and vary enormously between cells of different size and shapes. Typical measured curves are shown in Fig. 10. It is obvious that phase changes of up to  $90^\circ$  are introduced by the cell and attenuation of from 10 times to zero can be obtained between the input to the cell (current electrode) and the reference electrode. Similar curves are reported by other workers.<sup>6</sup>

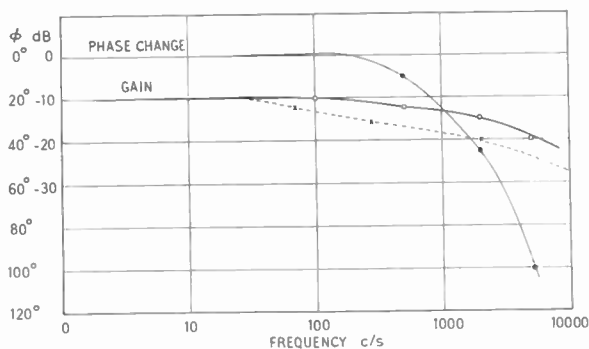


Fig. 10. Typical cell response.

For the required stability therefore and to provide voltage for all types of cells an error input of 1 mV should provide 20 V across the cell and a phase lag of  $90^\circ$  should be accommodated with zero attenuation across the cell.

The overall amplifier system therefore should have a d.c. gain of 20 000 with the gain falling to zero before the phase change has reached  $270^\circ$ . This is achieved by resistance-capacitance networks provided in the amplifier and stability has been found to be satisfactory using all cells so far encountered using both platinum and mercury electrodes.

The stability of the system is always based on a compromise. By restricting the frequency response a very stable system on all cells can be assured. But in order to maintain accuracy in the apparatus the response should be maintained to as high a frequency as possible because the stirrer revolves at approximately 2000 rev/min and the consequent variation of cell resistance must be counteracted by the apparatus.

The transfer function of the cell varies from cell to cell but in the sector from 10 c/s to 1 kc/s does appear to have a slope approximating to 6 dB/octave.

In order to obtain maximum frequency response together with stability, the gain of the amplifier is arranged so that only one attenuating network in the amplifier is operative when the open-loop response curve crosses the 0 dB line, and this is adjusted to happen before any attenuation takes place due to the cell. Once the networks C2 R10, C3 R13 have been arranged in the amplifier to do this no trouble with stability is normally experienced when cells of the same type are used. If a differently designed cell is used, the reference electrode voltage should be observed with an oscilloscope and if necessary the network adjusted to obtain stability.

#### 5. Read-out and Results

The output of the integrator is read on a five-digit voltmeter. Results have been obtained<sup>7</sup> which have a standard deviation and accuracy of better than 0.1%. Several complete sets of apparatus are working at A.W.R.E. and it has been possible to arrange for one digital voltmeter to read results from several machines.

#### 6. Acknowledgments

Thanks are due to Mr. G. C. Goode, Chemistry Division, A.W.R.E., for his help in the appreciation of the problems and to Mr. R. F. C. Bennett for guidance in the early stages of the project. I would also like to thank the Director of the Atomic Weapons Research Establishment for permission to publish this paper.

#### 7. References

1. J. J. Lingane, "Electro-analytical Chemistry", 2nd ed. (Interscience Publishers, London, 1958.)
2. P. Delahay, "New Instrumental Methods in Electrochemistry" (Interscience Publishers, London, 1954).
3. M. T. Kelly, H. C. Jones and D. J. Fisher, "Electronic controlled potential coulometric titrator", *Anal. Chem.* **31**, No. 4, pp. 848-956, April 1959.
4. A. Hickling, "Studies in electrode polarisation (Part 4: automatic control of potential of a working electrode)", *Trans. Faraday Soc.*, **38**, pp. 27-33, 1942.
5. N. J. Wadsworth, "A Controlled Cathode Potential Electrodeposition Apparatus", R.A.E. Technical Note, Met. 309, March 1959.
6. J. J. Rockett, "A Constant Potential Coulometric Titration Equipment using Transistors", H.M. Stationery Office, November 1961.
7. G. C. Goode, J. Herrington and G. Hall, "The determination of uranium in the presence of plutonium by controlled potential coulometry", *Anal. Chim. Acta.*, **30**, pp. 109-13, 1964.

Manuscript first received by the Institution on 29th June 1964 and in final form on 1st February 1965. (Paper No. 981.)

© The Institution of Electronic and Radio Engineers, 1965

(cont. from p. 296)

**A Tunnel Diode Oscillator with Wide Tuning Range (0.7-4.9 Gc/s)**

D. R. PERSSON. (*Decca Radar Limited, Hersham, Surrey.*)

The tunnel diode is coupled weakly to a relatively high  $Q$  resonator essentially of the hybrid coaxial type. This construction ensures a wide tuning range and a frequency of oscillation that is relatively insensitive to temperature change, supply voltage variations and interchange of diodes. In the basic form of the oscillator, using a 2 mA peak current germanium diode, stable and continuous oscillation is sustained over the full tuning range of 0.7 to 5 Gc/s with a power output greater than 1 mW up to 4 Gc/s. Alternative forms of the oscillator still under development give power outputs approaching 1 mW at some cost in frequency stability and tuning range.

**Parametric Multi-Port Networks for Microwave Signal Processing**

H. B. HENNING. (*Advanced Development Laboratory, Raytheon Company, Sudbury, Massachusetts.*)

This paper investigates multi-port linear networks in which pumped variable capacitances shunt and interconnect the several ports. A preliminary example of a two-varactor parametric amplifier is followed by a general analysis and reduction to a practical synthesis technique. Further examples include a negative impedance converter, impedance transformer, non-reciprocal coupler, three-port and  $N$ -port circulators, distributed parametric amplifiers and "steerable amplifiers" for phased array receiving antennas.

**Applications of Parametric Amplifiers in Satellite Communications**

H. N. DAGLISH AND D. CHAKRABORTY. (*Post Office Research Station, Dollis Hill, London.*)

Varactor diode parametric amplifiers have been used for a number of applications in satellite communication earth stations. The paper describes some of these applications, illustrating them by reference to experimental parametric amplifiers designed and constructed at the Post Office Research Station, Dollis Hill, and at the Post Office Radio Laboratory at Backwell, for use at Goonhilly Satellite System Earth Station. These include uncooled and refrigerated non-degenerate communication amplifiers and a cooled degenerate amplifier intended for a radiometric measurement of aerial gain. The likely requirements for devices for use as first stage amplifiers in future operational satellite communication systems are discussed.

**Parametric Amplifiers in Radioastronomy**

R. D. DAVIES. (*University of Manchester, Nuffield Radio Astronomy Laboratories.*)

The operating requirements for parametric amplifiers when used in radioastronomy will be discussed in this paper. Extraterrestrial signals with an intensity corresponding to aerial temperatures as low as 0.01°K are currently being studied. Their detection requires a parametric amplifier with a low system temperature and a high overall stability. With appropriate switching techniques a stability of 1 in  $10^4$  is achievable in a system.

In spectral line studies 1 dB bandwidths of 10-20 Mc/s are desirable. Interferometry experiments involving two aeriels and receiving systems require phase stabilities of several degrees per hour. It is expected that workable systems cooled to liquid nitrogen temperatures will soon be available for radioastronomy.

**A Survey of Possible Applications of Tunnel Diodes in Antenna Systems**

PROFESSOR DR. H. H. MEINKE. (*Institut für Hochfrequenztechnik, Technische Hochschule, Munich.*)

It is well known that tunnel diodes integrated with antenna-systems can be used for amplification and mixing. It may become more important to influence the current distribution on radiators and so influence the radiation pattern. We can also change the mutual coupling between parallel radiators and find combinations with very low mutual coupling. In broadband problems new possibilities have arisen, because the input impedance of radiators loaded with tunnel diodes offers frequency dependent curves which in combination with passive networks may solve some broadband problems. As in all applications of negative resistances some stability problems arise. In some cases the stability problem is alleviated if the tunnel diode works in its current maximum (infinite resistance) and is pumped by an auxiliary frequency. In this mixer case the diode has an interesting frequency-dependent input impedance, which can be changed by idler circuits. This impedance integrated with a rod antenna in an appropriate position can produce broadband qualities.

# Impedance Characteristics of Glow-discharge Tubes in the Frequency Range 200 c/s-70Mc/s

By

F. A. BENSON, D.Eng., Ph.D.†

AND

M. W. BRADSHAW, B.Eng.,  
Ph.D.†

*Reprinted from the Proceedings of the Symposium on "Cold Cathode Tubes and their Applications" held in Cambridge from 16th-19th March 1964.*

**Summary:** Impedance-frequency characteristics of glow-discharge tubes, filled with pure neon, over the frequency range 200 c/s-70 Mc/s have been obtained at several values of steady tube current. Molybdenum, nickel, zirconium and tantalum were used as cathode materials and in the case of molybdenum tubes the gas pressure was also varied.

The measurements confirm that there are several delayed effects in the glow discharge which affect the impedance characteristics considerably. A detailed analysis of the results for a tantalum-cathode tube gives the magnitudes of the consequent delay times and the complete equivalent circuit of the tube.

## 1. Introduction

The impedance presented to a small alternating signal, superimposed on the steady operating voltage of a glow-discharge tube, increases with frequency. In some tube applications it is desirable to have a low audio-frequency impedance and in certain voltage-stabilizer circuits the transient response of the tube is an important factor which can be assessed if its equivalent circuit is known.

Many attempts have been made to explain the origin of the effects observed when impedance-frequency characteristics are measured.<sup>1-9</sup> An early theory due to van Geel,<sup>3</sup> derived by considering perturbations about the steady-state maintenance condition and assuming that physical quantities in the discharge are functions of the instantaneous current and voltage alone predicts that the impedance loci (reactance-resistance curves) should be semi-circles (neglecting displacement current). The impedance locus of a tube has the form predicted by this theory if it is extended to include several delayed effects.<sup>7</sup> Secondary processes of electron production can be regarded as retarded functions of current and voltage since they are associated with a delay time; these affect the tube impedance locus considerably.

Impedance measurements on glow-discharge tubes have been carried out by Benson,<sup>7, 10</sup> Chalmers,<sup>7</sup> Mayo,<sup>10</sup> Reed,<sup>8</sup> Dix,<sup>8, 9</sup> Ahsmann,<sup>11-13</sup> Oskam,<sup>11</sup> Marx<sup>14</sup> and Weston.<sup>15, 16</sup> The complex impedance of the discharge in a rare gas has been observed by Ahsmann and Oskam<sup>11</sup> to be considerably reduced by the addition of another rare gas of lower ionization

potential, in fact, both the real and imaginary parts decrease. The impedance is nearly independent of the anode distance provided an anode fall does not develop. The addition of one rare gas to another of higher ionization potential also strongly influences the recovery time of the discharge.

Reed<sup>8</sup> and Dix<sup>8, 9</sup> have made spectral-noise measurements on 85A2 reference tubes in the frequency band 20 c/s to 10 Mc/s and have correlated the noise properties with the measured impedances of the tubes. Weston<sup>15, 16</sup> has measured the variation of the impedance of glow-discharge tubes with gas pressure in the audio-frequency range. No simple law could be obtained relating the impedance or its measured components with pressure. Weston attempted to correlate his results with van Geel's theory. Parallel-plate tubes were used for the initial experiments but it was found that the results were unaffected by geometry provided there was no anode fall. Later tubes therefore had wire anodes. Tubes were constructed with different cathode areas and filled to pressures within the range 15 to 100 torr with a 99% neon-1% argon mixture. Weston also investigated the effect of current and cathode material on impedance; molybdenum, zirconium and nickel were used.

Crawford<sup>17</sup> obtained impedance-frequency characteristics of hot-cathode d.c. mercury-vapour plasmas at a pressure of about 1 $\mu$  using several values of anode current and frequencies up to 2 Mc/s. Many other investigators have commented on the increase of impedance of a glow-discharge tube with frequency<sup>18-26</sup> or the dynamic characteristics of tubes.<sup>27</sup> Some dynamic aspects of the cathode-fall region of a d.c. glow discharge have been studied by Severin<sup>28</sup>

† Department of Electronic and Electrical Engineering, University of Sheffield.

and the properties of an a.c. glow discharge have been investigated by Deutsch.<sup>29</sup>

In an attempt to confirm theoretical predictions Benson and Chalmers<sup>7</sup> made measurements over the frequency range 300 c/s to 5 Mc/s on tubes with pure-neon fillings at various pressures and several neon-argon mixtures. To understand the impedance-frequency characteristics of tubes better and to obtain more information about the physics of the discharge, the delayed effects and the equivalent circuit of a tube the measurements have now been extended up to a frequency of 70 Mc/s using pure-neon tubes having cathodes of various materials with several gas pressures and steady tube currents. The results of these measurements are presented and discussed here. The tubes used for the investigations each had a rod anode 1 mm in diameter and a cylindrical cathode 7.5 mm in diameter and 10 mm long. The electrode structure was mounted in a glass envelope having a volume of about 8 cm<sup>3</sup>. The tubes were sputtered before examination using standard reference-tube technique.

**2. Theoretical Treatment**

The impedance (*Z*) of the discharge tube, derived by considering *n* delayed effects has the following form<sup>7</sup>:

$$Z = a_0 - \left( \frac{a'}{1 + j\omega\tau'} \right) - \sum_{k=1}^{k=n} \frac{a_k}{1 + j\omega\tau'_k} \dots\dots(1)$$

where *a*<sub>0</sub>, *a'*, *a*<sub>1</sub> . . . *a*<sub>*k*</sub> . . . *a*<sub>*n*</sub>, have the dimensions of resistance and  $\tau'_1$   $\tau'_2$  . . .  $\tau'_k$  . . .  $\tau'_n$  are time-constants associated with the various delay processes. The second term of this expression, which itself involves a delay time  $\tau'$ , may be regarded as the contribution from the discharge process itself and the last term is attributed to the secondary mechanisms or delayed-effect processes which were called after-effects by van Geel.

If two such delayed processes only are considered as an example the impedance may be written in the form:

$$Z = R_0 - \frac{R_1}{1 + j\omega\tau_1} - \frac{R_2}{1 + j\omega\tau_2} - \frac{R_3}{1 + j\omega\tau_3} \dots\dots(2)$$

where *R*<sub>0</sub>, *R*<sub>1</sub>, etc., have been used instead of the previous *a* terms.

Impedance loci satisfying this equation can be represented by the sum of three vectors whose individual loci are semi-circles of diameters *R*<sub>1</sub>, *R*<sub>2</sub> and *R*<sub>3</sub>. For positive values of *R*<sub>1</sub>, *R*<sub>2</sub> and *R*<sub>3</sub> and  $\tau_1 > \tau_2 > \tau_3$  the locus is shown on Fig. 1 and the construction has been discussed by Benson and Chalmers.<sup>7</sup>

When (*n* - 1) delayed effects are considered the quantity *R*<sub>0</sub> in equation (2) is given by:

$$R_0 = R_T + R_1 + R_2 + \dots + R_n \dots\dots(3)$$

where *R*<sub>*T*</sub> is the slope of the static voltage-current characteristic.

Thus, for (*n* - 1) delayed effects:

$$Z = R_T + \frac{R_1 j\omega\tau_1}{1 + j\omega\tau_1} + \frac{R_2 j\omega\tau_2}{1 + j\omega\tau_2} + \dots + \frac{R_n j\omega\tau_n}{1 + j\omega\tau_n} \dots\dots(4)$$

Defining

$$L_1 = R_1\tau_1, \quad L_2 = R_2\tau_2, \text{ etc.,}$$

$$Z = R_T + \frac{R_1 j\omega L_1}{R_1 + j\omega L_1} + \frac{R_2 j\omega L_2}{R_2 + j\omega L_2} + \dots + \frac{R_n j\omega L_n}{R_n + j\omega L_n} \dots\dots(5)$$

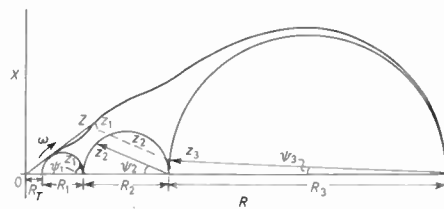


Fig. 1. Theoretical impedance locus, where  $\tau_1 : \tau_2 : \tau_3$  as 100 : 10 : 1.

The second and subsequent terms of equation (5) represent a parallel combination of *L* and *R* and the equivalent circuit, including the effective tube capacitance, takes the form shown in Fig. 2(a). Each parallel combination has a time-constant associated with a particular process in the discharge mechanism.

Benson and Chalmers<sup>7</sup> observed that the effective tube capacitance of all the tubes approached a limiting value at frequencies above about 4 Mc/s (higher in the case of pure-neon tubes of 40 torr pressure and pure-argon tubes) seemingly independent of frequency. This capacitance, which was found to be independent of the anode-cathode spacing and electrode geometry, was taken to be the effective capacitance *C*<sub>*d*</sub> of the discharge. It was found to be of the order of the capacitance of the cathode-dark-space region of the discharge. To compare the results with theory, which does not take into account displacement current, the effective tube capacitance had to be subtracted from the measured values of capacitance. The resulting modified impedance loci, when analysed graphically according to the theory, could be represented approximately by a series of vectors whose individual loci were semi-circles each having a different time-constant.

It appeared from the results of Benson and Chalmers<sup>7</sup> that if the frequency was increased beyond their upper limit of 5 Mc/s the unmodified impedance loci would move towards the origin as would be expected if *C*<sub>*d*</sub> alone shunts the circuit of Fig. 2(a).

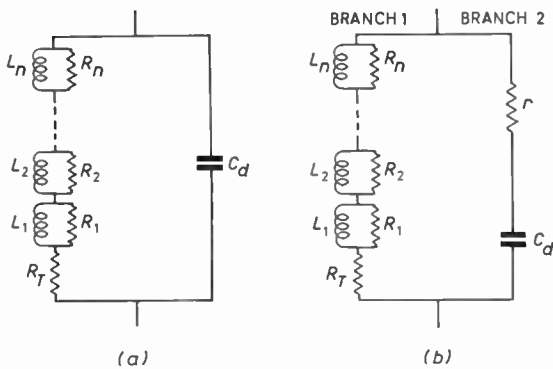


Fig. 2. Equivalent circuits of discharge.

Reed<sup>8</sup> and Dix<sup>8, 9</sup> have shown, however, that there is a resistance  $r$  in series with capacitance  $C_d$  which represents the dielectric loss due to gas molecules. They found that for the 85A2 type of tube  $r$  varies from  $160\Omega$  when the direct tube current is 10 mA to  $2\text{ k}\Omega$  when the current is 1 mA. The complete equivalent circuit of a tube is therefore that shown in Fig. 2(b).

3. Measurements

Impedance measurements were made in the three frequency ranges 200 c/s–50 kc/s, 50 kc/s–5 Mc/s, and 5 Mc/s–70 Mc/s. For the first range a balanced transformer bridge as designed by Weston<sup>16</sup> was used and a tunable twin-T network was employed for eliminating harmonics from the input signal to the detector. For the other two frequency ranges Wayne-Kerr transformer bridges type B601 and B801 were used respectively with radio receivers as detectors. With the B601 instrument (in which the normal wire-wound main resistance-dial potentiometer was replaced by a low-capacitance carbon one) it was sufficient to place the tube mounting and circuit on a Perspex board above the terminals but with the B801 bridge the tube mounting was actually built on the terminals to keep the connecting leads as short as possible.

The alternating signal was applied to the tubes through the bridge in all three cases and its voltage was maintained at a sufficiently low level (always  $< 100\text{ mV}$  and  $< 50\text{ mV}$  at frequencies below 1 kc/s) to avoid any effect on the measured impedance.

The accuracy of the measurements was studied in some detail since the computational method used in analysing the results depended to a great extent on the mean deviation to be expected on each experimental reading. The accuracies of the frequency and direct-tube-current measurements were both about 1%. With the low-frequency bridge the accuracy of the resistance measurement was approximately 2% or

$\pm 1\Omega$  and that of the capacitance measurement 3% or  $\pm 20\text{ pF}$ . With the B601 bridge resistance could be determined to within 2% and capacitance to within 2% or  $\pm 0.05\text{ pF}$ . The corresponding figures for the B801 instrument were (resistance/1000) % above  $10\text{ k}\Omega$  (and generally 10% in the range used) and  $\pm 0.5\text{ pF}$  (approximately 10% in the range used).

The results were obtained in the form of an equivalent parallel tube resistance ( $R_p$ ) and capacitance ( $C_p$ ) at various frequencies and tube currents. The cathode materials used in the tubes were molybdenum, zirconium, tantalum and nickel and the gas filling was pure neon at a pressure of 40 torr. For tubes having molybdenum cathodes pressures of 30 and 50 torr were also used. Measurements were made at direct currents of 10, 8, 6 and 4 mA.

4. Results

The typical curves illustrated in Fig. 3 show the variations of the measured values of parallel resistance and capacitance for a zirconium-cathode tube. Figure 4 gives an enlarged view of these curves at the higher frequencies.

Impedance loci were plotted to facilitate the analysis of the results and to compare them with the theoretical predictions. For this purpose the equivalent series resistance ( $R_s$ ) and reactance ( $X_s$ ) were used as they give a better picture of the characteristics, particularly where  $X_s \rightarrow 0$ . The necessary conversion from the experimental results was done using the formulae:

$$X_s = X_p / \{1 + (X_p/R_p)^2\}, \quad R_s = R_p / \{1 + (R_p/X_p)^2\}$$

where  $X_p = 1/\omega C_p$ .

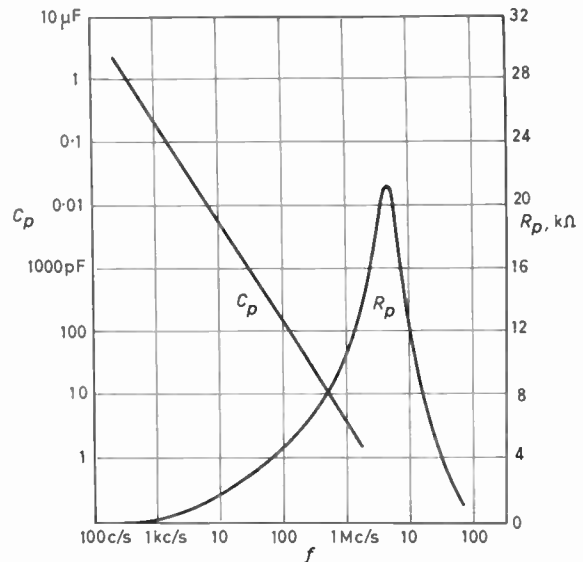


Fig. 3. Typical curves of measured capacitance and resistance. Tube: 40 torr neon, zirconium cathode at 6 mA.

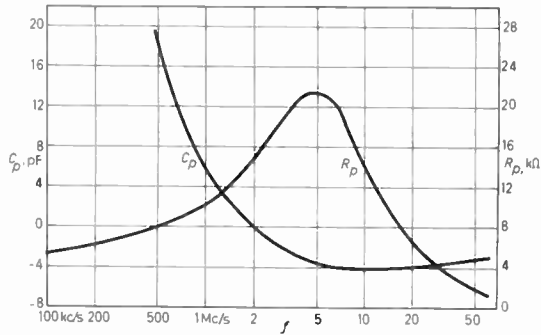


Fig. 4. High frequency detail of Fig. 3.

Measurements were made on several tubes with the same structure, gas filling, pressure and cathode material. No significant differences were observed in the results at frequencies above 10 kc/s. Below 10 kc/s, however, the differences become significant being about 5% at 10 kc/s and as much as 100% at 400 c/s. This divergence between results for different tubes of the same kind was also observed by Reed<sup>8</sup> and Dix.<sup>8, 9</sup>

Figure 5 shows typical impedance loci for a molybdenum-cathode tube with a pressure of 40 torr at various direct tube currents. Enlargements of these curves at the high- and low-frequency ends are given on Fig. 6. Typical loci for tubes with different cathode materials are compared in Fig. 7. The effects of changing the gas pressure on the impedance loci of

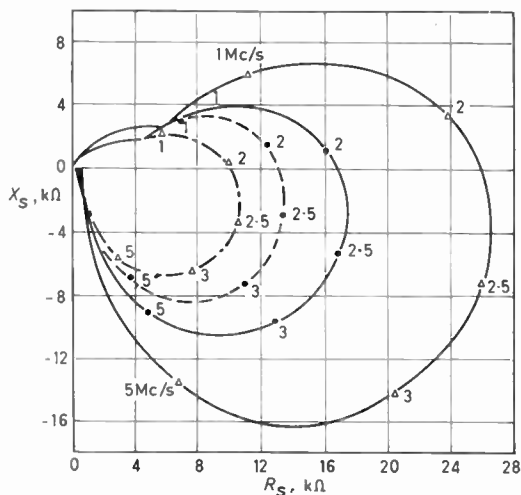


Fig. 5. Typical impedance loci at various tube currents. Tube: 40 torr, neon, molybdenum cathode.

- △— 4 mA
- 6 mA
- - - ● - - - 8 mA
- . . . △ - . . . 10 mA

molybdenum-cathode tubes can be seen from Figs. 8-10.

It may be noted from the various curves and particularly from Fig. 6 that the loci have definite intercepts on the resistance axis at frequency  $f = 0$  and also when  $f \rightarrow \infty$ . Table 1 gives the intercepts as  $f \rightarrow \infty$  for all the tubes tested at various currents. It is evident from Fig. 2(b) that these intercepts give the values of  $r$ . For the zirconium-cathode tubes values of  $r$  were also found at currents of 12 mA and 3 mA and these are included in Table 1. The results show that  $r$  is inversely proportional to the direct tube current  $I$ .

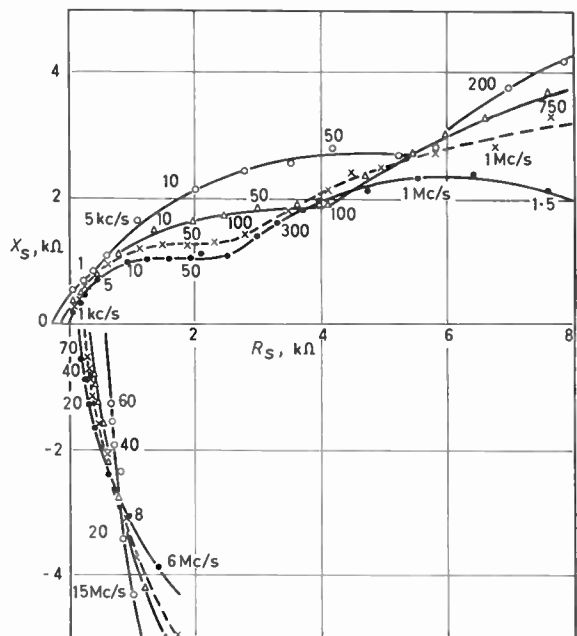


Fig. 6. Upper and lower frequency characteristics. Tube: 40 torr, neon, molybdenum cathode.

- 4 mA
- △— 6 mA
- - - × - - - 8 mA
- 10 mA

From the circuit of Fig. 2(b) when  $f = 0$ ,  $Z = R_T$ . Table 2 compares the low-frequency intercepts and the gradients of the static voltage-current characteristics of the tubes ( $dV/dI$ ) at corresponding currents. There is reasonable agreement between  $R_T$  and  $dV/dI$ . The lack of agreement in certain cases is mainly due to the difficulty of extrapolating from  $f = 200-400$  c/s to  $f = 0$ .

From Fig. 4 it is seen that, for  $f > 8$  Mc/s,  $C_p$  is nearly constant and is approximately the capacitance of the cathode-fall region. Benson and Chalmers<sup>7</sup>

**Table 1**  
Values of  $r$  for tubes filled with pure neon

Tube type		$r$ (ohms) at various direct tube currents					
Cathode	Pressure (torr)	12 mA	10 mA	8 mA	6 mA	4 mA	3 mA
Molybdenum	30	—	150	180	250	400	—
Molybdenum	50	—	200	300	400	1300	—
Molybdenum	40	—	160	200	300	550	—
Nickel	40	—	180	250	350	650	—
Zirconium	40	140	180	200	400	550	750
Tantalum	40	—	180	250	350	550	—

**Table 2**  
Values of  $R_T$  (i.e.  $Z$  at  $f = 0$ ) and  $dV/dI$  for tubes filled with pure neon

Tube type		Direct tube currents (mA)							
		10		8		6		4	
Cathode	Pressure (torr)	$R_T$ ( $\Omega$ )	$dV/dI$ ( $\Omega$ )	$R_T$ ( $\Omega$ )	$dV/dI$ ( $\Omega$ )	$R_T$ ( $\Omega$ )	$dV/dI$ ( $\Omega$ )	$R_T$ ( $\Omega$ )	$dV/dI$ ( $\Omega$ )
Molybdenum	30	510	526	470	526	400	426	0	0
Molybdenum	50	0	0	-50	-90	-100	-300†	-200	-600†
Molybdenum	40	0	-77	-50	-175	-150	-175	-250	-275
Nickel	40	500	600	400	400	400	300	200	200
Zirconium	40	0	80	0	20	-50	-53	-150	-125
Tantalum	40	250	260	50	67	300	268	100	60

† The  $V/I$  characteristic of this tube, at  $I < 8$  mA, had large steps due to the glow jumping from one glow area to another. Hence, the value of  $dV/dI$  was difficult to assess.

took this to be exactly so. The effect of  $r$ , which is to make  $C_p < C_d$ , becomes more pronounced, however, as the frequency increases (see Fig. 4).

The loci intercepts  $R_{(X=0)}$  at  $f \approx 2$  Mc/s are approximately proportional to  $1/I$ , e.g. considering the molybdenum-cathode-tube results of Fig. 5, Table 3 is obtained.

Comparison of Figs. 7 and 10 shows that changes in cathode material do not seem to affect the frequency  $f_{(X=0)}$  at which  $X_s$  goes through zero (i.e. changes from inductive to capacitive) but changes in pressure  $p$  do. As  $p$  increases so does  $f_{(X=0)}$ . This may be explained by the dark-space capacitance being inversely proportional to pressure, as stated by Benson and Chalmers.<sup>7</sup> Since  $f_{(X=0)}$  is the frequency at which the inductance of branch 1 of Fig. 2(b) balances the capacitance of

branch 2 any decrease in capacitance will cause an increase in  $f_{(X=0)}$  (the inductance will tend to increase

**Table 3**

Values of the impedance loci intercepts  $R_{(X=0)}$  for a molybdenum-cathode tube filled with pure neon at a pressure of 40 torr

Tube current (mA)	$R_{(X=0)}$ (k $\Omega$ )
10	10
8	13
6	16.5
4	25.8

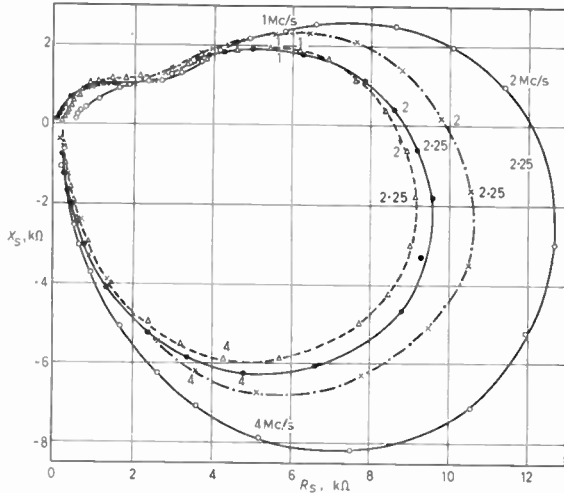


Fig. 7. Impedance loci for tubes with various cathode materials.  
Tubes: 40 torr, neon, at 10 mA current.

- Δ --- Tantalum
- ● — Zirconium
- × ····· Molybdenum
- · - · - Nickel

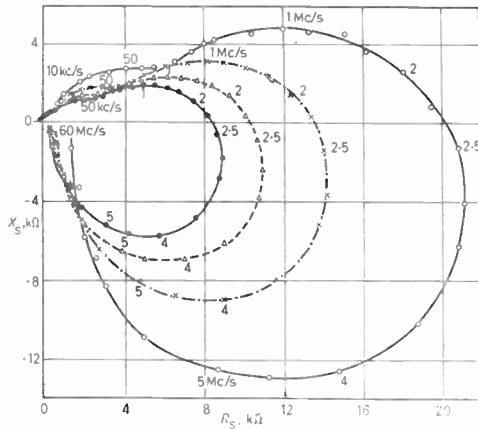


Fig. 9. Impedance loci for various tube currents.  
Tube: 50 torr, neon, molybdenum cathode.

- ○ — 4 mA
- × --- 6 mA
- Δ --- 8 mA
- ● — 10 mA

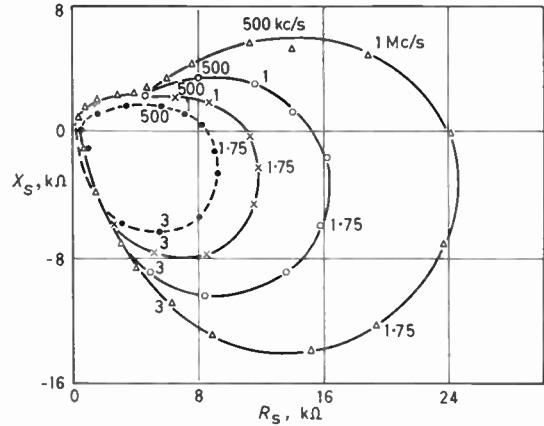


Fig. 8. Impedance loci for various tube currents.  
Tube: 30 torr, neon, molybdenum cathode.

- Δ — 4 mA
- ○ — 6 mA
- × — 8 mA
- ● — 10 mA

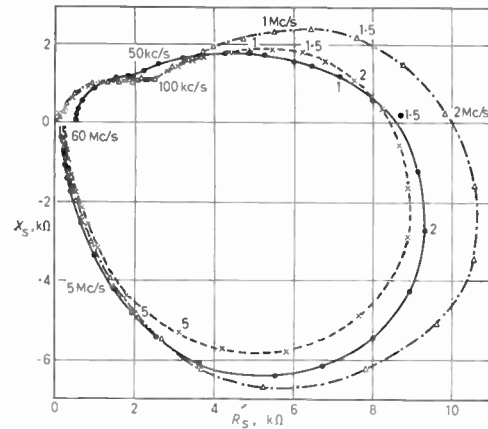


Fig. 10. Impedance loci for tubes with various gas pressures.  
Tubes: neon, molybdenum cathode at 10 mA.

- × --- 50 torr
- ● — 30 torr
- Δ --- 40 torr

with  $p$  due to the increase in collision frequency and will reduce the effect of capacitance).

Definite bumps are present in the various impedance loci, which may be associated with individual delayed effects, but the number and magnitudes of the delayed effects are difficult to determine from the curves. It was therefore decided to analyse the results using digital-computational techniques. Previous analyses

have been mainly limited to graphical methods which are very approximate. Benson and Chalmers<sup>7</sup> concluded from their graphical analysis that for pure-neon tubes and neon-argon tubes with less than 0.1% argon there are five time-constants to consider but one of these involved a negative inductance. For neon-argon tubes with more than 0.1% argon only four time-constants seemed to be involved. Since their measure-

ments were made only at frequencies up to 5 Mc/s the effect of  $r$  was not observed. Reed<sup>8</sup> and Dix<sup>8, 9</sup> made measurements up to 30 Mc/s and discovered the effect of  $r$ . They were using a neon-argon tube and by construction found only three time-constants. It is evident from the previous studies that the general form of the equivalent circuit evolved is basically correct. There is difficulty, however, in determining the number of delayed effects and the exact values of the resistances and inductances in branch 1 of Fig. 2(b). It is also desirable to get a more accurate picture of the other constants involved, i.e.  $R_T$ ,  $r$  and  $C_d$ .

The analytical method used was the 'least-squares best-fit' one.<sup>30</sup> In this method the theory is assumed and programmed into the computer. The computer is then fed with estimated values of the parameters, i.e.  $r$ ,  $R_T$ ,  $C_d$ ,  $R_1$ ,  $L_1$ , etc., from which it calculates the values of the equivalent parallel capacitance  $C_{pt}$  and resistance  $R_{pt}$  predicted by the theory. The computer is also fed with the measured values of  $C_p$  and  $R_p$  at the various frequencies together with standard deviation for each value of  $C_p$  and  $R_p$ . It compares the theoretical and measured values of resistance and capacitance and then makes corrections to the values of the estimated parameters so as to obtain a better fit between the two sets of values. The cycle of events is repeated using the corrected values of the estimated parameters until the best fit is obtained (if the first estimates are within 50% this is probably after six cycles). The program prints out the theoretical and the measured values of  $C_p$  and  $R_p$  at the various frequencies for comparison and also the overall error of the fit  $\Delta$ . It will also, on direction from the console, print out the theoretical values of  $X_s$  and  $R_s$  for comparison with the  $X_s$ - $R_s$  graphs.

Initially it was decided to divide the fitting procedure into the high- and low-frequency sections. At the high-frequency end ( $f > 10$  Mc/s) the circuit was approximated to by the arrangement of Fig. 11 and the values of  $R$ ,  $r$  and  $C_d$  determined. The values of  $r$  and  $C$  were 'removed' mathematically from the circuit as in Fig. 2(b), thus effectively isolating branch 1 and the fitting procedure repeated on the pseudo experimental results. This method proved unsatisfactory due mainly to the fact that it requires the high-frequency results to be very accurate since the 'removal' of branch 2 involves the subtraction of two numbers of approximately-equal magnitude (i.e. the values of  $C_d$  and  $C_p$ ) the difference of which is of the same order as the experimental error. This only applies for  $f > 3$  Mc/s as below this frequency the method is valid and is effectively the same as the graphical methods used previously.<sup>7-9</sup> It was then decided to use the best-fit method on the results as a whole and this proved to be satisfactory.

The locus for a zirconium-cathode tube at a current of 6 mA was chosen to test the theory since this tube had the smoothest voltage-current characteristic and 6 mA is about its optimum current. The least-squares best-fit procedure was tried for a total of three, four, five and six time-constants (i.e.  $P = 3, 4, 5$  or 6). Figure 12 gives a comparison of the practical curve with the various theoretical ones. It can be seen that  $P = 5$  gives the best fit to the experimental points. Although  $P = 6$  was tried the final error was almost the same as  $P = 5$  but the program could not clearly define six time-constants probably because (a) the data were not sufficiently accurate to permit the resolution of six time-constants involving fifteen parameters or (b) there was no sixth time-constant present or if there was it was too small to be resolved and so would not greatly affect the component values in branch 1 of Fig. 2(b) obtained by assuming  $P = 5$ .

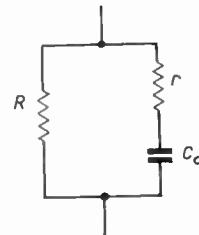


Fig. 11. Approximate high frequency equivalent circuit.

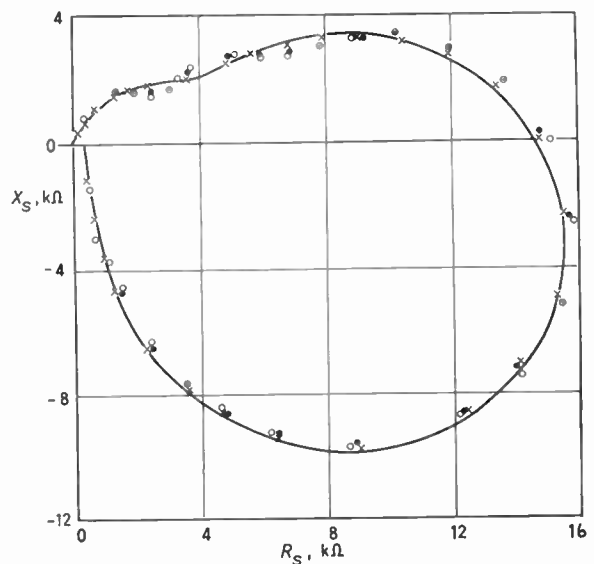


Fig. 12. Comparison of various theoretical loci with measured locus.

Tube: 40 torr, neon, zirconium cathode, 6 mA.

- Measured
- ×  $P = 5$
- $P = 4$
- $P = 3$

**Table 4**

Circuit parameters for  $P = 3, 4$  and  $5$  for a zirconium-cathode tube filled with pure neon at 40 torr

	$P = 3$	$P = 4$	$P = 5$
$r(\Omega)$	367	377	391
$C_d(\text{pF})$	4.28	4.29	4.32
$R_T(\Omega)$	203	18.5	12.5
$L_1(\text{mH})$		61	64.4
$R_1(\Omega)$		319	297
$L_2(\text{mH})$	38	30.3	30
$R_2(\text{k}\Omega)$	2.55	2.76	2.34
$L_3(\text{mH})$	3.49	2.66	3.44
$R_3(\text{k}\Omega)$	3.79	3.63	1.67
$L_4(\text{mH})$			1.18
$R_4(\text{k}\Omega)$			2.81
$L_5(\mu\text{H})$	648	626	589
$R_5(\text{k}\Omega)$	22	22.9	24.6
$\Delta$	342.2	79.34	43.52

**Table 5**

Circuit parameters and time-constants for a zirconium-cathode tube filled with pure neon at 40 torr

$I(\text{mA})$	10	8	6	4
$r(\Omega)$	179	259	391	691
$C_d(\text{pF})$	6.48	5.46	4.32	3.11
$R_T(\Omega)$	-5.68	64.4	12.5	-65.8
$L_1(\text{mH})$	44.8	50.3	64.4	107
$R_1(\Omega)$	180	224	297	435
$\tau_1(\mu\text{s})$	249	225	217	245
$L_2(\text{mH})$	20.3	22.5	30	45.2
$R_2(\text{k}\Omega)$	1.47	1.82	2.34	3.37
$\tau_2(\mu\text{s})$	13.8	12.4	12.8	13.4
$L_3(\text{mH})$	2.3	2.65	3.44	4.94
$R_3(\text{k}\Omega)$	1.08	1.24	1.67	2.46
$\tau_3(\mu\text{s})$	2.14	2.14	2.06	2.01
$L_4(\text{mH})$	0.787	0.937	1.18	1.69
$R_4(\text{k}\Omega)$	1.85	2.16	2.81	3.99
$\tau_4(\mu\text{s})$	0.425	0.433	0.420	0.424
$L_5(\text{mH})$	0.328	0.429	0.589	0.939
$R_5(\text{k}\Omega)$	15.7	19.6	24.6	33.07
$\tau_5(\mu\text{s})$	$2.08 \times 10^{-2}$	$2.186 \times 10^{-2}$	$2.39 \times 10^{-2}$	$2.84 \times 10^{-2}$
$\Delta$	61.53	32.79	43.52	67.25

Table 4 gives the various parameters found by the best-fit procedure for  $P = 3, 4$  and  $5$  and also the overall error  $\Delta$  where  $\Delta$  is given by:

$$\Delta = \sum_{i=1}^N \frac{[F(Z_i) - f(Z_i)]^2}{[\varepsilon(Z_i)]^2} \quad \dots(6)$$

where  $N$  is the number of experimental results.

$F(Z_i)$  is the experimental result

$f(Z_i)$  is the corresponding theoretical result at the same frequency, and

$\varepsilon(Z_i)$  is the error in  $F(Z_i)$ , i.e. the experimental error.

Table 5 lists the parameters and time-constants obtained, assuming  $P = 5$ , for a zirconium-cathode tube and several tube currents ( $I$ ).

### 5. Discussion of Results

Since a complete analysis was performed on the results of one tube alone only general conclusions may be drawn from the comparative graphs of Figs. 7 and 10. However, from a consideration of the impedance loci and the actual measured results it follows that:

- (a) Tubes with zirconium, molybdenum and tantalum cathodes will yield similar results. Tubes having nickel cathodes will give somewhat different results, as can be seen from Fig. 7, probably due to the running voltage being about 140 V compared with about 104 V for the other cathode materials used.
- (b) Changes in pressure affect the impedance to a greater extent than cathode material due to the pressure dependency of diffusion, collision frequency, mean-free path, etc.

The approximate values of  $C_d$  obtained for the molybdenum-cathode tubes with different pressures and a tube current of 8 mA are:

$$p = 30 \text{ torr, } C_d \approx 6.5 \text{ pF}$$

$$p = 40 \text{ torr, } C_d \approx 4.8 \text{ pF}$$

$$p = 50 \text{ torr, } C_d \approx 4.5 \text{ pF}$$

which are in agreement with the theory.<sup>7</sup>

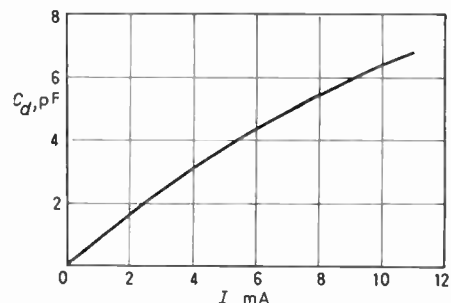


Fig. 13. Variation of dark-space capacitance with tube current. Tube: 40 torr, neon, zirconium cathode.

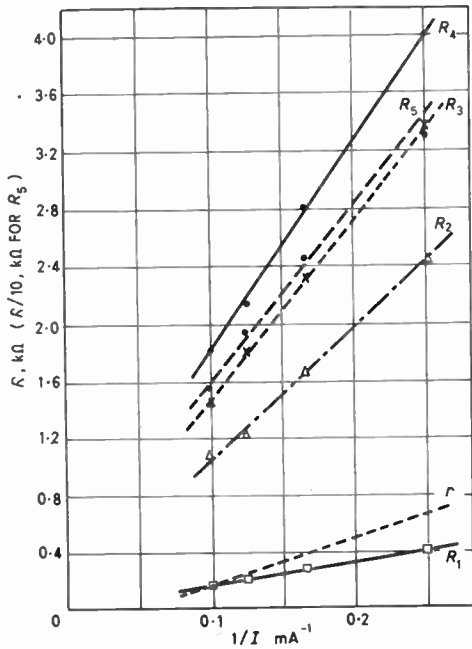


Fig. 14. Resistance values for theoretical circuit obtained by analysis of zirconium tube.

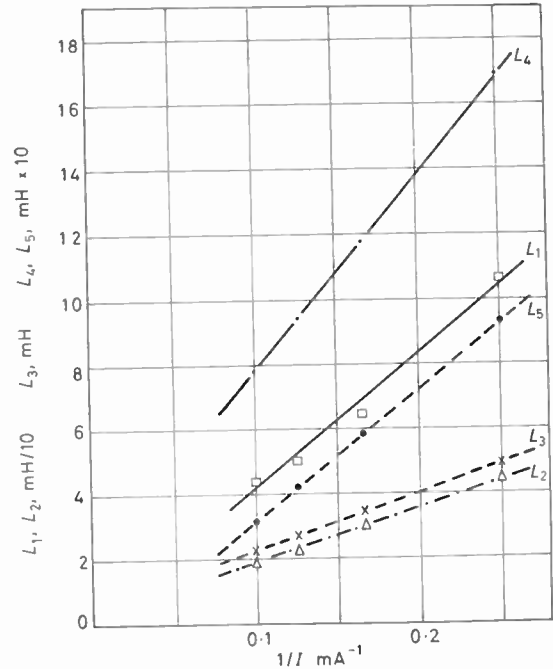


Fig. 15. Inductance values for theoretical circuit obtained by analysis of zirconium tube.

By reference to Fig. 12 and Table 4 it can be seen that the theory assuming  $P = 5$  is a good fit to the practical results; better than 3% for the most part. It may be noted that for  $P = 3$  the computer eliminated the first time-constant, which is defined by only a few results and effectively resolved the same delayed effects as  $P = 4$ . Also, whatever value of  $P$  was chosen, the parameters and hence the time-constant ( $\tau_5$ ) for the last delayed effect are approximately the same.

Figure 13 shows that the dark-space capacitance  $C_d$  is proportional to the current  $I$ . This is expected for a normal glow discharge with a constant current density. The slight divergence of the proportionality at  $I > 8$  mA is thought to be due to cathode edge effects. From Figs. 14 and 15 it can be seen that  $r, R_1, R_2 \dots R_n$  and  $L_1, L_2 \dots L_n$  are inversely proportional to  $I$ .

The respective time-constants given in Table 5 for each current are the same and on average are:

$$\begin{aligned} \tau_1 &= 234 \mu\text{s}, & \tau_2 &= 13.1 \mu\text{s}, & \tau_3 &= 2.09 \mu\text{s}, \\ \tau_4 &= 0.425 \mu\text{s}, & \tau_5 &= 0.024 \mu\text{s}. \end{aligned}$$

Thus, it may be concluded that for this tube the mechanics of the discharge are the same for any value of  $I$  provided the discharge is normal.

The relative values of  $R_1, R_2, R_3, R_4$  and  $R_5$  should give an insight into the importance of their respective mechanisms as current carriers in the discharge. It is found that:

$$R_5 : R_4 : R_3 : R_2 : R_1 :: 1 : 9 : 16 : 11 : 86$$

The values of  $R_T$  found by analysis are not consistent with the slopes of the voltage-current characteristics for the particular zirconium-cathode tube considered. This may be expected because the values of  $R_T$  are small in this case and the data does not clearly define any effects below 400 c/s.

It is not proposed at this stage to attribute all the various delayed effects to any particular discharge phenomena but merely to suggest some of the agencies which may be associated with them. It is hoped to make a detailed correlation in a later paper when all the results have been analysed and some further measurements have been made on both the tubes used during the present investigations and on tubes with different gas fillings.

When the delayed effects are small and  $\tau_1 \gg \tau_2 \gg \tau_3$ , then  $\tau_1$  and  $\tau_2$  are associated with  $T_1$  and  $T_2$  respectively, the time-constants of the two delayed effects on which the transport factor is dependent.<sup>7</sup> Further,  $\tau_3$  is associated with the degression time which in turn is associated with the time taken for the space-charge to change. Benson and Chalmers<sup>7</sup> thought that a larger delay time could be due to thermal lag connected with the heat-conduction mechanism from the cathode and that another possible delayed effect may be associated with the lateral growth of the discharge. The expansion or contraction of the cathode glow due to a change of current will depend on the nature of the

cathode surface and the results do in fact show spreads for tubes of the same type at frequencies below 10 kc/s where the effects of the larger time-constants are predominant. Differences in results for a given type of tube were also reported by Reed<sup>8</sup> and Dix.<sup>8, 9</sup>

Tubes having more than 0.1% argon in neon were found by Benson and Chalmers<sup>7</sup> to have one less delay process than tubes filled with pure neon. This may be attributed to the fact that in the former tubes a delay time associated with the lifetime of neon metastable atoms is reduced to a negligibly small value by ionizing collisions with argon atoms.

It is well-known that nearly all the potential drop in a glow discharge is across the cathode-fall region and it has been stated by many previous workers that there is a delayed effect due to the transit time of positive ions across this region. By analysis of ion energies at the cathode of a glow discharge Davis and Vanderslice<sup>31</sup> showed that for a normal glow discharge the ions arriving at the cathode, having suffered multiple charge-transfer collisions *en route* from the space-charge to the cathode, are predominantly low-energy ones. Severin<sup>28</sup> assumed that appreciable fractions of the ion momentum are transferred to the atoms during collisions and summed the transit times between collisions, there being  $d_c/l$  collisions in all. The resulting transit time  $\tau$  is found to be

$$\tau = 2\sqrt{2}(d_c/l)^{\frac{1}{2}}/\Omega, \text{ provided that } d_c \gg l,$$

where  $d_c$  is the width of the cathode-fall region  $l$  is the mean-free path and  $\Omega$  is the ion plasma frequency as defined by Severin.

For the pure-neon zirconium-cathode tubes  $d_c$  was estimated to be  $2.4 \times 10^{-2}$  cm from the capacitance measurements and  $\Omega = 1.28 \times 10^8$ . Thus, for  $I = 10$  mA, since  $l = 5.157 \times 10^{-4}$  cm,  $\tau = 15 \times 10^{-2}$   $\mu$ s, and for  $I = 4$  mA, since  $l = 4.69 \times 10^{-4}$  cm,  $\tau = 15.8 \times 10^{-2}$   $\mu$ s.

Severin<sup>28</sup> deduced an alternative value of  $\tau$  derived from a non-conservative differential equation, i.e. one including a dissipative term. This gave

$$\tau = 3(d_c/l)^{\frac{1}{2}}/2\Omega$$

This expression gives:

$$\begin{aligned} \text{for } I = 10 \text{ mA, } \quad \tau &= 7.98 \times 10^{-2} \mu\text{s} \\ \text{and for } I = 4 \text{ mA, } \quad \tau &= 8.38 \times 10^{-2} \mu\text{s} \end{aligned}$$

An alternative method of calculating  $\tau$  has been derived by Benson and Gillespie.<sup>31</sup> This method divides the cathode fall into high- and low-field regions and then makes use of the relationship between drift velocity and field strength proposed by Hornbeck.<sup>33</sup> The expression for  $\tau$  is:

$$\tau \simeq \frac{3\sqrt{3}(d_c)^{\frac{1}{2}}p^{\frac{1}{2}}}{2\sqrt{5}k_2(V_n)^{\frac{1}{2}}} \left[ 1 - \left( \frac{d}{d_c} \right)^{\frac{1}{2}} \right] + \frac{6d_c dp}{5k_1(d/d_c)^{\frac{1}{2}}V_n}$$

where  $V_n$  is the normal cathode fall,  $d$  is the extent of the low-field region in the cathode-fall space, and  $k_1$  and  $k_2$  are coefficients relating the positive-ion velocity and (electric field strength/ $p$ ) in the low-field and high-field regions of the cathode-fall space.

For the particular zirconium-neon tube under consideration this gives  $\tau \simeq 17.4 \times 10^{-2}$   $\mu$ s.

The delay time  $\tau_5$  in Table 5 is thought to be related to the positive-ion transit time. The above calculations, which involved preliminary estimates of  $d_c$  based on  $C_d$  and the current density are somewhat higher than the practical results. Inaccuracies in current density and  $d_c$  may account for some of the errors but space-charge distribution in the cathode-fall will modify the simplified calculations to some extent. It may be seen from Table 5 that as  $I$  increases  $\tau_5$  decreases and the reductions are about the same as those predicted by the calculations considering changes in mean-free path with variations in temperature caused by tube current.

## 6. Conclusions

The impedance locus of a glow-discharge tube can be explained effectively by the extended form of van Geel's theory developed by Benson and Chalmers<sup>7</sup> which takes into account several delayed effects. These delay processes affect the impedance locus considerably. Detailed analysis of the impedance locus gives the magnitudes of the various delay times and the complete equivalent circuit of the tube which is quite complex. It has been concluded that for a tube with a zirconium cathode containing pure neon at a pressure of 40 torr there are a total of five delay processes having time-constants:

$$\begin{aligned} \tau_1 &= 234 \mu\text{s}, & \tau_2 &= 13.1 \mu\text{s}, & \tau_3 &= 2.09 \mu\text{s}, \\ \tau_4 &= 0.425 \mu\text{s}, & \text{and } \tau_5 &= 0.024 \mu\text{s}. \end{aligned}$$

## 7. Acknowledgments

The work described has been carried out in the Department of Electrical Engineering at the University of Sheffield. The authors wish to thank Professor A. L. Cullen for facilities afforded in the laboratories of this Department and Dr. R. N. Maddison of the Mathematics Department for his valuable help with the computing. They also wish to acknowledge the kindness of the English Electric Valve Company in supplying special tubes for examination, for financial assistance and for the loan of equipment.

## 8. References

1. M. O. Williams, "Inertia effects in cold-cathode tubes", *Strowger J.*, 8, p. 106, 1952.
2. Report by Margaret J. Potter, "The impedance of voltage stabilizer and reference tubes", *Mullard Tech. Commun.*, 1, p. 219, 1954.

3. C. van Geel, "Untersuchungen von Gasentladungen mit Rücksicht auf ihre dynamischen Eigenschaften und ihre Stabilität", *Physica*, 6, p. 806, 1939.
4. C. J. D. M. Verhagen, "Impedanzmessungen an Gasentladungsröhren", *Physica*, 8, p. 361, 1941 and "Theorie en Metingen over de Impedantie en de Stabieleit van Gasontladungen", Thesis submitted to the University of Delft, 1942.
5. C. van Geel, "Zelfinductie en Nawerking in Gasontladungen", Thesis submitted to the University of Delft, 1955.
6. C. van Geel, "Influence of self-inductance and after-effect in gas discharges on their stability", *Applied Scientific Research*, B5, p. 79, 1955-56.
7. F. A. Benson and P. M. Chalmers, "Impedance-frequency characteristics of glow-discharge reference tubes", *Proc. Instn. Elect. Engrs*, 107B, p. 199, 1960.
8. K. B. Reed and J. F. Dix, "Cold cathode discharge tubes—impedance and noise properties", *Electronic Technology*, 39, p. 31, 1962.
9. J. F. Dix, "An experimental study of noise initiated electrically, with particular reference to gas discharge tubes", Ph.D. Thesis, University of London, 1961.
10. F. A. Benson and G. Mayo, "Impedance-frequency variations of glow-discharge voltage-regulator tubes", *Electronic Engineering*, 26, p. 206, 1954.
11. G. J. M. Ahsmann and H. J. Oskam, "Impedance and recovery time of glow discharges in mixtures of rare gases", *J. Appl. Phys*, 29, p. 1768, 1958.
12. G. J. M. Ahsmann, "On the impedance of the anode fall region of a glow discharge in the noble gases", *Proceedings of the Third International Conference on Ionization Phenomena in Gases*, Venice 1957, p. 19.
13. G. J. M. Ahsmann, "The impedance and recovery time of glow discharges in mixtures of rare gases", *Proceedings of the Fourth International Conference on Ionization Phenomena in Gases*, Uppsala, 1959, p. IIA, 309.
14. G. Marx, "Irregular oscillations of cold-cathode tubes and their eliminations", *Nachrichtentechnische Fachberichte*, 9, p. 32, 1957.
15. G. F. Weston, "Impedance pressure characteristics of glow-discharge tubes", *Proceedings of the Fifth International Conference on Ionization Phenomena in Gases*, Munich, 1961, 1, p. 528.
16. G. F. Weston, "The effect of current and pressure on the impedance of cold-cathode glow-discharge tubes", *J. Electronics & Control*, 12, p. 379, 1962.
17. F. W. Crawford, "Impedance characteristics of a low-pressure mercury-vapour plasma", Stanford University Microwave Laboratory Report No. 761, November, 1960.
18. M. A. Townsend and W. A. Depp, "Cold-cathode tubes for transmission of audio-frequency signals", *Bell Syst. Tech. J.*, 32, p. 1371, 1953.
19. F. A. Benson and G. Mayo, "Impedance-frequency characteristics of some glow-discharge tubes", *Electronic Engineering*, 28, p. 124, 1956.
20. D. W. Hill, "A cold-cathode speech tube", *A.T.E. J.*, 11, p. 129, 1955.
21. J. E. P. Hunt, "Some limitations in voltage stabilizers", *Institution of Electrical Engineers Students' Quarterly Journal*, 23, p. 12, 1952.
22. J. Groszkowski, "Glow-discharge tube as an inductance", *Kwartalnik Telekomunikacyjny*, No. 1, 1948.
23. A. M. Andrew, "The design of series-parallel voltage stabilizers", *Electronic Engineering*, 24, p. 385, 1952.
24. F. Iannone and H. Baller, "Gas-tube coupling for d.c. amplifier", *Electronics*, 19, p. 106, October 1946.
25. Y. Hatta, T. Sato and M. Sakata, "The measurement of the low-frequency impedance of the gaseous electric discharge", *Electrotechnical Papers, Japan*, 4, No. 1, p. 46, 1952.
26. F. A. Benson and L. J. Bental, "Glow-discharge stabilizers", *Wireless Engineer*, 32, p. 330, 1955.
27. H. J. Reich and W. A. Depp, "Dynamic characteristics of glow-discharge tubes", *J. Appl. Phys.*, 9, p. 421, 1938.
28. P. J. Severin, "Some dynamic aspects of the cathode fall region in a d.c. glow discharge", *Physica*, 29, p. 83, 1963.
29. H. Deutsch, "Gas mixture processes in alternating-current discharges", *Annalender Physik*, 6, p. 355, 1960.
30. R. N. Maddison, "Optical model analysis of the electric scattering of low energy deuterons", *Proc. Phys. Soc. Lond.*, 79, Part 2, p. 264, 1962.
31. W. D. Davis and T. A. Vanderslice, "Ion energies at the cathode of a glow-discharge", *Phys. Rev.*, 131, p. 219, 1963.
32. F. A. Benson and E. F. F. Gillespie, "The influence of argon content on the characteristics of glow-discharge tubes", *Proc. Elec. Engrs*, 104B, p. 498, 1957.
33. J. A. Hornbeck, "The drift velocities of molecular and atomic ions in helium, neon and argon", *Phys. Rev.*, 84, p. 615, 1951.

Manuscript received by the Institution on 24th January 1964.  
(Paper No. 982.)

© The Institution of Electronic and Radio Engineers, 1965

## DISCUSSION

**Mr. T. Poorter:** The frequency response measurements made by Dr. Benson have resulted in a complex equivalent circuit for a gas discharge diode valid for small sinusoidal variation of voltage and current superimposed on a d.c. level. It is desirable from the circuit engineer's point of view to have available a more simple equivalent circuit that might be a first approximation to the one presented and that should give a response sufficiently accurate for actual practice. It may be possible that such a circuit can be derived more easily from step response measurements; in

any case this approach will give a result which has a closer connection with the kind of operation actually met in practice thus indicating the relevant parameter more clearly.

Moreover, measurements could be done on step response excitation of lower amplitude which would be of still more interest in practical cases; those responses cannot be derived from the frequency response data because of the non-linearity involved.

It appears that the equivalent circuit presented by Dr. Benson could be regarded as a first step in the attempt to come to an equivalent circuit that can be handled by a circuit designer and can produce quantitative information of a sufficient accuracy about circuit operation. It presents a link between circuit operation and the physical processes involved such that it might be possible to design a gas discharge tube according to the circuit operating requirements.

In the transistor field, starting from a frequency response approach, a simple and approximate charge control theory has evolved, based on a qualitative insight into the physical processes involved, leaving out details which complicate the equivalent circuit and do not give a great improvement in accuracy of response. This has brought the quantitative treatment of transistor transient response within the grasp of the circuit designer and might well account for the ready acceptance of the transistor as a fast switching device.

Moreover, it has been possible to define from this approach several important parameters characterizing the transistor as a switching device. These parameters can easily be measured and are used in comparing the switching performance of different transistors. In addition it has been possible to extend this approach to other devices such as vacuum tubes and photoelectric devices so that now vacuum tubes and transistors can be compared more easily in their ability to perform similar operations. It would be of great interest if this approach could be extended to gas-filled tubes.

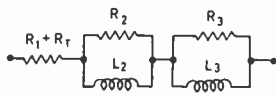


Fig. A.

In this respect it is of interest that an analogy can be drawn between a semiconductor diode and a gas-filled diode. The cathode-fall region in a gas-filled diode can be compared with the depletion layer in a semiconductor diode, both being regions containing an electric field and carrying nearly the full voltage drop. The plasma region of a gas-filled diode can be compared with the bulk region adjacent to the depletion layer of a semiconductor diode service in both the current flows by ambipolar diffusion in which the electric field is virtually zero and they do not carry a substantial voltage drop.

It should be pointed out that, in the case of the semiconductor diode and the transistor, a crude approximation of the density distribution of holes and electrons together with an assumed constant mean-lifetime of the minority

carrier, already gives rise to an equivalent circuit which is sufficiently accurate over a wide frequency range; moreover a fairly accurate transient response can be obtained from the equivalent circuit for large current step excitations.

Dr. F. A. Benson (*in reply*): Figure 2(b) of the paper shows the complete equivalent circuit for the discharge tube over the frequency range investigated, i.e. 200 c/s–70 Mc/s. For a restricted frequency band within this range, however, the equivalent circuit may be simplified. The impedance of a parallel combination of inductance and resistance may be approximated to by a resistance at high frequencies and an inductance at low frequencies. Further, since the value of  $C_d$  is small (of the order of 6 pF) it may be neglected at low frequencies. Thus, for example, at audio frequencies the equivalent circuit may be reduced to that shown in Fig. A and at megacycle frequencies it may be approximated by Fig. B.

We have not made any step-response measurements. Mackay and Morrist† observed the transient responses of a number of glow discharges and showed that the performance of tubes in pulse circuits may be poor. Each tube (1/25 watt neon or argon tubes were used) was placed in series with a resistor and fixed bias source. Superimposed on this fixed voltage was a square-wave signal (rise and fall times of less than 0.3  $\mu$ s with no overshoot), the response to which was observed across the resistor. From the response time of several microseconds and the characteristic overshoot it was suggested that a tube could be replaced by an equivalent circuit consisting of a combination of resistance and inductance.

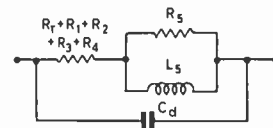


Fig. B.

Dr. C. Grey Morgan: Have you observed any pressure dependence of the delay times?

Dr. Benson (*in reply*): From Severin's formula for transit time  $\tau$  given in Section 5 of the paper it is found that  $\tau \propto 1/p$ . Measurements on pure-neon tubes with molybdenum cathodes and gas pressure of 30, 40 and 50 torr show that as the pressure decreases the various time constants increase. Further measurements are now being undertaken over a wider pressure range in an attempt to confirm the result predicted by Severin's expression.

† R. S. Mackay and H. D. Morris, "Transient response of glow-discharges with applications", *Proc. I.R.E.*, 42, p. 961, 1954.

# A Light Absorption Detector for a Computer Controlled Film Scanner

By

P. de BRUYNE, B.Sc.  
(Associate Member)†

**Summary:** Computers can process photographically recorded data both rapidly and efficiently. It is shown that a general purpose computer may be readily adapted to read film information. A standard computer display monitor is used as a scanning source. The detector employs a photomultiplier and transfers the digitized data to the computer.

## 1. Introduction

Scientific data photographs may be selectively scanned under control from a programmed computer in a way similar to punched data cards. Instead of using a number of bulbs and phototransistors, a spot from a cathode-ray tube is focused on the film. The transmitted light is detected by photomultipliers. The spot may be programmed to scan in a fashion most efficient to the work at hand and is thus more versatile and faster than a conventional flying spot scanner. Extraction of data and computation of results can proceed simultaneously at a high speed even though the plotting of a single point may take much longer (50  $\mu$ s) than with a flying spot scanner. No time need be wasted scanning unfruitful areas and only the required data are read out and in the required sequence for rapid processing. The computer need not permanently store all data. It may use temporary storage and write on tape only the results as soon as they are produced. What can be done is limited by the imagination of the programmer; it is not limited by a mechanical raster scanner.

Although undoubtedly useful in other areas (satellite data photographs, star mapping, etc.) the scanner was primarily built for the analysis of nuclear tracks in spark chambers. Spark chamber pictures can be analysed with a micrometer microscope but the method is tedious for the large numbers of such pictures usually involved.

The equipment to be described is designed for use with a medium-speed general-purpose computer and consists of a film transport mechanism, light absorption detector and data buffer.

## 2. Description of System

The computer‡ has a display unit capable of addressing  $1028 \times 1028$  points on a monitor tube (Raytheon 16A7DP34). The spot size is about 0.8 mm. The

useful area is  $235 \times 235$  mm and the measured aberration is maximum 1.5 mm and generally less than 0.5 mm.

An optical box (Fig. 1) containing a lens and an automatic film transport for 70-mm film was made to fit the monitor housing. A half-silvered mirror and two photomultiplier tubes are used to detect film

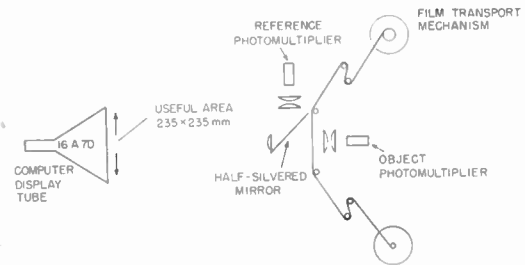


Fig. 1. Optical arrangement.

density. It was found advantageous to use two tubes connected differentially because the random variations in spot brightness on the screen were of the order of 2 to 1. By adding the dynode current of the reference tube to the anode current of the object tube (or vice versa for positives), the resulting signal applied to an emitter follower allows detection of less than 10% absorption in the film.

The two photomultipliers 6199 are connected as shown in Fig. 2. Dynode-anode operation can be interchanged using switches so that either negative or positive film may be used. Photomultiplier voltages are always adjusted so that the anode-connected tube current slightly exceeds the magnitude of the dynode-connected tube current. The summed current is thus predominantly negative with positive excursions at positions of film data.

† Cyclotron Laboratory, Harvard University, Cambridge, Massachusetts, U.S.A.

‡ Type PDP1, Digital Equipment Corporation, Maynard, Mass., U.S.A.

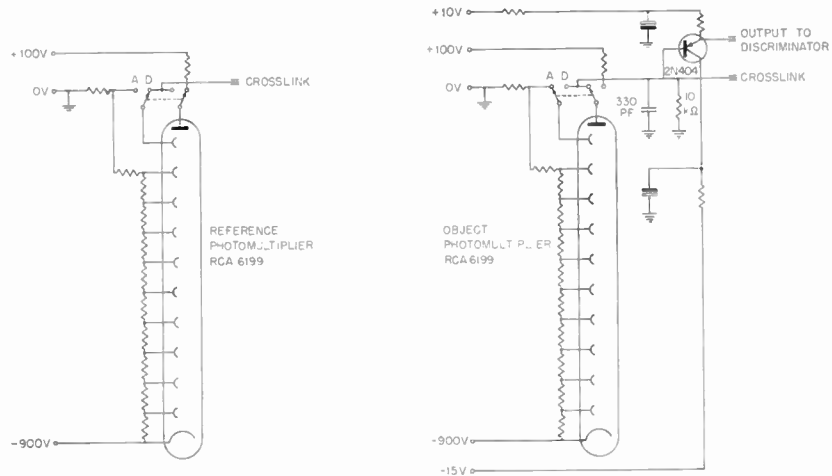


Fig. 2. Photomultiplier corrections.

### 3. Computer Interface Circuits

The peak negative output voltage of the summed photomultiplier signal is detected and stored by the use of an operational amplifier, a diode and a capacitor (Fig. 3). This voltage corresponds to maximum spot brightness at non-data positions on the film. The stored voltage is allowed to decay with a time-constant adjustable from 1 millivolt per millisecond to 100 millivolts per millisecond. The instantaneous output voltage of the emitter follower is constantly compared with a set fraction of this negative stored voltage using a second operational amplifier. The open loop voltage gain of each amplifier is about 5000. The output of this second amplifier is standardized to the logic levels -3 V for negation and 0 V for data assertion. It is then sampled in a gate with a strobe pulse at the time the scanning point has reached a maximum brightness.

The output of this gate sets a flip-flop which may be sampled by the computer. The flip-flop is reset to zero at the beginning of each brightening pulse.

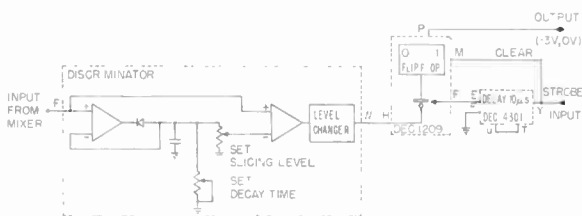


Fig. 3. Logic diagram.

The two operational amplifiers and level standardizer are mounted on a blank module card (Fig. 4). The gate and flip-flop and delay units are standard modules. The delay is set to a value such

that the output pulse is obtained when the spot is at maximum brightness.

The only other controls besides those for the photomultiplier voltages are the slicing level or sensitivity control at the input of the second operational amplifier, and the decay time control.

The photomultiplier voltages are set around 900 V so that each tube by itself would produce about 3 V across the 10-kΩ load. As the currents are in opposite directions they subtract and should leave about 0.2 V negative in the 'no data' positions during brightening of the spot.

The slicing level may be set to about 0 V for photographs with normal detail. This then requires a difference voltage of 0.2 V or more to obtain assertion.

By setting the decay control to a long decay, large numbers of assertions may be stored consecutively. Each time a single negation is obtained the storage capacitor is recharged to the peak negative voltage.

A short decay time is permissible for most spark chamber photographs as the lines are only a few positions wide. The operation can then be made relatively insensitive to variations in film base density and optical differences which produce slow variations in the negative peak voltage.

### 4. Resolution

The capacity of the store is such that only about 4000 locations of assertion may be stored. This, however, proves to be sufficient to hold all the tracks of an average spark chamber photograph. Operation of the equipment was checked and adjusted by re-displaying the locations of assertion on the monitor screen. Dark lines of 25 microns width on clear film could be recorded over the entire film window of 63 mm × 72 mm.



# Radio Engineering Overseas . . .

The following abstracts are taken from Commonwealth, European and Asian journals received by the Institution's Library. Abstracts of papers published in American journals are not included because they are available in many other publications. Members who wish to consult any of the papers quoted should apply to the Librarian, giving full bibliographical details, i.e. title, author, journal and date, of the paper required. All papers are in the language of the country of origin of the journal unless otherwise stated. Translations cannot be supplied.

## ANALYSIS OF A TUNNEL DIODE STORE BY ANALOGUE SIMULATION

In the course of designing a store consisting of a current-biased Esaki tunnel diode combined with two conventional diodes and characterized by high speed of operation and large level of read-out signal, the authors of a Japanese paper had to choose appropriate values for parameters specifying both the cell itself and driving waveforms.

For this purpose, an analogue simulation technique seemed to be highly suitable, in which non-linear characteristics of the elements would be approximated in linear piecewise manner by an appropriate limiter circuit using vacuum-tube diodes.

The method adopted and the resulting data are described in the paper. The results may be summarized as follows:

(1) Assuming the read-drive is fixed, the read-out level is an increasing function of  $C_{ED}$  (junction capacitance of Esaki diode) and independent of  $C_{D1}$  (junction capacitance of read diode). On the other hand, the noise level is independent of  $C_{ED}$  and proportional to  $C_{D1}$ .

(2) The function of so-called current-reading which is basic to the cell is much improved by addition of an appropriate capacitor parallel to the Esaki diode. In this case, it is found that the switching time of the cell still remains within practical limits; typically it does not exceed 10 ns.

"Analysis of an Esaki diode memory cell by analog simulation", Teruhiko Bessho and Keijichi Tsukada *Review Electrical Communications Laboratory, NTT*, 12, 7-8, pp. 447-68, July-August 1964.

## VARIATION OF IONIZATION IN THE IONOSPHERE

The solar wave radiation responsible for the production of the ionization in the ionosphere varies in its intensity in close correlation with the period of the 11-years' sunspot cycle. Furthermore, intensity variations with a quasi-persistent 27-days' period can occur in cases where sunspots are unsymmetrically distributed in heliographic longitude and where the sun in the course of its rotation in about 27 days exhibits alternatively disks with many spots and with few spots.

In a paper published in Germany recently it is shown that such intensity variations produce considerable 27-day variations with the same phase in the critical frequencies of the  $F_1$ -,  $F_2$ -, and  $E_1$ -layers as well as in the MUF 3000 (maximum usable frequency for the 3000-km distance), but 27-day variations with reversed phase in the M3000 factor (conversion factor from vertical to oblique-incidence critical frequency for the 3000-km distance); 27-day quasi-persistent variations in the average temperature of

the F-layer may be responsible for the production of these M3000 variations. Numerical data are given for magnitude and seasonal variation of the average relative amplitude of the 27-day variations of the ionospheric data mentioned above.

"Ionization variations in the mid-latitudes of the ionosphere and the variation of the usable frequencies for long distance short wave propagation, with 27-day period as the effect of solar wave radiations", G. Lange-Hesse and E. Schott. *Archiv der Elektrischen Übertragung*, 19, No. 1, pp. 59-65, January 1965.

## HORN ANTENNA CHARACTERISTICS

The authors of this Czech paper have investigated the influence of the reflector on a microwave horn antenna with various reflector distances, using multiple reflections between the antenna and the reflector. Experimental measurements of the reflection factor corroborate the theoretical conclusion that the resultant reflection factor forms a family of concentric circles around a centre point determined solely by the reflection factor of the antenna alone; the radii of the circles indicate the reflection factor for a given distance. The measurement results are being used for determining the gain of a horn antenna.

"Determining the influence of reflector distance on a horn antenna", F. F. Hanna and A. M. Bishai. *Slaboproudý Obzor (Prague)*, 26, No. 2, pp. 85-7, February 1965.

## TELEVISION TRANSMISSION SIGNAL/NOISE RATIO IMPROVEMENT

Methods are described by a German engineer for utilizing the correlation of the brightness values of television picture elements which are adjacent in time and space, to effect an improvement of the signal/noise ratio. Possible fields of application are, among others, magnetic picture recording, television programme relay links, television broadcasting, television satellites, and space probes.

"Methods for improving the signal/noise ratio in television transmission systems", G. Krause. *Archiv der Elektrischen Übertragung*, 18, No. 10, pp. 601-6, October 1964.

## TUNNEL DIODE SAMPLER-QUANTIZER

A video sampler-quantizer which uses a tunnel diode as the threshold switching device is described in a recent Australian paper. Sampling the waveform allows backlash to be reduced by means of a set-reset method of operation. By using a parallel connected system the speed of operation is reduced to a minimum. A rise-time of 40 ns has been measured.

"A sampler-quantizer for television waveforms", J. O. Limb. *Proceedings of the Institution of Radio and Electronics Engineers Australia*, 26, No. 3, pp. 113-17, March 1965.